



Fabian Veider, BSc

**NLO corrections for $e^-e^+ \rightarrow \mu^-\mu^+$ in a
 $SU(2) + BEH$ theory via augmented
perturbation theory**

Master's Thesis

to achieve the university degree of
Master of Science
Master's degree programme: Physics

submitted to

University of Graz

Supervisors

Axel T. Maas, Simon Plätzer

Affidavit

I declare that I have authored this thesis independently, that I have not used other than the declared sources/resources, and that I have explicitly indicated all material which has been quoted either literally or by content from the sources used. The text document uploaded to UNIGRAZonline is identical to the present master's thesis.

01.09.2023

Date



Signature

Abstract

The standard model (SM) stands as a cornerstone in particle physics, providing remarkable insight into the fundamental interactions of nature. While the Higgs field therein resolved the electroweak interaction puzzle, the elementary particles are lacking gauge invariance with respect to the weak interaction. Therefore, it may seem surprising that the usual treatment of leptonic scattering in terms of gauge-variant elementary leptons is in strong agreement with experimental results. This master thesis sheds light on this tension through the Fröhlich-Morchio-Strocchi (FMS) mechanism. It posits gauge-invariance of external leptons by introducing bound states of the elementary fields and the scalar Higgs doublet. This effects can then be analyzed via an augmented perturbation theory (APT), with its leading contribution corresponding to the standard perturbative treatment of elementary particles. By taking into account the scalar bound-state contribution in the scattering process $e_L^- e_L^+ \rightarrow \mu_L^- \mu_L^+$ of massless left-handed leptons at NLO, we obtain new and yet unaccounted matrix elements in addition to the standard contributions. These could be essential for an accurate theoretical description of (differential) cross sections, especially for high-energy collisions in future lepton colliders.

Acknowledgement

I would like to express my sincere gratitude to my two supervisors, Axel Maas and Simon Plätzer, for their unwavering guidance, invaluable insights, and continuous support throughout the journey of this master thesis. Their expertise and encouragement have been instrumental in shaping the direction of this research.

I would also like to extend my thanks to my colleague, Franziska Reiner, whose thoughtful discussions and proofreading added depth to my work and enriched the overall experience. Furthermore, my thanks extends to my friend David Gulda, whose support and fruitful discussions about my path in science had a strong impact in shaping this thesis.

Lastly, I am deeply thankful to my family for their boundless love, encouragement, and patience. Their unwavering belief in me has been the driving force behind my accomplishments.

Each of you has played an integral role in the realization of this work, and I am truly grateful for all of your contributions.

Contents

1. Introduction	2
2. Physical leptons in the weak sector of the SM	4
2.1. The weak sector of the SM	4
2.2. Renormalization	7
2.3. FMS formalism	8
2.3.1. Gauge-invariance and physical leptons	8
2.3.2. FMS expansion	9
2.4. Scattering Theory	11
2.4.1. Differential cross section	11
2.4.2. Invariant matrix elements	12
2.4.3. Bound states	14
2.4.4. FMS expansion of our leptonic scattering	16
2.4.5. Matrix elements and cross sections in APT	18
3. Technical tools	20
3.1. Spinor-helicity (SH) formalism	20
3.1.1. Introduction	20
3.1.2. Spinor chains	23
3.1.3. Simplification rules	24
3.2. Integral reduction	25
3.2.1. Scalar Integrals	25
3.2.2. Tensor decomposition	29
3.2.3. Reduction Summary	31
4. Software and packages	32
4.1. QGraf	32
4.1.1. Introduction	32
4.1.2. Input files	32
4.2. Our Mathematica tools	37
4.2.1. Overview	37
4.2.2. Example calculation	38
5. Results	40
5.1. Tree level	40
5.2. Regular loop expressions	43
5.2.1. Feynman diagrams	43

5.2.2. Reduced algebraic expressions	47
5.3. FMS loop expressions	55
5.3.1. Feynman diagrams	55
5.3.2. Reduced algebraic expressions	57
6. Conclusion and Future Work	62
A. Conventions	68
A.1. Units	68
A.2. Minkowski space	68
A.3. Mandelstam variables	69
A.4. Dirac & Pauli matrices	70
B. Tree level for the full EW model	72
C. Feynman rules in Weyl representation	76
C.1. Elementary external legs	76
C.2. External bound states	77
C.3. Propagators	78
C.4. Interaction vertices	78
D. Scalar integrals	80
D.1. Convention	80
D.2. Tadpole integral	81
D.3. Bubble integrals	81
E. QGraf	84
E.1. Model file	84

List of Figures

2.1.	Tree-level Feynman diagram for our process of order g^2	13
2.2.	NLO Feynman diagram with a fermionic loop of order g^4	13
2.3.	Operator insertions of the leptons $L = E, M$ as a Feynman rule, approximated by an elementary spinor attached to a lepton and scalar propagator with an integration of the relative momenta of constituent particles.	15
2.4.	All types of n-point functions occurring after the FMS expansion. Each insertion of a bound state is marked by a cross and translates to an integration over the relative momentum of one of its constituents. One representation for each type of n-point function was chosen.	17
2.5.	Two suggestive plots that highlight different behaviour for the deviation of $d\sigma$ due to a gauge-invariant treatment, here for fixed t and SM values v_{exp} , g_{exp} and λ_{exp}	19
3.1.	Momentum and mass conventions for our choice of master integrals.	27
4.1.	Fermionic self-energy diagram of the process $e_L^- e_L^+ \rightarrow \mu_L^- \mu_L^+$	35
4.2.	Triangle diagram due to the expanded six-point function from FMS contributions in the final state	36
4.3.	Accurate representation of the bound-state insertion with our cross-notation from the Feynman rules of figure (2.3)	36
4.4.	Snail-diagram of the process $e_L^- e_L^+ \rightarrow \mu_L^- \mu_L^+$	38
4.5.	Tensor expression of our loop diagram in Mathematica	39
4.6.	Scalar expression of our loop diagram in Mathematica	39
4.7.	Final reduced expression of our loop diagram in Mathematica	39
5.1.	Differential cross section of the tree-level process in terms of the CM-energy \sqrt{s} and the scattering angle θ	42
5.2.	Differential cross section of the tree-level process in terms of the CM-energy \sqrt{s} and the pseudorapidity η	42
5.3.	Differential cross section of the tree-level process in terms of the CM-energy \sqrt{s} for fixed angles	43
5.4.	Full list of all bubble diagrams	44
5.5.	Full list of all snail diagrams	45
5.6.	Full list of all tadpole diagrams	45

5.7.	Full list of all triangle diagrams	46
5.8.	Full list of all box diagrams	46
5.9.	Full list of all triangle diagrams arising from six-point functions	55
5.10.	Full list of all box diagrams arising from eight-point functions . .	56
5.11.	Exemplary FMS contribution	57
6.1.	Summary of all types of matrix elements due to the gauge-invariant description of external leptons. Red lines symbolize all possible propagator types that are consistent with Feynman rules of the weak sector, and crosses correspond to operator insertions of the composite scalar-lepton fields. The terms $\phi_a \in \{h, \chi, \phi^\pm\}$ represent the would-be Goldstone bosons in (6.1) and (6.2). . . .	64
B.1.	Tree level diagrams for the scattering process in the full EW sector	72
B.2.	Differential cross sections at tree-level for the full EW model and our $SU(2)$ model in terms of the CM-energy \sqrt{s} and the pseudorapidity η	73
B.3.	Differential cross section of the tree-level process in terms of the CM-energy \sqrt{s} and fixed angle $\theta = 0$ of the full EW model and our $SU(2)$ model (above). The comparison $d\sigma_{SU(2)}/d\sigma_{EW}$ shows strong agreement for energies far above the pole of the vector boson (below).	74
C.1.	Full list of all leptonic external legs	76
C.2.	Operator insertion of the bound states	77
C.3.	Full list of all propagators.	78
C.4.	Full list of all interactions containing four particles.	78
C.5.	Full list of all interactions containing three particles.	79

1. Introduction

The fundamental requirement of theories like the standard model is the gauge invariance of experimental observables [1, 2, 3, 4]. However, a paradox seems to arise in the electroweak sector, as the elementary particles that appear in the Lagrangian do not strictly adhere to gauge invariance [1, 2, 3]. Despite this, when treated within perturbation theory, they remarkably provide a very good explanation for experimental outcomes [5, 6].

The solution to this seemingly paradox situation comes through the Fröhlich-Morchio-Strocchi (FMS) mechanism [3, 7]. It introduces gauge-invariant composite states that are a mixture of the standard elementary fields. These bound states can be compared with the perturbative elementary states through a FMS expansion, given that we choose a gauge fixing where perturbation theory can be applied [8]. Empirical support for this concept is given by lattice simulations for static properties of particles [4, 9, 10]. This can have an effect on dynamical quantities such as cross sections [11], where the scattering of bound states primarily derives from the scattering process involving their elementary constituents [3, 7], akin to the scattering behavior observed in QCD bound states [5]. Nevertheless, a crucial distinction exists. In the usual treatment of the electroweak sector, only one constituent from the actual bound-state operators contributes to all orders of perturbation theory. Incorporating the contribution from the second component necessitates moving beyond the boundaries of conventional perturbation theory, augmenting the calculations by including additional Green's functions of higher orders than the standard elementary ones. The effects of this augmented perturbation theory (APT) have been tested in an isolated study of the full gauge-invariant propagators in the scalar and weak sector of the standard model [12, 13], and prior studies of collisions in the flavour sector using parton distribution functions (PDFs) suggest a small deviation from usual calculations in fermionic scattering processes [14]. Furthermore, this change to external bound states has implications on the Bloch-Nordsieck theorem [15]. However, no full treatment using APT for fermions at loop-order has been done yet. This master thesis sets out to fill this gap. To do so, we analytically calculate the matrix elements of the process

$$e_L^- e_L^+ \rightarrow \mu_L^- \mu_L^+ \quad (1.1)$$

with massless left-handed leptons at next-to-leading-order (NLO) by introducing gauge-invariant bound states of elementary leptons with the Higgs doublet.

We isolate the weak sector of the standard model to avoid complications such as infrared divergences due to massless photons.

This thesis is structured as follows: First, we introduce in chapter (2) the theoretical basics of our analysis. After shortly reviewing the usual picture of the renormalized weak sector in (2.1) and (2.2) along with our augmented picture that incorporates gauge-invariance for leptons (2.3), we highlight the impact on particle phenomenology and its effect on the calculation of matrix elements and (differential) cross sections (2.4). Then, we present the main technical tools (3) that went into our calculations, namely the spinor-helicity formalism in section (3.1) and the integral reduction of loop expressions in section (3.2). In chapter (4) we will highlight the main software tools created and used in the process of our research. The diagram generation via QGraf (4.1) and our implementation of tools for loop calculations within Mathematica (4.2) are emphasized here. Finally, we present our results in (5), splitting the resulting matrix elements into tree level (5.1), regular one-loop (5.2) and new terms (5.3) at NLO. To conclude, a brief summary and outlook into future research is presented in chapter (6).

2. Physical leptons in the weak sector of the SM

We showcase the usual picture of the weak sector of the SM with massless Weyl fermions in sections (2.1) and (2.2). Imposing gauge invariance on our external leptons via the FMS formalism then yields bound states of elementary leptons and Higgs particles in section (2.3). We link these objects to perturbation theory through a FMS expansion, where we end up with an extended expression for matrix elements and the differential cross section for perturbative calculations at NLO in section (2.4).

2.1. The weak sector of the SM

The electroweak theory is the unified theory of two fundamental forces in nature: electromagnetism and the weak interaction. It was developed in the 1960s by Sheldon Glashow, Abdus Salam, and Steven Weinberg [16, 17, 18]. It is based on the principles of gauge theories that describe interactions between particles using symmetry principles. The symmetry group of the electroweak interaction is $SU(2)_W \times U(1)_Y$, where $SU(2)_W$ represents the weak isospin symmetry and $U(1)_Y$ represents the weak hypercharge symmetry. For the description of bound states in our leptonic scattering process, it is sufficient to only consider the weak interaction with two generations of massless fermions. The Lagrangian density of the theory then reads

$$\mathcal{L}_W = -\frac{1}{4}W_{\mu\nu}^a W^{a,\mu\nu} + \frac{1}{2}\text{tr}\left\{(D_\mu X)^\dagger(D^\mu X)\right\} - \frac{\lambda}{4}\left(\text{tr}\left\{X^\dagger X\right\} - v^2\right)^2 + \mathcal{L}_{\text{Fermion}} \quad (2.1)$$

where $W_{\mu\nu}^a = \partial_\mu W_\nu^a - \partial_\nu W_\mu^a + g\epsilon^{abc}W_\mu^b W_\nu^c$ ($a, b, c = 1, 2, 3$) are the field strength tensors in terms of the three weak gauge fields W_μ^a , the weak coupling g and the Levi-Civita tensor ϵ^{abc} . For practical purposes, we made use of the matrix

representation of the complex scalar doublet $\phi = (\phi_1, \phi_2)^T$

$$X = \begin{pmatrix} \phi_2^* & \phi_1 \\ -\phi_1^* & \phi_2 \end{pmatrix} \quad (2.2)$$

The covariant derivative D_μ reads

$$D_\mu = \partial_\mu \mathbb{1} - ig \frac{\sigma^a}{2} W_\mu^a \quad (2.3)$$

with the generators $\frac{\sigma^a}{2}$ of the symmetry group $SU(2)_W$. The first two vector bosons are combined into the charged fields

$$W_\mu^\pm = \frac{1}{\sqrt{2}} (W_\mu^1 \mp iW_\mu^2) \quad (2.4)$$

The interactions for two generations of massless Weyl spinors are incorporated through the fermionic term

$$\mathcal{L}_{\text{Fermion}} = \sum_{j=1}^2 \left[\bar{\psi}_L^j i \not{D} \psi_L^j + \bar{\kappa}_R^j i \not{\partial} \kappa_R^j + \bar{q}_L^j i \not{D} q_L^j + \bar{a}_R^j i \not{\partial} a_R^j + \bar{b}_R^j i \not{\partial} b_R^j \right] \quad (2.5)$$

where we used the following short forms for the gauged left-handed doublets ψ_L^j / q_L^j and the ungauged right-handed singlets κ_R^j, a_R^j and b_R^j

$$\begin{aligned} \psi_L^1 &= \begin{pmatrix} \nu_{eL} \\ e_L^- \end{pmatrix}, & \psi_L^2 &= \begin{pmatrix} \nu_{\mu L} \\ \mu_L^- \end{pmatrix} \\ \kappa_R^1 &= e_R^-, & \kappa_R^2 &= \mu_R^- \\ q_L^1 &= \begin{pmatrix} u_L \\ d_L \end{pmatrix}, & q_L^2 &= \begin{pmatrix} c_L \\ s_L \end{pmatrix} \\ a_R^1 &= u_R, & a_R^2 &= d_R \\ b_R^1 &= c_R, & b_R^2 &= s_R \end{aligned} \quad (2.6)$$

The dashed expressions in (2.5) represent the corresponding anti-particles. Expanding the complex Higgs doublet in terms of the would-be Goldstones

$$\phi = \begin{pmatrix} \phi^+ \\ \frac{1}{\sqrt{2}}(v + h + i\chi) \end{pmatrix}, \quad (\phi^+)^{\dagger} = \phi^- \quad (2.7)$$

so that it has a non-vanishing vacuum expectation value (vev) v

$$\langle \phi \rangle = \begin{pmatrix} 0 \\ \frac{v}{\sqrt{2}} \end{pmatrix}, \quad \langle X \rangle = \frac{v}{\sqrt{2}} \mathbb{1} \quad (2.8)$$

2. Physical leptons in the weak sector of the SM

leads to the "spontaneous symmetry breaking" of the weak sector. This allows for the vector bosons to acquire masses and is famously known as the Brout-Englert-Higgs (BEH) mechanism [19, 20]. Expanding the Lagrangian using (2.3) and (2.8), we can read off the masses of the neutral vector bosons from their kinematic terms

$$\frac{g^2 v^2}{8} W_\mu^3 W^{3,\mu} = \frac{m^2}{2} W_\mu^3 W^{3,\mu} \rightarrow m = \frac{gv}{2} \quad (2.9)$$

The same mass appears for the term $W_\mu^+ W^{-,\mu}$ of the charged vector bosons. Similarly, the kinematic part of the real scalar Higgs field h yields its mass in terms of the self-interaction λ and the vev v

$$\lambda v^2 h^2 = \frac{m_h^2}{2} h^2 \rightarrow m_h = \sqrt{2\lambda} v \quad (2.10)$$

Quantization and higher-order loop corrections demand a specific gauge choice [21]. We employ here the renormalizable 't Hooft gauge with the gauge-fixing functionals

$$C^\pm = \partial^\mu W_\mu^\pm \mp im \tilde{\zeta}'_+ \phi^\pm, \quad C^W = \partial^\mu W_\mu^3 - m \tilde{\zeta}'_W \chi \quad (2.11)$$

leading to the gauge-fixing Lagrangian

$$\mathcal{L}_{\text{Gauge}} = -\frac{1}{2\tilde{\zeta}_W} (C^W)^2 - \frac{1}{2\tilde{\zeta}_\pm} C^\pm C^\mp \quad (2.12)$$

We can further choose $\tilde{\zeta}'_W = \tilde{\zeta}_W$ and $\tilde{\zeta}'_\pm = \tilde{\zeta}_\pm$ to obtain simple expressions for the masses of our would-be Goldstone bosons

$$m_{\phi^\pm} = \sqrt{\tilde{\zeta}_\pm} m, \quad m_\chi = \sqrt{\tilde{\zeta}_W} m \quad (2.13)$$

In order to retrieve perturbative gauge-invariance, we need unphysical virtual states called Faddeev-Popov ghosts [5]. Their Lagrangian is

$$\mathcal{L}_{\text{Ghost}} = - \int d^4 y \bar{u}^r(x) \frac{\delta C^r(x)}{\delta \theta^s(y)} u^s(y), \quad r, s = W, \pm \quad (2.14)$$

with a variation of the gauge-fixing functions C^r in terms of infinitesimal gauge transformations and the Faddeev-Popov (anti-)ghost fields u^s, \bar{u}^r . Their masses are the same for the Goldstone bosons. By adding (2.1), (2.12) and (2.14) we obtain the full quantized Lagrangian necessary for loop calculations

$$\mathcal{L}_W^{\text{Full}} = \mathcal{L}_W + \mathcal{L}_{\text{Gauge}} + \mathcal{L}_{\text{Ghost}} \quad (2.15)$$

In a generalized treatment of the massive standard model, the covariant derivative is expanded to include the hypercharge field B_μ , which leads to three massive vector fields with two distinct masses and the massless photon field after rotating them around the Weinberg angle θ_W . There, the BEH mechanism is also responsible for the generation of masses for the elementary fermions via Yukawa interactions. The Weyl fermions then combine into the usual Dirac fermions [22].

2.2. Renormalization

The final part of the Lagrangian arises from the renormalization of our theory. It cancels all appearing ultraviolet (UV) divergences and can be obtained in a future work via counterterm diagrams that modify the Feynman rules. The starting point is to split the bare parameters of the Lagrangian in terms of renormalized parameters (denoted by the subscript R) and corresponding counterterms. We briefly list the necessary steps here for an on-shell scheme [21], where we set the renormalized masses to the poles of the elementary propagators. Then, our coupling and masses read

$$\begin{aligned} m^2 &= m_R^2 + \delta m_R^2, \quad m_h^2 = m_{h,R}^2 + \delta m_{h,R}^2 \\ g &= Z_g g_R = g + \delta g \end{aligned} \quad (2.16)$$

Additionally, we need to introduce renormalization coefficients for the bare fields. Expanding them at NLO yields

$$W^\pm = Z_+^{1/2} W_R^\pm = \left(1 + \frac{1}{2} \delta Z_+\right) W_R^\pm, \quad W = Z_W^{1/2} W_R = \left(1 + \frac{1}{2} \delta Z_W\right) W_R \quad (2.17)$$

Inserting these expressions into the full Lagrangian would already cancel all UV-divergences of the S-matrix elements and the Green's functions with only physical external particles [21]. For a full renormalization it is necessary to further introduce renormalization factors of the unphysical sector related to the would-be Goldstone bosons and ghost fields

$$\begin{aligned} \chi &= Z_\chi^{1/2} \chi_R = \left(1 + \frac{1}{2} \delta Z_\chi\right) \chi_R, \quad \phi^\pm = Z_\phi^{1/2} \phi_R^\pm = \left(1 + \frac{1}{2} \delta Z_\phi\right) \phi_R^\pm, \\ u^\pm &= \tilde{Z}_\pm u_R^\pm = (1 + \delta \tilde{Z}_\pm) u_R^\pm, \quad u^W = \tilde{Z}_W u_R^W = (1 + \tilde{Z}_W) u_R^W, \\ \bar{u}^W &= \bar{u}_R^W, \quad \bar{u}^\pm = \bar{u}_R^\pm \end{aligned} \quad (2.18)$$

At NLO, the gauge-parameters do not need to be renormalized and the would-be Goldstone bosons decouple from the scalar gauge bosons. Inserting these transformations into the bare Lagrangian (2.15) allows us to perform the split

$$\mathcal{L}_W^{\text{Full}}(\Phi_i, g_i) = \mathcal{L}_W^{\text{Full}}(\Phi_{i,R}, g_{i,R}) + \mathcal{L}^{\text{CT}}(\Phi_{i,R}, g_{i,R}, \delta Z_i) \quad (2.19)$$

into the full Lagrangian in terms of renormalized fields $\Phi_{i,R}$, the parameters $g_{i,R} = \{g_R, m_R^2, m_{h,R}^2\}$ and the counterterm Lagrangian \mathcal{L}^{CT} containing all terms proportional to δZ_i .

2.3. FMS formalism

2.3.1. Gauge-invariance and physical leptons

There is a problem with the picture given before: The apparent breaking of the electroweak gauge symmetry is forbidden due to Elitzur's theorem [23]. It states that only operators with non-vanishing expectation values are invariant under local gauge transformations. However, there are gauge-fixing choices where the vev v of the Higgs field vanishes, and the usual modification via Wilson loops (as can be done in QED) is not sufficient to amend gauge invariance for the weak sector. This is directly linked to the Gribov-Singer ambiguity of non-abelian gauge groups such as $SU(2)_W$ [24]. In reality, the electroweak symmetry group only distinguishes different gauge charges, similar to color charges in QCD. A solution has been given by Fröhlich, Morchio and Strocchi via the FMS formalism, which can be separated into two parts [3, 7]. For the SM, the modification of leptonic external states is relatively simple. It turns out that the scalar Higgs sector has a global $SU(2)_C$ symmetry for vanishing Yukawa couplings. It acts on the scalar doublet X in (2.2) as a right-side multiplication with a matrix d in the fundamental representation of $SU(2)_C$. This custodial symmetry group is the same as the gauged electroweak symmetry group $SU(2)_W$. Consequently, we can construct gauge-invariant bound states by multiplying the left-handed leptonic doublet with the Higgs doublet

$$\psi_{L,f}^1 \rightarrow \Psi_{L,f}^1 = X^\dagger \psi_{L,f}^1 = \begin{pmatrix} \phi_2 \nu_{eL} - \phi_1 e_L^- \\ \phi_1^* \nu_{eL} + \phi_2^* e_L^- \end{pmatrix} \quad (2.20)$$

$$\psi_{L,f}^2 \rightarrow \Psi_{L,f}^2 = X^\dagger \psi_{L,f}^2 = \begin{pmatrix} \phi_2 \nu_{\mu L} - \phi_1 \mu_L^- \\ \phi_1^* \nu_{\mu L} + \phi_2^* \mu_L^- \end{pmatrix} \quad (2.21)$$

These compound leptons can be identified with physical particles. They are now singlets with respect to the (electro-)weak gauge group, and instead obtain a global $SU(2)_C$ charge from the scalar sector that differentiates the two components f of Ψ_L^1 and Ψ_L^2 . Right-handed leptons are not charged under $SU(2)_W$, so they can remain unchanged. Furthermore, all other elementary particles that interact weakly need to be formulated in terms of compound states. Their construction for the rest of the fermionic sector and the bosonic sector in the SM follows along similar lines [25]. Importantly, it is a specific feature of the SM that the global symmetry of the scalar sector aligns with the non-abelian gauge group of the vector bosons. This correspondence is potentially lost in beyond the Standard Model theories [26].

2.3.2. FMS expansion

These bound states can be related to perturbation theory via a FMS expansion. This is the second part of the FMS formalism that requires a gauge fixing where the scalar field obtains a non-vanishing vev that minimizes the scalar potential in (2.1). One can then apply the splitting of the scalar field into the vev v and fluctuation fields η to analyze the resulting objects in terms of elementary ones. The leading term of this expansion in powers of v is the usual expression we encounter in perturbation theory. For our model, the expanded scalar doublet X has the form

$$X = \frac{v}{\sqrt{2}}\mathbb{1} + \eta = \begin{pmatrix} \frac{1}{\sqrt{2}}(v + h - i\chi) & \phi^+ \\ -\phi^- & \frac{1}{\sqrt{2}}(v + h + i\chi) \end{pmatrix} \quad (2.22)$$

with the real scalar Higgs field h and the would-be Goldstone bosons χ and ϕ^\pm that we already encountered in (2.7). The compound leptons in (2.20) yield after expansion

$$\Psi_L^1 = \begin{pmatrix} N_{eL} \\ E_L^- \end{pmatrix} = \frac{1}{\sqrt{2}} \begin{pmatrix} v\nu_{eL} + (h + i\chi)\nu_{eL} - \sqrt{2}\phi^+ e_L^- \\ \nu_{eL}^- + (h - i\chi)e_L^- + \sqrt{2}\phi^- \nu_{eL} \end{pmatrix} \quad (2.23)$$

where we introduce capital letters to differentiate the elementary from the bound-state leptons. The usual elementary electron e_L^- and electron neutrino ν_{eL} are retained (up to a prefactor) if we neglect the scalar fluctuation fields

$$\begin{pmatrix} N_{eL} \\ E_L^- \end{pmatrix} = \frac{v}{\sqrt{2}} \begin{pmatrix} \nu_{eL} \\ e_L^- \end{pmatrix} + \mathcal{O}(v^0) \quad (2.24)$$

Notably, the charged would-be Goldstone bosons mix the elementary leptons within each generation. The situation is the same for the corresponding anti-particles

$$\bar{\Psi}_L^1 = \begin{pmatrix} \bar{N}_{eL} \\ E_L^+ \end{pmatrix}^T = \frac{1}{\sqrt{2}} \begin{pmatrix} v\bar{\nu}_{eL} + (h - i\chi)\bar{\nu}_{eL} - \sqrt{2}\phi^- e_L^+ \\ \nu_{eL}^+ + (h + i\chi)e_L^+ + \sqrt{2}\phi^+ \bar{\nu}_{eL} \end{pmatrix}^T \quad (2.25)$$

and the second generation of leptons. Let us first take the bound-state propagator for the electron as a simple example of this expansion. By inserting the expanded bound-state leptons of (2.23) and (2.25), its gauge-invariant form in terms of elementary fields reads

$$\begin{aligned}
 \langle 0 | \Psi_{L,2}^1(x_1) \bar{\Psi}_{L,2}^1(x_2) | 0 \rangle &\equiv \langle E_L^- E_L^+ \rangle \\
 &= \frac{v^2}{2} \langle e_L^- e_L^+ \rangle + \frac{v}{2} \left(\sqrt{2} \langle e_L^- [\phi^+ \bar{\nu}_{eL}] \rangle + \sqrt{2} \langle [\phi^- \bar{\nu}_{eL}] e_L^+ \rangle + \langle [he_L^-] e_L^+ \rangle \right. \\
 &\quad \left. + \langle e_L^- [he_L^+] \rangle - i \langle e_L^- [\chi e_L^+] \rangle - i \langle [\chi e_L^-] e_L^+ \rangle \right) \\
 &+ \frac{1}{2} \left(\langle [he_L^-] [he_L^+] \rangle - i \langle [\chi e_L^-] [he_L^+] \rangle \right. \\
 &\quad \left. + i \langle [he_L^-] [\chi e_L^+] \rangle + \langle [\chi e_L^-] [\chi e_L^+] \rangle \right) \\
 &+ \frac{1}{\sqrt{2}} \left(\langle [he_L^-] [\phi^+ \bar{\nu}_{eL}] \rangle + \langle [\phi^- \nu_{eL}] [he_L^+] \rangle \right. \\
 &\quad \left. - i \langle [\chi e_L^-] [\phi^+ \bar{\nu}_{eL}] \rangle + i \langle [\phi^- \nu_{eL}] [\chi e_L^+] \rangle \right) + \langle [\phi^- \nu_{eL}] [\phi^+ \bar{\nu}_{eL}] \rangle \quad (2.26)
 \end{aligned}$$

where $|0\rangle$ is the vacuum of the free theory and square brackets denote the compound fields at the same spacetime point. The original elementary propagator appears as the leading term in v^2 , with fifteen subleading n-point functions (six three-point functions with prefactor v and nine four-point functions without v). Only the full sum of all sixteen terms is gauge-invariant.

In conclusion, expanding the bound-state particles into elementary ones by splitting the Higgs doublet around the vev v via a FMS expansion leads to additional terms in n-point functions, the starting point for any perturbative scattering calculation in quantum field theory. A general study of this expansion that also sheds light on the group structure and different breaking patterns can be found in [26].

2.4. Scattering Theory

2.4.1. Differential cross section

The physical quantity we want to compare to experiment in the future is the (differential) cross section $d\sigma$ of our leptonic scattering in the center-of-mass (CM) frame. Derived from the cross sectional area, its definition in a quantum theory is

$$d\sigma = \frac{1}{tF} dP \quad (2.27)$$

where $dP = \frac{N}{N_i}$ is the differential probability of scattered particles N over incident particles N_i , t represent the collision time and F the incoming flux of particles. In our CM frame, the flux F is just the difference between velocities of the two incoming particles normalized by the total volume $|\vec{v}_1 - \vec{v}_2|/V$

$$d\sigma = \frac{V}{t} \frac{1}{|\vec{v}_1 - \vec{v}_2|} dP \quad (2.28)$$

For theoretical calculations, we assume that all interactions happen in a finite time interval and the asymptotic states at $t = \pm\infty$ are free of interactions. We can then take the limits $V \rightarrow \infty$, $t \rightarrow \infty$ for the cross section in (2.28). The probability for our initial state $|i\rangle$ to evolve into a final state $|f\rangle$ is calculated via amplitudes. In quantum field theory, they are obtained (up to normalization) from the scattering or S matrix and the phase-space region of outgoing momenta $d\Pi$

$$dP = |\langle f|S|i\rangle|^2 d\Pi \quad (2.29)$$

For our perturbative calculation, we can split the S-matrix into a free and an interaction part

$$S = \mathbb{1} + i\mathbb{T} \quad (2.30)$$

Subtracting the one, factoring out a factor for momentum conservation and sandwiching (2.30) between initial and final states, we obtain the invariant matrix element \mathcal{M}_{fi}

$$\langle f|S - \mathbb{1}|i\rangle = i(2\pi)^4 \delta^{(4)}\left(\sum_{in} p_i - \sum_{out} p_j\right) \langle f|\mathcal{M}|i\rangle, \quad \langle f|\mathcal{M}|i\rangle \equiv \mathcal{M}_{fi} \quad (2.31)$$

for physical momenta. After some algebra, the differential cross section can be expressed in terms of the solid angle $d\Omega = \sin(\theta)d\theta d\phi$ and the Heaviside function H as

$$\left(\frac{d\sigma}{d\Omega}\right)_{CM} = \frac{1}{64\pi^2 E_{CM}^2} \frac{|\vec{p}_f|}{|\vec{p}_i|} |\mathcal{M}|^2 H(E_{CM} - m_3 - m_4) \quad (2.32)$$

where we drop the indices of the matrix elements. Our external states are all massless, so this expression further reduces to

2. Physical leptons in the weak sector of the SM

$$\left(\frac{d\sigma}{d\Omega}\right)_{CM} = \frac{1}{64\pi^2 E_{CM}^2} |\mathcal{M}|^2 \quad (2.33)$$

We use equation (2.33) for the tree-level calculation of our scattering process in section (5.1).

2.4.2. Invariant matrix elements

The matrix elements $\langle f|S|i\rangle$ themselves are related to Green's functions of quantum fields via the LSZ formula [27]. These Green's functions are time-ordered products of field operators sandwiched between the interacting vacuum states $|\Omega\rangle$. For the leptonic process with $\langle f| = \langle M_L^- M_L^+ |$ and $|i\rangle = |E_L^- E_L^+\rangle$ the LSZ relation reads

$$\langle M_L^- M_L^+ | S | E_L^- E_L^+ \rangle \sim \langle \Omega | T \left(\Psi_{L,2}^2(x_3) \bar{\Psi}_{L,2}^2(x_4) \Psi_{L,2}^1(x_1) \bar{\Psi}_{L,2}^1(x_2) \right) | \Omega \rangle \quad (2.34)$$

where in the right-hand expression we have the time ordering of fields $T(\dots)$ and the ground-state of the interacting theory $|\Omega\rangle$. The matrix elements of the interacting fields are given by

$$\begin{aligned} & \langle \Omega | T \left(\Psi_{L,2}^2(x_3) \bar{\Psi}_{L,2}^2(x_4) \Psi_{L,2}^1(x_1) \bar{\Psi}_{L,2}^1(x_2) \right) | \Omega \rangle \\ &= \frac{\langle 0 | T \left(M_L^-(x_3) M_L^+(x_4) E_L^-(x_1) M_L^+(x_2) e^{i \int d^4x \mathcal{L}_{int}} \right) | 0 \rangle}{\langle 0 | T \left(e^{i \int d^4x \mathcal{L}_{int}} \right) | 0 \rangle} \end{aligned} \quad (2.35)$$

with the interaction part of the Lagrangian $\mathcal{L}_{int} = \mathcal{L} - \mathcal{L}_{free}$ that is free of kinetic terms. Doing a perturbative expansion in our small coupling parameter g yields the invariant matrix elements at a desired order in the weak coupling

$$\begin{aligned} & \langle 0 | T \left(M_L^-(x_3) M_L^+(x_4) E_L^-(x_1) E_L^+(x_2) e^{i \int d^4x \mathcal{L}_{int}} \right) | 0 \rangle \\ &= \langle 0 | T \left(M_L^-(x_3) M_L^+(x_4) E_L^-(x_1) E_L^+(x_2) \right) | 0 \rangle \\ &+ \sum_k ig \int d^4x \langle 0 | T \left(M_L^-(x_3) M_L^+(x_4) E_L^-(x_1) E_L^+(x_2) \Phi_k(x) \right) | 0 \rangle + \mathcal{O}(g^2) \end{aligned} \quad (2.36)$$

with $\Phi_k(x)$ representing field operators from our Lagrangian density \mathcal{L}_{int} . The calculations of our invariant matrix elements \mathcal{M} can be represented visually through Feynman diagrams. These serve as a pictorial representation of the calculations within (2.36), where each diagram consists of lines and vertices that correspond to algebraic expressions we can translate via Feynman rules.

These diagrams are a standard tool for the perturbative calculation of invariant matrix elements [5]. For example, the tree-level Feynman diagram arising in the lowest-order of g for the four-point function $\langle e_L^- e_L^+ \mu_L^- \mu_L^+ \rangle$ is given in figure (2.1). It features two interactions with an overall power of g^2 from the expansion (2.36).

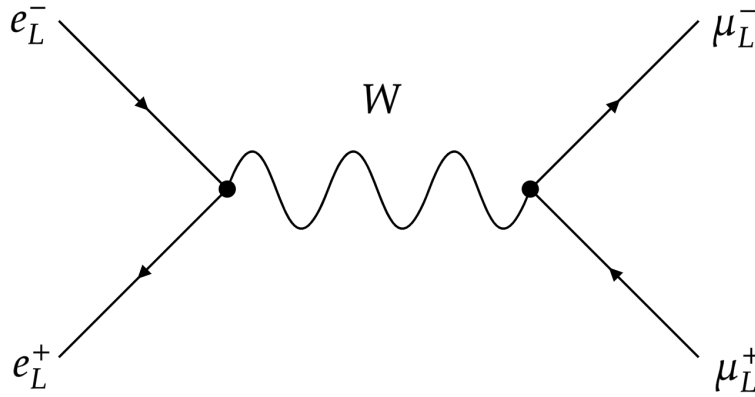


Figure 2.1.: Tree-level Feynman diagram for our process of order g^2

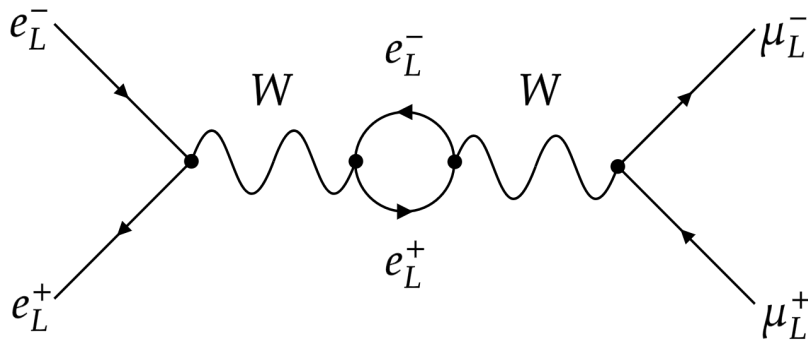


Figure 2.2.: NLO Feynman diagram with a fermionic loop of order g^4

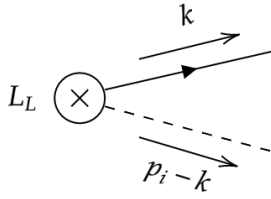
Regular loop diagrams arise from higher order terms in the coupling parameter such as the fermionic bubble diagram in figure (2.2), and their algebraic expressions are the main result in section (5). A list of all relevant Feynman rules of our theory, including all other interaction vertices, propagators and external lines, is given in appendix (C).

2.4.3. Bound states

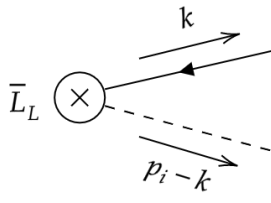
The approach via the LSZ formalism to calculate invariant matrix elements \mathcal{M} works for bound states as well, but we need to introduce Bether-Salpeter (BS) amplitudes ρ_L [5]. These are the amplitudes of one-particle states composed of multiple elementary particles. For example, the BS-amplitude for the elementary electron e_L^- with momentum p_{11} and the real scalar Higgs field h with momentum p_{12} reads

$$\rho_L(p_{11}, p_{12})\delta(p_{11} + p_{12} - p_1) = \frac{1}{(2\pi)^d} \int d^d x_1 \int d^d x_2 \langle 0 | T \left(h(x_1) e_L^-(x_2) \right) | M_e, p_1 \rangle e^{i(p_{11}x_1 + p_{12}x_2)} \quad (2.37)$$

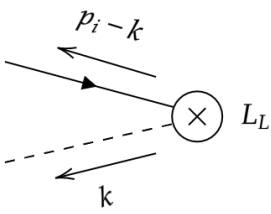
with the bound state carrying the momentum p_1 in the end. We approximate the amplitude by the elementary spinors of the leptons. Why this approximation is sufficient at NLO is related to the lepton mass of the elementary particles being equal to the bound state particle ($M_e = m_e$), and the details will be explained in a future work by Maas, Plätzer and Sondenheimer. In terms of Feynman rules, the insertion of external bound-state leptons corresponds to an integration over the relative momenta with respect to the scalar and fermion propagators of the elementary constituents. This is similar to a regular loop integration of internal propagators, minus the dependence of loop momenta that can arise in interaction vertices as seen in figure (2.3) and appendix (C). The loop integral is regularized in dimensional regularization (DR) as explained in section (3.2), and we include the external wavefunction renormalization K_i for the state with momentum p_i to ensure that the final invariant matrix elements stay dimensionless.



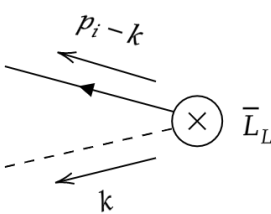
$$= -\frac{K_i \mu^{4-d}}{(2\pi)^d} \int d^d k \frac{\gamma^\alpha k_\alpha}{k^2 [(p-k)^2 - m_S^2]} |p], \quad S = h, \chi, \phi^\pm$$



$$= -\langle p| \frac{K_i \mu^{4-d}}{(2\pi)^d} \int d^d k \frac{\gamma^\alpha k_\alpha}{k^2 [(p-k)^2 - m_S^2]}, \quad S = h, \chi, \phi^\pm$$



$$= -\langle p| \frac{K_i \mu^{4-d}}{(2\pi)^d} \int d^d k \frac{\gamma^\alpha k_\alpha}{k^2 [(p-k)^2 - m_S^2]}, \quad S = h, \chi, \phi^\pm$$



$$= -\frac{K_i \mu^{4-d}}{(2\pi)^d} \int d^d k \frac{\gamma^\alpha k_\alpha}{k^2 [(p-k)^2 - m_S^2]} |p], \quad S = h, \chi, \phi^\pm$$

Figure 2.3.: Operator insertions of the leptons $L = E, M$ as a Feynman rule, approximated by an elementary spinor attached to a lepton and scalar propagator with an integration of the relative momenta of constituent particles.

2.4.4. FMS expansion of our leptonic scattering

Our calculation focuses on the bound-state lepton collision of a left-handed electron-positron pair scattering to a left-handed muon-antimuon pair

$$E_L^- E_L^+ \rightarrow M_L^- M_L^+ \quad (2.38)$$

This potentially deviates the most from its elementary counterpart since all four leptons are now composite states with additional Higgs fields. All other chiral combinations vanish in our model at NLO due to the neglect of Yukawa interactions and photons that would allow for a coupling of right-handed elementary leptons and quarks. As a first step, we apply the FMS expansion and relate the four-point function of the process (2.38) to n-point functions in terms of elementary particles. We abbreviate the Green's functions by skipping the explicit spacetime dependence and again group particles at the same spacetime point via square brackets. Inserting the expansion of our compound leptons in equations (2.23) and (2.25) leads to

$$\begin{aligned} & \langle \Omega | T \left(\Psi_{L,2}^1(x_1) \bar{\Psi}_{L,2}^1(x_2) \Psi_{L,2}^2(y_1) \bar{\Psi}_{L,2}^2(y_2) \right) | \Omega \rangle \\ & \equiv \langle E_L^- E_L^+ M_L^- M_L^+ \rangle \\ & = \frac{v^4}{4} \langle e_L^- e_L^+ \mu_L^- \mu_L^+ \rangle \\ & + \frac{v^3}{4} \left(\langle [he_L^-] e_L^+ \mu_L^- \mu_L^+ \rangle + \langle e_L^- [he_L^+] \mu_L^- \mu_L^+ \rangle \right. \\ & \left. + \langle e_L^- e_L^+ [h\mu_L^-] \mu_L^+ \rangle + \langle e_L^- e_L^+ \mu_L^- [h\mu_L^+] \rangle + \dots \right) \\ & + \frac{v^2}{4} \left(\langle [he_L^-] [he_L^+] \mu_L^- \mu_L^+ \rangle + \dots \right) + \frac{v}{4} \left(\langle [he_L^-] [he_L^+] [h\mu_L^-] \mu_L^+ \rangle + \dots \right) \\ & + \langle [he_L^-] [he_L^+] [h\mu_L^-] [h\mu_L^+] \rangle + \dots \end{aligned} \quad (2.39)$$

The FMS expansion results in 256 different n-point functions, consisting of the regular four-point function, twelve five-point functions, 54 six-point functions, 108 seven-point functions and 81 eight-point functions. All of these new contributions can in principle contribute to the perturbative treatment of the collision, and only the sum of all terms generates a gauge-invariant result. An illustration of the different groups of n-point functions based on the number of scalar fields is given in figure (2.4)

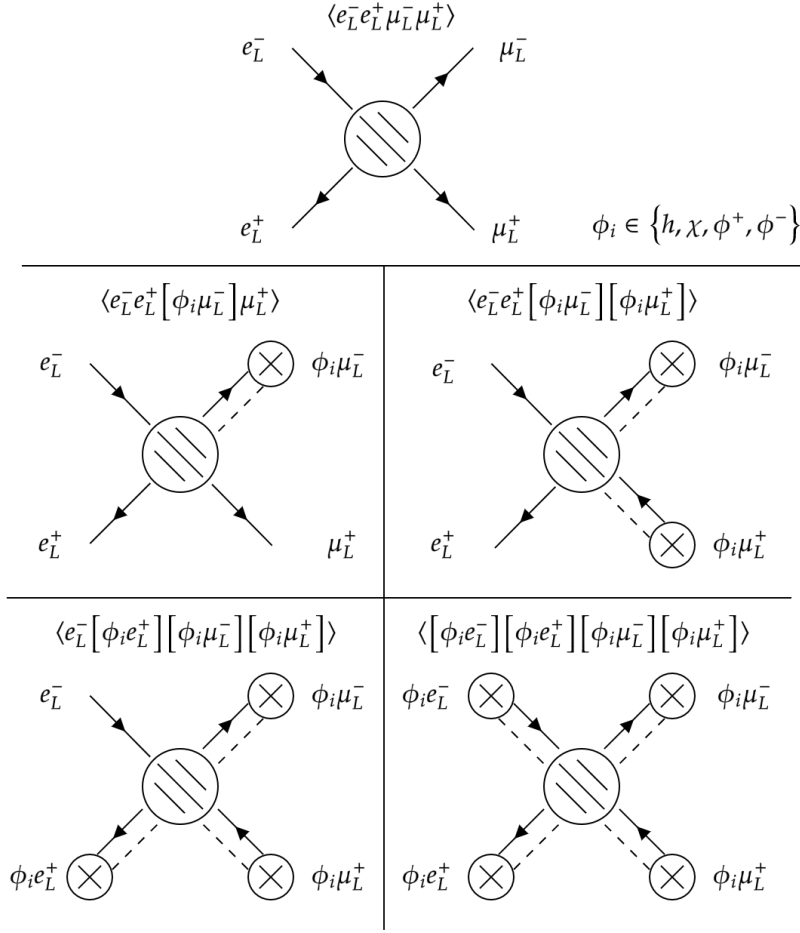


Figure 2.4.: All types of n-point functions occurring after the FMS expansion. Each insertion of a bound state is marked by a cross and translates to an integration over the relative momentum of one of its constituents. One representation for each type of n-point function was chosen.

The leading term is the usual four-point function, with higher-order terms being suppressed by powers of the vev v . This kinematic suppression could be a simple explanation of why the four-point function has been sufficient for predictions of scattering experiments so far. Nevertheless, understanding how the higher order terms affect the differential cross section and how these terms scale especially at high-energy collisions (where no comparison of theory and experiment can be done yet) necessitates a calculation of matrix elements for the scattering process with bound states. The study of these new n-point functions allows us to either verify the validity of the usual approach, namely the isolated treatment of the first term in (2.39), or we obtain an experimentally significant discrepancy for the differential cross section, and future studies of the FMS formalism could become crucial.

2.4.5. Matrix elements and cross sections in APT

We split the invariant matrix elements into tree-level expressions \mathcal{M}_{LO} at order g^2 , regular NLO expressions $\mathcal{M}_{NLO,R}$ at order g^4 and new contributions $\mathcal{M}_{NLO,FMS}$ due to the FMS formalism. We factor out the dependence of the expansion parameter g and obtain for a description at NLO

$$\mathcal{M} = g^2 \mathcal{M}_{LO} + g^4 \mathcal{M}_{NLO,R} + g^n \mathcal{M}_{NLO,FMS}, \quad n \leq 4 \quad (2.40)$$

where the new invariant matrix elements could generally be of a lower order in g compared to the usual loop diagrams. Let us see how the new term in (2.40) changes the expression for differential cross sections. If we plug (2.40) into equation (2.33) and only keep terms up to order g^6 we obtain

$$\begin{aligned} \left(\frac{d\sigma}{d\Omega} \right)_{FMS} &\equiv d\sigma_{FMS} = \frac{1}{64\pi^2 s} \left(g^4 |\mathcal{M}_{LO}|^2 + g^{2n} |\mathcal{M}_{NLO,FMS}|^2 \right. \\ &+ 2g^6 \text{Re}(\mathcal{M}_{LO}^* \mathcal{M}_{NLO,R}) + 2g^{2+n} \text{Re}(\mathcal{M}_{LO}^* \mathcal{M}_{NLO,FMS}) \\ &\left. + 2g^{4+n} \text{Re}(\mathcal{M}_{NLO,R}^* \mathcal{M}_{NLO,FMS}) \right) \end{aligned} \quad (2.41)$$

Higher orders in g require the inclusion of NNLO contributions to the matrix elements since the interference term $2g^8 \text{Re}(\mathcal{M}_{LO}^* \mathcal{M}_{NNLO})$ would contribute as well. Now, if we compare this with the differential cross section at NLO in regular perturbation theory

$$\left(\frac{d\sigma}{d\Omega} \right)_R \equiv d\sigma_R = \frac{1}{64\pi^2 s} \left(g^4 |\mathcal{M}_{LO}|^2 + 2g^6 \text{Re}(\mathcal{M}_{LO}^* \mathcal{M}_{NLO,R}) \right) \quad (2.42)$$

we can quantify the deviation of the usual perturbative calculation compared to our augmented perturbation theory (APT)

$$\begin{aligned} A^{NLO}(s, t, g, v, \lambda) &\equiv \frac{d\sigma_{FMS}}{d\sigma_R}(s, t, g, v, \lambda) \\ &= 1 + \frac{2g^{2+n} \text{Re}(\mathcal{M}_{LO}^* \mathcal{M}_{NLO,FMS})}{g^4 |\mathcal{M}_{LO}|^2 + 2g^6 \text{Re}(\mathcal{M}_{LO}^* \mathcal{M}_{NLO,R})} \\ &\quad + \frac{2g^{4+n} \text{Re}(\mathcal{M}_{NLO,R}^* \mathcal{M}_{NLO,FMS}) + g^{2n} |\mathcal{M}_{FMS}|^2}{g^4 |\mathcal{M}_{LO}|^2 + 2g^6 \text{Re}(\mathcal{M}_{LO}^* \mathcal{M}_{NLO,R})} \end{aligned} \quad (2.43)$$

This quantity can depend on the external momenta via two independent Mandelstam variables s and t as defined in (A.3), the electroweak coupling g , the Higgs self-interaction λ and the vev v . One could fix the values for v , λ and g to the values of the SM and investigate the deviations due to a full treatment via the FMS formalism in the weak sector. Two exemplary curves of A^{NLO} with fixed t are shown in figure (2.5).

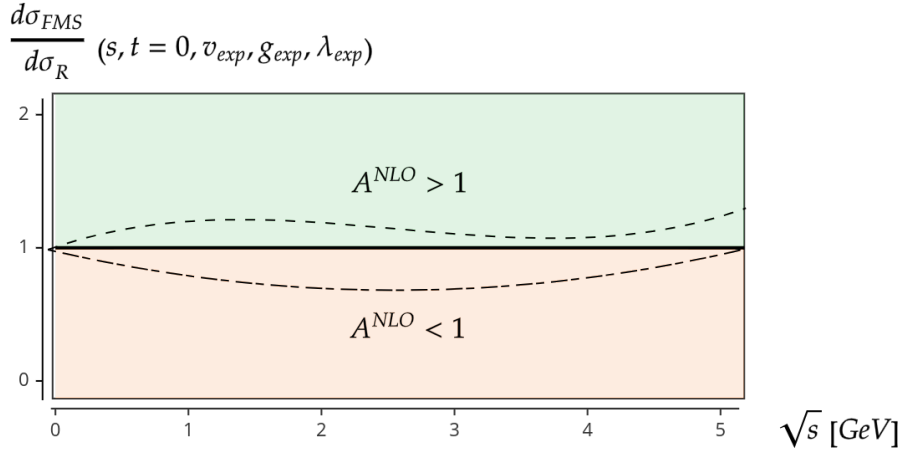


Figure 2.5.: Two suggestive plots that highlight different behaviour for the deviation of $d\sigma$ due to a gauge-invariant treatment, here for fixed t and SM values v_{exp} , g_{exp} and λ_{exp}

To sum up, applying perturbation theory in a leptonic scattering with the requirement of gauge-invariance for our external states yields additional higher-order Greens's functions with additional Higgs content that affects invariant matrix elements and potentially the differential cross section at NLO (2.43).

3. Technical tools

While the prior chapter shed light on the improved phenomenology of the weak sector of the SM, we now take a look at the main technical ingredients in order to calculate the invariant matrix elements \mathcal{M} outlined in (2.43). To start off, section (3.1) addresses the main aspects of the spinor-helicity (SH) formalism that introduces chiral Weyl spinors as a basis for our leptons [28]. This section concludes with a full list of simplification rules that this formalism offers in our Mathematica package 'spinorhelicity.m' [29] in (3.1.3). The calculation of loop contributions requires the reduction of tensor integral and the regularization of divergences. Section (3.2) addresses these topics, where we highlight the rules employed by our second Mathematica package 'oneloop.m' [30].

3.1. Spinor-helicity (SH) formalism

3.1.1. Introduction

Since we are only concerned with massless Weyl spinors, the usage of a chirality basis is a convenient choice for our calculations. This means we trade the usual spinors with four components for two-dimensional Weyl spinors

$$\begin{aligned} u_L(p_i) &= v_R(p_i) = \begin{pmatrix} |i] \\ 0 \end{pmatrix} = \begin{pmatrix} \tilde{\lambda}_i^{\dot{\alpha}} \\ 0 \end{pmatrix} \\ \bar{u}_L(p_i) &= \bar{v}_R(p_i) = ([i|, 0) = ((\tilde{\lambda}_i)_{\dot{\alpha}}, 0) \\ u_R(p_i) &= v_L(p_i) = \begin{pmatrix} 0 \\ |i\rangle \end{pmatrix} = \begin{pmatrix} 0 \\ (\lambda_i)_\alpha \end{pmatrix} \\ \bar{u}_R(p_i) &= \bar{v}_L(p_i) = (0, \langle i|) = (0, \lambda_i^\alpha) \end{aligned} \tag{3.1}$$

$$\tag{3.2}$$

where $u_R(p_i) = \frac{1}{2}(\mathbb{1} + \gamma_5)u(p_i)$ is the right-handed Dirac spinor and $|i\rangle$ is the corresponding Weyl spinor, and $u_L(p_i) = \frac{1}{2}(\mathbb{1} - \gamma_5)u(p_i)$ is the left-handed Dirac spinor with the corresponding Weyl spinor $|i]$. The spinor indices α and $\dot{\alpha}$ indicate the two different spinor representations of the Lorentz group. Throughout the calculations, we implore the ket-notation for Weyl spinors and drop these indices in the final expressions of our calculations. Notably, for massless momenta the negative-energy solutions are equal to positive-energy solutions with flipped chirality. Both Dirac and Weyl spinors naturally fulfill

the massless Dirac equation

$$\begin{aligned} \not{p}_i u_R(p_i) = p_i^\mu \sigma_\mu |i\rangle = 0, \not{p}_i u_L(p_i) = p_i^\mu \bar{\sigma}_\mu |i] = 0 \\ \bar{u}_L(p_i) \not{p}_i = [i| p_i^\mu \sigma_\mu = 0, \bar{u}_R(p_i) \not{p}_i = \langle i| p_i^\mu \sigma_\mu = 0 \end{aligned} \quad (3.3)$$

Lorentz-invariant quantities can be constructed via the contraction of Weyl spinors with the antisymmetric tensors $\epsilon^{\alpha\beta}$ and $\epsilon^{\dot{\alpha}\dot{\beta}}$

$$\epsilon^{\alpha\beta} = -\epsilon_{\alpha\beta} = \epsilon^{\dot{\alpha}\dot{\beta}} = -\epsilon_{\dot{\alpha}\dot{\beta}} = \begin{pmatrix} 0 & 1 \\ -1 & 0 \end{pmatrix} \quad (3.4)$$

Similar to the metric tensor $g^{\alpha\beta}$ for four-momenta, they act by raising and lowering spinor indices, with the caveat that the index ordering is important as $\epsilon^{\alpha\beta}$ is antisymmetric. Spinor products are defined as

$$\langle ij \rangle \equiv \epsilon^{\alpha\beta} (\lambda_i)_\alpha (\lambda_j)_\beta = \bar{u}_R(p_i) u_R(p_j) \quad (3.5)$$

$$[ij] \equiv \epsilon_{\dot{\alpha}\dot{\beta}} \tilde{\lambda}_i^{\dot{\alpha}} \tilde{\lambda}_j^{\dot{\beta}} = \bar{u}_L(p_i) u_L(p_j) \quad (3.6)$$

Due to λ_i and λ_j being commuting numbers, the products of Weyl spinors are antisymmetric

$$\langle ij \rangle = -\langle ji \rangle, [ij] = -[ji] \quad (3.7)$$

and inner products of identical momenta disappear

$$\langle ii \rangle = [ii] = 0 \quad (3.8)$$

while products of opposite chirality cancel in general

$$\langle ij \rangle = [ij] = 0 \quad (3.9)$$

The Fierz identity allows us to simplify spinor chains reads

$$(\sigma^\mu)_{\alpha\dot{\alpha}} (\sigma_\mu)_{\dot{\beta}\beta} = 2\delta_\alpha^\beta \delta_{\dot{\alpha}}^{\dot{\beta}} \quad (3.10)$$

Slashed momenta decompose into an outer products of Weyl spinors

$$\not{p}_i = \begin{pmatrix} 0 & |i\rangle\langle i| \\ |i\rangle[i| & 0 \end{pmatrix} \quad (3.11)$$

as massless momenta can be factorized into an outer product of our Weyl spinors $(\lambda_i)^\alpha$ and $(\tilde{\lambda}_i)^{\dot{\alpha}}$

$$p_i^{\alpha\dot{\alpha}} = (\lambda_i)^\alpha (\tilde{\lambda}_i)^{\dot{\alpha}} \quad (3.12)$$

For complex massless momenta, we have three complex degrees of freedom, since we have two degrees of freedom per spinor and a scale symmetry under the transformation

$$\lambda^\alpha \rightarrow z\lambda^\alpha, \tilde{\lambda}^{\dot{\alpha}} \rightarrow z^{-1}\tilde{\lambda}^{\dot{\alpha}} \quad (3.13)$$

3. Technical tools

keeps the product of Weyl spinors unchanged. For real momenta the scaling turns into a simple phase

$$\lambda^\alpha = (\tilde{\lambda}^{\dot{\alpha}})^\dagger \rightarrow z = e^{i\phi}, \phi \in \mathbb{R} \quad (3.14)$$

and complex conjugation of spinor products reduces to a chirality flip

$$[ij] = \langle ij \rangle^* \quad (3.15)$$

This comes in handy when we calculate complex conjugates of matrix elements for the differential cross section as we can simplify spinor products in terms of Mandelstam variables

$$2p_i \cdot p_j = \frac{1}{2}(\tilde{\lambda}_i)_{\dot{\alpha}}(\sigma^\mu)^{\dot{\alpha}\alpha}(\lambda_i)_\alpha(\tilde{\lambda}_i)_{\dot{\beta}}(\sigma^\mu)^{\dot{\beta}\beta}(\lambda_i)_\beta = \langle ij \rangle [ji] \quad (3.16)$$

The spinor products themselves are roots of the Mandelstam variables

$$\langle ij \rangle = \sqrt{2p_i \cdot p_j} e^{i\phi_{ij}}, [ij] = \sqrt{2p_i \cdot p_j} e^{-i\phi_{ij}} \quad (3.17)$$

where $2p_i \cdot p_j = s, t, u$ as seen in (A.3). Energy conservation for the scattering process with four external legs implies $\sum_j^4 p_j^\mu = 0$ for incoming momenta. Translated to helicity spinors we have

$$\sum_{j=1}^4 (\lambda_j)_\alpha (\tilde{\lambda}_j)^{\dot{\alpha}} = |1\rangle[1| + |2\rangle[2| + \dots + |n\rangle[n| = 0 \quad (3.18)$$

Multiplying this with Weyl spinors from both sides gives us sixteen equations of the form

$$\sum_{j=1}^4 \langle ij \rangle [jk] = 0 \quad (3.19)$$

In our two-to-two scattering process, this allows us to rewrite Weyl products in terms of Mandelstam variables. Expressions such as

$$\langle 13 \rangle [32] \langle 24 \rangle \stackrel{(3.19)}{=} -\langle 14 \rangle [42] \langle 24 \rangle \stackrel{(3.16)}{=} -\langle 14 \rangle t \quad (3.20)$$

often appear in intermediate calculations of loop diagrams, especially when spinor chains with multiply gamma matrices appear.

3.1.2. Spinor chains

We define spinor n -chains as products of Weyl spinors being embedded into massless Dirac spinors, with n Dirac matrices in the Weyl basis as follows

$$[i|_D \gamma^{\alpha_1} \dots \gamma^{\alpha_n} |j\rangle_D = ([i|, 0) \begin{pmatrix} 0 & \sigma^{\alpha_1} \\ \bar{\sigma}^{\alpha_1} & 0 \end{pmatrix} \dots \begin{pmatrix} 0 & \sigma^{\alpha_n} \\ \bar{\sigma}^{\alpha_n} & 0 \end{pmatrix} \begin{pmatrix} 0 \\ |j\rangle \end{pmatrix} \quad (3.21)$$

This way, we can use Feynman rules in the usual Dirac picture and apply all of the simplifications for Weyl spinors presented in the previous section. The final reduced expressions of our calculations are then written in terms of simple spinor products, so we drop the index of the initial Dirac spinors to simplify the notation. In case of our massless loop diagrams, up to three Dirac matrices can appear between spinors that disappear depending on the helicity and number of matrices. Concretely, spinor chains of different helicities only survive with an uneven number of Dirac matrices

$$[i|\gamma^{\alpha_1} \dots \gamma^{\alpha_{2n}} |j\rangle = \langle i|\gamma^{\alpha_1} \dots \gamma^{\alpha_{2n}} |j\rangle = 0 \quad (3.22)$$

Spinor chains with the same helicity on both ends only remain for an even number of Dirac matrices

$$[i|\gamma^{\alpha_1} \dots \gamma^{\alpha_{2n+1}} |j\rangle = \langle i|\gamma^{\alpha_1} \dots \gamma^{\alpha_{2n+1}} |j\rangle = 0 \quad (3.23)$$

and all other spinor chains automatically evaluate to zero. Four-momenta can be reconstructed from spinor chains via

$$[i|\gamma^\mu |i\rangle \equiv (\tilde{\lambda}_i)_{\dot{\alpha}} (\sigma^\mu)^{\dot{\alpha}\alpha} (\lambda_i)_\alpha = 2q_i^\mu \quad (3.24)$$

and the Fierz identity of the Pauli matrices in (3.10) reads for spinor chains

$$\langle i|\gamma^\mu |j\rangle \langle k|\gamma_\mu |l\rangle = 2\langle ik\rangle [lj] \quad (3.25)$$

Sometimes it is helpful to reduce a n -chain with more than one Dirac matrix into an expression only containing one-chains before contracting it with an external momentum or metric tensor. This can be done by inserting a $\mathbb{1}$ of the form

$$\mathbb{1} = \frac{\not{p}_i \not{p}_j + \not{p}_j \not{p}_i}{2p_i p_j} \quad (3.26)$$

between two spinors. If we use (3.8), (3.11) and (3.16), one can reformulate it solely in terms of Weyl spinors

$$\begin{aligned} \mathbb{1} &= \frac{(|i\rangle\langle i| + |i\rangle[i|])(|j\rangle\langle j| + |j\rangle[j|])}{\langle ij\rangle[ji]} + \frac{(i \leftrightarrow j)}{\langle ij\rangle[ji]} \\ &= \frac{|i\rangle[j| - |j\rangle[i|]}{[ji]} + \frac{|i\rangle\langle j| - |j\rangle\langle i|}{\langle ji\rangle} \end{aligned} \quad (3.27)$$

With the help of (3.24), we can break down a two-chain

$$\langle i|\gamma^\mu\gamma^\nu|j\rangle = \langle i|\gamma^\mu\left(\frac{|i\rangle\langle j| - |j\rangle\langle i|}{[ji]}\right)\gamma^\nu|j\rangle = \frac{1}{[ji]}\left(4p_i^\mu p_j^\nu - \langle i|\gamma^\mu|j\rangle\langle j|\gamma^\nu|i\rangle\right) \quad (3.28)$$

Similar reductions can be achieved if we insert the $\mathbb{1}$ of (3.27) between every product of Dirac matrices in higher n-chains.

3.1.3. Simplification rules

The full list of simplification rules offered by our package 'spinorhelicity.m' is listed below

$$\begin{aligned} \langle ij\rangle &= -\langle ji\rangle, [ij] = -[ji], [ii] = \langle ii\rangle = \langle ij\rangle = [ij] = 0 \\ [ij]\langle ji\rangle &= s_{ij}, s_{ij} = s, t, u \\ \langle i|\gamma^\mu|j\rangle\langle k|\gamma_\mu|l\rangle &= 2\langle ik\rangle[lj] \\ \langle i|\gamma^{\alpha_1}\dots\gamma^{\alpha_k}\dots\gamma^{\alpha_n}|j\rangle g_{\alpha_k\beta} &= \langle i|\gamma^{\alpha_1}\dots\gamma_\beta\dots\gamma^{\alpha_n}|j\rangle \\ \langle i|\gamma^{\alpha_1}\dots\gamma^{\alpha_k}\dots\gamma^{\alpha_n}|j\rangle p_{i,\alpha_k} &= \langle i|\gamma^{\alpha_1}\dots\not{p}_i\dots\gamma^{\alpha_n}|j\rangle \\ [i|\gamma^{\alpha_1}\dots\gamma^{\alpha_{2n+1}}|j\rangle &= \langle i|\gamma^{\alpha_1}\dots\gamma^{\alpha_{2n+1}}|j\rangle = 0 \\ [i|\gamma^{\alpha_1}\dots\gamma^{\alpha_{2n+1}}|j\rangle &= \langle i|\gamma^{\alpha_1}\dots\gamma^{\alpha_{2n+1}}|j\rangle = 0 \\ \not{p}_i &= |i\rangle\langle i| + |i\rangle[i| \\ \mathbb{1} &= \frac{|i\rangle\langle j| - |j\rangle\langle i|}{[ji]} + \frac{|i\rangle\langle j| - |j\rangle\langle i|}{\langle ji\rangle} \end{aligned} \quad (3.29)$$

with the addition of contraction rules for Dirac matrices as seen in appendix (A.4). The contraction of momenta and metric tensors in (3.29) extends to all other chirality configurations, only one example is shown. Strictly speaking, the Fierz identity is only guaranteed to hold for momenta in four dimensions, and an extension to the d-dimensional case is not fully clear yet [31]. For simplicity, we claim that it holds equally in the case of loop calculations, and future studies will hopefully bring clarity. Furthermore, calculations within the SH formalism can be extended to massive spinors [32], so an investigation for massive fixed-spin collisions can be studied in a similar fashion.

3.2. Integral reduction

Here we give a short overview of the tensor reduction of our loop integrals at NLO. First, we treat the regularization and evaluation of scalar integrals in section (3.2.1). How these are extracted from the tensor structures of the matrix elements at loop-level is then covered in section (3.2.2). Finally, the main reduction formulas are listed in section (3.2.3).

3.2.1. Scalar Integrals

Dimensional regularization (DR) is employed for the treatment of UV- and IR-divergences that will appear in our scattering process. All divergent integrals are therefore evaluated in $d = 4 - 2\epsilon$ dimensions, and the divergences appear then as poles in terms of ϵ^{-1} (UV divergences) and ϵ^{-2} (IR divergences). The general expression of the appearing scalar integrals is

$$\begin{aligned}
 & S^d_{(v_1, v_2, \dots, v_n)}(0, q_1^2, q_2^2, \dots, q_{n-1}^2 | m_1^2, m_2^2, \dots, m_n^2) \\
 &= h(\epsilon) \int \frac{d^d k}{i\pi^{d/2}} \frac{1}{[k^2 - m_1^2]^{v_1} [(k + q_1)^2 - m_1^2]^{v_2} \dots [(k + q_{n-1})^2 - m_n^2]^{v_n}}
 \end{aligned} \tag{3.30}$$

where we suppress an imaginary part $+i\delta$ within each propagator for brevity. The prefactor $h(\epsilon)$ contains the rest of the π -factors that result from the loop integration and a dimensional factor of μ^{4-d} that ensures the right mass dimension for final expressions. In addition, an overall factor r_Γ is removed

$$h(\epsilon) \equiv \frac{\mu^{4-d}}{(4\pi)^{d/2} r_\Gamma} = \frac{\mu^{2\epsilon}}{(4\pi)^{2-\epsilon} r_\Gamma} \tag{3.31}$$

$$r_\Gamma \equiv \frac{\Gamma^2(1-\epsilon)\Gamma(1+\epsilon)}{\Gamma(1-2\epsilon)} = 1 - \epsilon\gamma_E + \epsilon^2 \left(\frac{\gamma_E^2}{2} - \frac{\pi^2}{12} \right) + \mathcal{O}(\epsilon^3) \tag{3.32}$$

which matches the convention of numerical software for future use in section (4). The terms q_i are linear combinations of the external momenta, and need to be chosen such that there is momentum conservation at each interaction vertex. We can shift away any external momentum possibly appearing in the first propagator, so one only needs $n - 1$ momentum variables. Furthermore, one can swap any two propagators within the integral

$$S^d(\dots, q_{i-1}^2, \dots, q_{j-1}^2, \dots | \dots, m_i^2, \dots, m_j^2, \dots) = S^d(\dots, q_{j-1}^2, \dots, q_{i-1}^2, \dots | \dots, m_j^2, \dots, m_i^2, \dots) \tag{3.33}$$

3. Technical tools

where $i, j = 1, \dots, n$. Depending on the number of propagators these integrals have special names for unit propagators that serve as a basis that we can reduce every loop expression to. Our choice of a sufficient basis of master integrals is

Tadpole integral $S^d(0|m^2)$:

$$h(\epsilon) \int \frac{d^d k}{i\pi^{d/2}} \frac{1}{[k^2 - m^2]} \quad (3.34)$$

Bubble integral $S^d(0, q^2|m_1^2, m_2^2)$:

$$h(\epsilon) \int \frac{d^d k}{i\pi^{d/2}} \frac{1}{[k^2 - m_1^2][(k+q)^2 - m_2^2]} \quad (3.35)$$

Triangle integral $S^d(0, q_1^2, q_2^2|m_1^2, m_2^2, m_3^2)$:

$$h(\epsilon) \int \frac{d^d k}{i\pi^{d/2}} \frac{1}{[k^2 - m_1^2][(k+q_1)^2 - m_2^2][(k+q_2)^2 - m_3^2]} \quad (3.36)$$

Box integral $S^d(0, q_1^2, q_2^2, q_3^2|m_1^2, m_2^2, m_3^2, m_4^2)$:

$$h(\epsilon) \int \frac{d^d k}{i\pi^{d/2}} \frac{1}{[k^2 - m_1^2][(k+q_1)^2 - m_2^2][(k+q_2)^2 - m_3^2][(k+q_3)^2 - m_4^2]} \quad (3.37)$$

To improve readability, we omit the subscripts in (3.30) whenever we encounter unit propagators. Graphically these integrals are depicted in (3.1). Due to power counting we can already infer that both tadpole and bubble integrals are UV-divergent, contrary to triangle and box integrals being UV-finite if all internal masses are non-zero. If the master integral is both UV- and IR-convergent we can set $\epsilon = 0$ and evaluate the integrals in four dimensions. We further omit the ϵ -dependence in the superscript and write $S^4(\dots)$ as we always expand around $d = 4 - 2\epsilon$ within the reduced matrix elements in terms of the scalar master integrals.

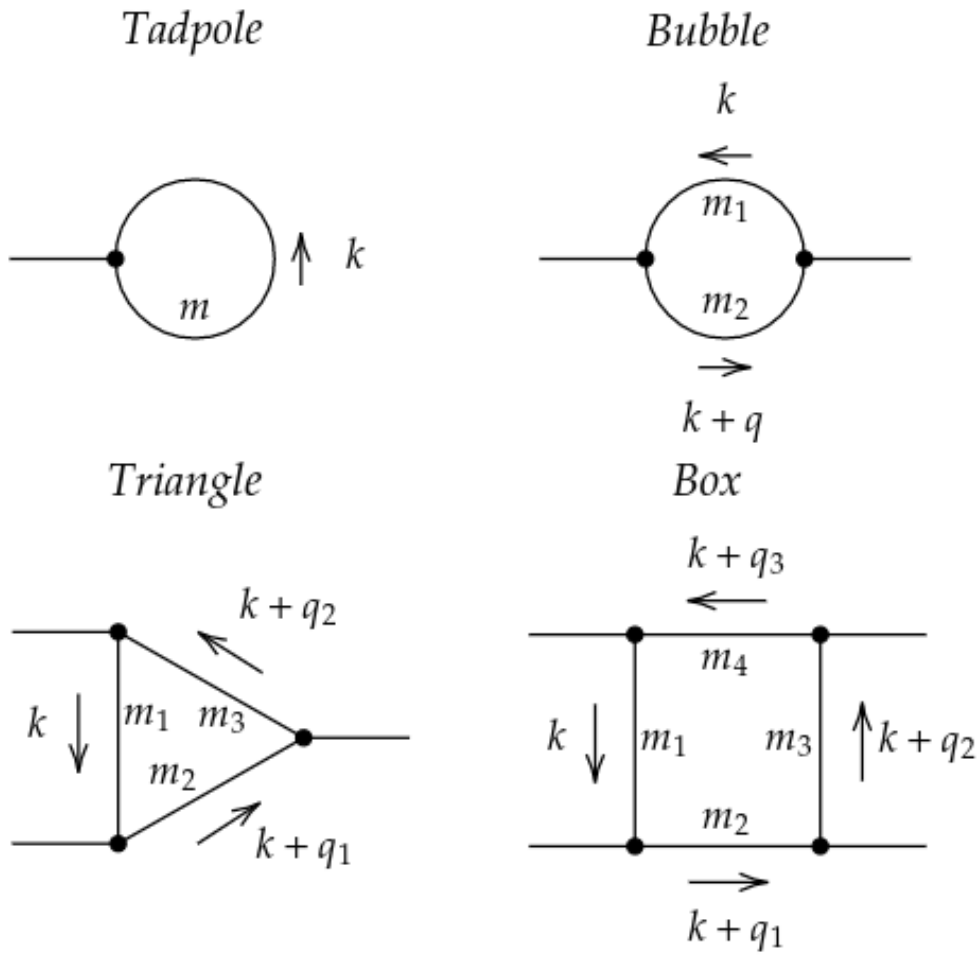


Figure 3.1.: Momentum and mass conventions for our choice of master integrals.

IR-divergences can be distinguished into soft- and collinear divergences [33]. They can be determined by from the Caley-matrix Y of an integral

$$Y_{ij} = (q_i - q_j)^2 - m_i^2 - m_j^2 \quad (3.38)$$

and they appear when there is an arrangement of momenta and masses such that the zero-entries in the Caley-matrix form a cross or a box

$$Y_{Soft} = \begin{bmatrix} \dots & 0 & \dots & \dots \\ 0 & 0 & 0 & \dots \\ \dots & 0 & \dots & \dots \\ \dots & \dots & \dots & \dots \end{bmatrix} \quad (3.39)$$

$$Y_{Collinear} = \begin{bmatrix} \dots & \dots & \dots & \dots \\ \dots & 0 & 0 & \dots \\ \dots & 0 & 0 & \dots \\ \dots & \dots & \dots & \dots \end{bmatrix} \quad (3.40)$$

3. Technical tools

All master integrals of our reduced loop expressions are IR-convergent in the 't Hooft gauge, so we can drop all ϵ^2 -terms that appear in the d-dimensional contractions of our spinor chains with metric tensors and momenta. Most of these integrals can be expressed in terms of logarithms and dilogarithms. The analytical expressions of all tadpole and bubble integrals are presented in appendix (D), for the analytical expressions of UV-divergent triangle and box integrals see [33]. In case of box integrals with complex masses (which are necessary for the treatment of unstable particles), no general algebraic expression exists. As a result, one would need to evaluate the scalar integrals numerically for a full reduction of matrix elements and the cross section, see section (4.2). For now, we turn our focus to the extraction of said scalar integrals from the tensor expressions within the one-loop matrix elements.

3.2.2. Tensor decomposition

In order to fully decompose matrix elements down to scalar kinematical factors and scalar integrals, we need to treat the tensor structure of the integration momentum that arises at loop-level. It is caused by the propagators of fermions, vector bosons and derivative couplings that contain the loop momentum. One very prominent method for the reduction is the Veltman-Passarino scheme [34], which uses the Lorentz-covariance of the loop integrals to rewrite them in terms of external momenta and metric tensors. We choose a similar approach called the Davydychev decomposition [35]. It allows us to decompose general tensor integrals of the form

$$S_{(v_1, v_2, \dots, v_n)}^{d, \mu_1 \mu_2 \dots \mu_m}(0, q_1^2, q_2^2, \dots, q_{n-1}^2 | m_1^2, m_2^2, \dots, m_n^2) \\ = h(\epsilon) \int \frac{d^d k}{i\pi^{d/2}} \frac{k^{\mu_1} k^{\mu_2} \dots k^{\mu_m}}{[k^2 - m_1^2]^{v_1} [(k + q_1)^2 - m_2^2]^{v_2} \dots [(k + q_n)^2 - m_n^2]^{v_n}} \quad (3.41)$$

by extracting the Lorentz structure and raising the dimensionality and powers of propagators within the loop integrals. This way, we can separate finite and divergent contributions at the level of scalar integrals, allowing us to study the divergence behaviour of the matrix elements at the level of unevaluated scalar integrals. The reduction reads

$$S_{(v_1, v_2, \dots, v_n)}^{d, \mu_1 \mu_2 \dots \mu_m}(0, q_1, q_2, \dots, q_n | m_1, m_2, \dots, m_n) = \\ \sum_{\lambda, x_1, x_2, \dots, x_n} \delta_{(2\lambda + \sum_i x_i - m)} \left(-\frac{1}{2}\right)^\lambda x_1! x_2! \dots x_n! \\ \times \left\{ g^\lambda q_1^{x_1} q_2^{x_2} \dots q_n^{x_n} \right\}^{\mu_1 \mu_2 \dots \mu_m} S_{(\dots, v_i + x_i, \dots)}^{d+2(m-\lambda)}(0, q_1, q_2, \dots, q_n | m_1, m_2, \dots, m_n) \quad (3.42)$$

with distinct vector-metric combinations $\{g^\lambda q_1^{x_1} q_2^{x_2} \dots q_n^{x_n}\}^{\mu_1 \mu_2 \dots \mu_m}$, where λ is the number of metric tensors $g^{\alpha\beta}$ and x_i the number of momentum variables q_i . Some examples are

3. Technical tools

$$\begin{aligned}
\{q_1 q_2\}^{\mu_1} &= q_1^{\mu_1} + q_2^{\mu_2}, \quad \{q_1 q_2\}^{\mu_1 \mu_2} = q_1^{\mu_1} q_2^{\mu_2} + q_1^{\mu_2} q_2^{\mu_1} \\
\{q_1 q_2 q_3\}^{\mu_1 \mu_2 \mu_3} &= q_1^{\mu_1} q_2^{\mu_2} q_3^{\mu_3} + q_1^{\mu_1} q_2^{\mu_3} q_3^{\mu_2} + q_1^{\mu_2} q_2^{\mu_1} q_3^{\mu_3} \\
&\quad + q_1^{\mu_2} q_2^{\mu_3} q_3^{\mu_1} + q_1^{\mu_3} q_2^{\mu_1} q_3^{\mu_2} + q_1^{\mu_3} q_2^{\mu_2} q_3^{\mu_1} \\
\{g q_1^2\}^{\mu_1 \mu_2 \mu_3 \mu_4} &= g^{\mu_1 \mu_2} q_1^{\mu_3} q_1^{\mu_4} + g^{\mu_1 \mu_3} q_1^{\mu_2} q_1^{\mu_4} + g^{\mu_1 \mu_4} q_1^{\mu_2} q_1^{\mu_3} \\
&\quad + g^{\mu_2 \mu_3} q_1^{\mu_1} q_1^{\mu_4} + g^{\mu_2 \mu_4} q_1^{\mu_1} q_1^{\mu_3} + g^{\mu_3 \mu_4} q_1^{\mu_1} q_1^{\mu_2}
\end{aligned} \tag{3.43}$$

All higher-dimensional scalar integrals that appear in the Davydychev decomposition can be calculated via recursion relations that depend on the kinematics of the integrals involved. First, we use the symmetric Caley matrix as defined in (3.38) to further declare the inverse Caley row b_i and Caley sum B

$$b_i = \sum_j Y_{ij}^{-1}, \quad B = \sum_i b_i = \sum_{ij} Y_{ij}^{-1} \tag{3.44}$$

if the inverse of Y_{ij} exists. Finally, we define the Gram matrix

$$G_{ij} = 2q_i q_j \tag{3.45}$$

and the sum of propagator powers

$$\sigma = \sum_{i=1}^n v_i \tag{3.46}$$

Then, via integration-by-parts, one can calculate a basic recursion relation valid for $n \leq 5$ and non-vanishing determinants of Y and G . Using the short forms of σ and B in (3.44) and (3.46) we obtain the following formula

$$(d - 1 - \sigma) B S_{(\{v_i\})}^d = S_{(\{v_i\})}^{d-2} - \sum_{i=1}^n S_{(\{v_i - \delta_{ii}\})}^{d-2} \tag{3.47}$$

This tells us that we can reduce a scalar integral of dimension d into a scalar integral with the dimension reduced by two and a sum of scalar integrals with reduced dimensionality and reduced propagator powers. A derivation of the recursive relation can be found in [36].

3.2.3. Reduction Summary

The two main algorithms that were implemented in our package 'oneloop.m' are the tensor reduction by Davydychev (3.42) and the simplification of scalar integrals with higher propagator powers (3.47) for all special cases of Y , G and number of external legs

$$\begin{aligned}
& S_{(v_1, v_2, \dots, v_n)}^{d, \mu_1 \mu_2 \dots \mu_m}(0, q_1, q_2, \dots, q_n | m_1, m_2, \dots, m_n) = \\
& \sum_{\lambda, x_1, x_2, \dots, x_n} \delta_{(2\lambda + \sum_i x_i - m)} \left(-\frac{1}{2}\right)^\lambda x_1! x_2! \dots x_n! \\
& \times \left\{ g^\lambda q_1^{x_1} q_2^{x_2} \dots q_n^{x_n} \right\}^{\mu_1 \mu_2 \dots \mu_m} S_{(\dots, v_i + x_i, \dots)}^{d+2(m-\lambda)}(0, q_1, q_2, \dots, q_n | m_1, m_2, \dots, m_n) \\
& (d-1-\sigma)BS_{(\{v_l\})}^d = S_{(\{v_l\})}^{d-2} - \sum_{i=1}^n S_{(\{v_l - \delta_{li}\})}^{d-2} \tag{3.48}
\end{aligned}$$

Additionally, one can access the Caley-matrix Y , the Gram-matrix G and all derived quantities (3.44) to check for IR-divergences as described in (3.39)

$$\begin{aligned}
& Y_{ij} = (q_i - q_j)^2 - m_i^2 - m_j^2, \quad G_{ij} = 2q_i q_j \\
& b_i = \sum_j Y_{ij}^{-1}, \quad B = \sum_i b_i = \sum_{ij} Y_{ij}^{-1} \tag{3.49}
\end{aligned}$$

4. Software and packages

The focus of this chapter is the software toolkit that was implemented in our calculations. We provide a workflow that generates Feynman diagrams automatically at NLO, along with their algebraic expressions. QGraf was used for all standard and new diagrams. Its implementation through the bash file 'fms_run.sh' is shown in (4.1) for both classes of standard and new diagrams. The algebraic expressions are then derived via our already-mentioned Mathematica packages 'spinorhelicity.m' and 'oneloop.m', along with additional replacement rules to transform Feynman rules into tensor integrals. Cross-checks by hand and through the usage of FeynCalc [37, 38, 39] helped to verify the validity of our routines. The main functions of our packages are presented in (4.2).

4.1. QGraf

4.1.1. Introduction

We make use of the flexibility of the Fortran program QGraf in order to generate connected diagrams for our weak model [40]. It creates Feynman diagrams based on a set of interaction rules, providing the sign of the anti-commutation relations and the symmetry factors of every diagram. The program requires two ingredients: A model file that specifies all kinds of interactions of the theory, and an instruction file with the specifics of the interaction process containing the order of expansion in our couplings. Both aspects are integrated into a workflow through a bash file with options directly linked to the QGraf program. In the following subsections, we first present our implementation of the weak sector of the SM in terms of helicity spinors, emphasizing the rules to create our new types of diagrams. Afterwards, we give two examples of output and comment on how to interpret it in section (4.1.2).

4.1.2. Input files

All types of particle propagators and interaction vertices are defined in a model file, where we split our description of fermions into left-handed and right-handed contributions. For example, the propagators for left-handed and right-handed leptons have the form

```
[ fi, fi_bar, - ], fi=eL,nueL,eR,mL,numL,mR
```

that account for both propagators of particles and antiparticles. The naming of particles within QGraf is irrelevant (up to the restriction of symbolic compatibility), and only the final sign is relevant as it assigns the anti-commutation properties of fermionic fields. The bosonic propagators are accounted for via

```
[ z, z, + ]
[ w_plus, w_minus, + ]
[ eta, eta, + ]
```

where the positive sign indicates the bosonic nature. The construction is the same for quarks, the would-be Goldstone bosons and ghosts. The external bound states enter via the declaration

```
[ P, P_bar, -, external]
P=UL,DL,CL,SL,EL,Nue,ML,NumL
```

for quarks and leptons of both generations. The keyword "external" ensures that the effects only occur in the external states of left-handed fermions. Interaction vertices are classified by the particles entering the vertex, the weak coupling g and the vev v . We have either $g = 1, 2$ for three-point and four-point interactions, and $v = 0, 1$ for standard vertices and insertions of the scalar component for the bound state. For example, two such declarations are

```
[ w, eta, chi; gpow = '1', vpow = '0']
[ EL_bar, eL, eta; gpow = '0', vpow = '1']
```

The parameters g and v are given by $gpow$ and $vpow$, respectively. The first line represents the neutral vector-scalar-scalar interaction $W\eta\chi$, and the second one represents an insertion of the elementary left-handed electron and the real Higgs field of the full bound state electron. The latter is treated as an interaction vertex within QGraf, but the rule should be understood in terms of operator insertions as explained in (2.4.3). The specifications for our scattering process are given in the input file. If one wants to generate the regular diagrams for the process $e_L^- e_L^+ \rightarrow \mu_L^- \mu_L^+$ at NLO, then its content reads

4. Software and packages

```
output = 'diagrams_dot.dat' ;
style = 'Styles/dot.sty' ;
model = 'Models/ewsm_reduced.model' ;
in = eL, eL_bar;
out = mL, mL_bar;
loops = 1;
loop_momentum = ;
options = onshell;
true = vsum[gpow, 4, 4] ;
true = vsum[vpow, 0, 0] ;
```

where the output is stored in 'diagrams_dot.dat', using the file dot.sty to immediately yield diagrams with Graphviz [41]. The model file 'ewsm_reduced.model' contains all Feynman rules, with the full file being presented in appendix E. The two lines containing *vsum* guarantee that only the first term in the FMS expansion at order g^4 appears. New diagrams are created by varying the parameters *gpow* and *vpow*. To test this efficiently, we created a bash file called 'fms_run.sh' with different flags for an automatic evaluation of the Feynman diagrams. Its options are

- -l: Number of loops implemented, with a warning for $l \geq 2$ as the number of diagrams grows immensely (more than 30000 regular loop diagrams for our process at $l = 2$)
- -g: Power in the coupling g
- -v: Number of operator insertions corresponding to loops containing the leptonic and scalar lines of the compound states
- -i: Specific operation insertions such as *Eemm*, *EEmm* for an insertion of scalar would-be Goldstones at the location of leptons with capital letters.
- -c: Different chirality configurations of the process (*LLLL*, *LLRR*, ...).

Two exemplary cases are shown in the next section.

Diagram output

Let us first consider a regular NLO diagram. With the command

```
bash fms_run.sh -l 1 -g 4 -v 0 -c LLLL -i eemm
```

we extract all regular NLO diagrams in terms of purely left-handed spinors without any additional Higgs insertion. One such diagram, a leptonic bubble diagram that contributes to the self-energy of the neutral vector boson, reads

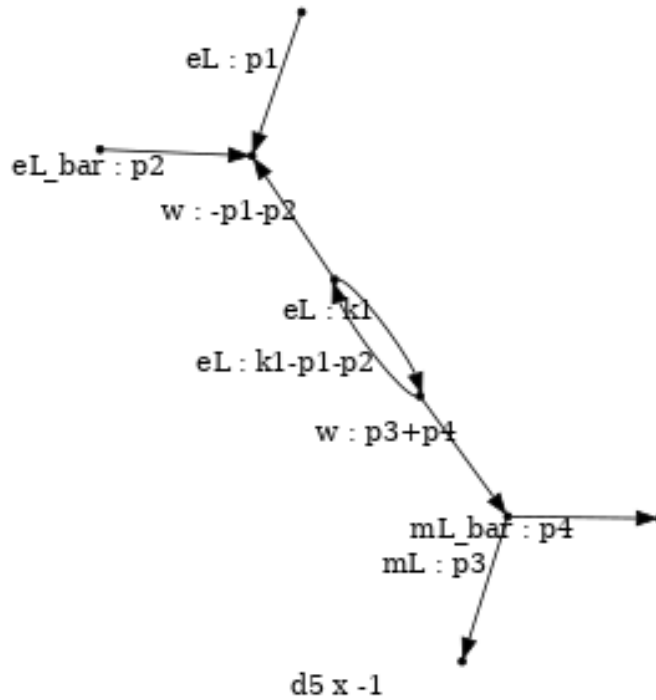


Figure 4.1.: Fermionic self-energy diagram of the process $e_L^- e_L^+ \rightarrow \mu_L^- \mu_L^+$

The label $d5x-1$ attached to the bottom of the diagram indicates the number in the generation process (here the fifth diagram), the negative sign from anti-commutation relations and the symmetry factor one. External particles are directed along their physical momenta, while internal momenta do not follow a specific direction and can vary based on the specific topology and process. A new diagram that arises due to the higher six-point function

$$\langle [e_L^- e_L^+ [h\mu_L^-] [\chi\mu_L^+]] \rangle \quad (4.1)$$

is represented in QGraf via figure (4.2). The loop arises since both bound-state operators share the fermionic line μ_L^\pm , while the integration, normally linked to the loop, arises from the integral over the relative momentum k_1 of the scalar contributions h and χ . One diagram of the Green's function in (4.1) is obtained

4. Software and packages

from the following command and yields the diagram in figure (4.2)

```
bash fms_run.sh -l 1 -g 2 -v 2 -c LLLL -i eeMM
```

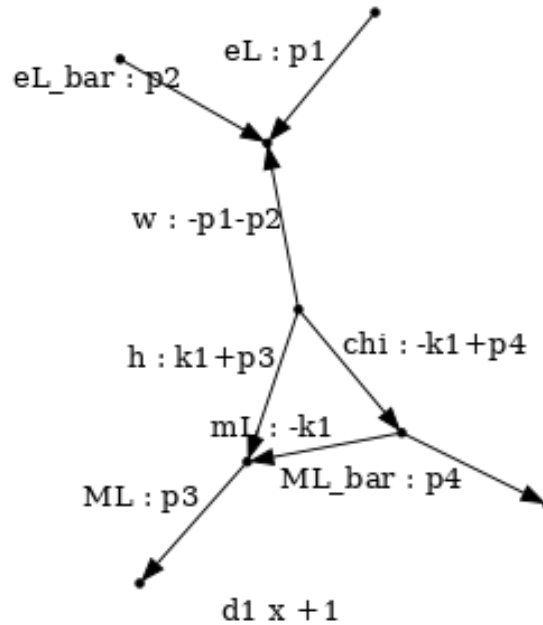


Figure 4.2.: Triangle diagram due to the expanded six-point function from FMS contributions in the final state

The capital labels correspond to the insertions of elementary particles (here η , χ and μ_L^-) and should not be confused with the full gauge-invariant bound state defined in (2.23). A more accurate representation consistent with our rules for bound states is given in figure (4.3).

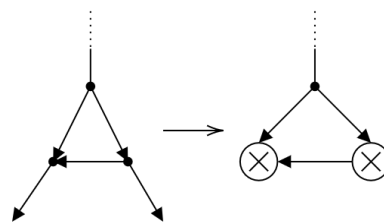


Figure 4.3.: Accurate representation of the bound-state insertion with our cross-notation from the Feynman rules of figure (2.3)

To increase clarity, we manually translate all diagrams of QGraf via Mathcha and present them in (5.2) and (5.3).

4.2. Our Mathematica tools

4.2.1. Overview

In order to calculate the algebraic expressions of matrix elements we created our own set of routines in Mathematica. We briefly list here the main functions used in the calculation of the reduced algebraic expressions in section (5). All functions and replacement rules were tested in Mathematica version (12.3).

- **SpinorString[...]**: Defines all the non-commutative rules of spinor chains, alongside all reduction rules such as the Fierz identity (3.25), the connection between Mandelstam variables and spinor products (3.16) and the sum rule (3.19). The main framework was created by Simon Plätzer in his package 'spinorhelicity.m' [29], with my extension to the d-dimensional case.
- **TensorReduce[...]**: The first main algorithm of the package 'oneloop.m' [30]. Its creation is a collaborative work between Simon Plätzer and me that implements the reduction of all tensor integrals with arbitrary propagator powers and tensor expressions.
- **ReduceScalarIntegral[...]**: The second main algorithm of 'oneloop.m'. It is again a joint development of Simon Plätzer and me that reduces the generalized scalar integrals. Special solutions based on the determinant of the Caley matrix (3.38), the Gram matrix (3.45) and the number of external legs within the loop integrals are contained as well.
- **LoopReduction[...]**: My own toolkit of replacement rules that allows for the translation of Feynman rules into general tensor integrals. These can then be reduced with the functions mentioned above.

In order to showcase the functionality of our Mathematica toolkit, we will give a detailed example calculation that contains all of the relevant functions listed above.

4.2.2. Example calculation

We analyse the snail diagram with a four-vector interaction within the W-boson propagator. The corresponding output of our bash file for QGraf is

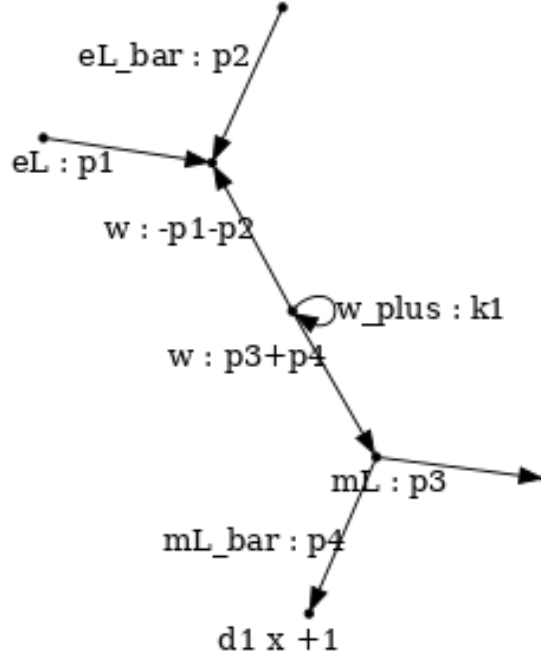


Figure 4.4.: Snail-diagram of the process $e_L^- e_L^+ \rightarrow \mu_L^- \mu_L^+$

The algebraic expression in Mathematica can be obtained by first writing down the Feynman rules as follows

- **SpinorString[MinusBarSpinor[p1], VerWFFbar[g, μ], PlusSpinor[p2]]:** The initial spinor chain $[1|\gamma^\mu|2\rangle$ containing the external spinors and the interaction vertex for $W e_L^- e_L^+$.
- **VProp[p1 + p2, m, μ , α , xiW]** and **VProp[p3 + p4, m, μ , α , xiW]**: The neutral vector propagators with momenta pointing in the positive time-direction and gauge-parameter ξ_W .
- **SpinorString[MinusBarSpinor[p4], VerWFFbar[g, μ], PlusSpinor[p3]]:** The almost identical final-state spinor string $[4|\gamma_\mu|3\rangle$, where we do not need to differentiate between upper and lower indices.
- **LoopReduction[VerWpWmWW[g, σ , ρ , α , β] VProp[k, m, σ , ρ , xiP]]:** The term containing the loop contribution, where **LoopReduction** needs to be wrapped around all terms that involve the loop momentum k .

First we load the two packages 'spinorhelicity.m' and 'oneloop.m' into our Mathematica notebook. Inserting the prior set of rules thus yields after expansion (4.5).

$$-\frac{1}{4} g^4 \frac{1}{-m^2+s} \frac{1}{-m^2+s} (\langle p2|\rho|p1\rangle \langle p3|\sigma|p4\rangle (S_{(1,1)}^{(\sigma,\rho)}[\{\theta, \theta\}, \{\theta, m^2\}] - \text{xIP} S_{(1,1)}^{(\sigma,\rho)}[\{\theta, \theta\}, \{\theta, m^2 \text{xIP}\}]) + 4 [p1p4] \langle p2p3\rangle ((-3+2 \text{eps}) S_{(1)}^4[\{\theta\}, \{m^2\}] + g^{\rho\sigma} (S_{(1,1)}^{(\sigma,\rho)}[\{\theta, \theta\}, \{\theta, m^2\}] - \text{xIP} S_{(1,1)}^{(\sigma,\rho)}[\{\theta, \theta\}, \{\theta, m^2 \text{xIP}\}])))$$

Figure 4.5.: Tensor expression of our loop diagram in Mathematica

Next, by applying **TensorReduce[...]** to the former expression, we obtain the matrix element in terms of scalar integrals (4.6).

$$-\frac{1}{4} g^4 [p1p4] \langle p2p3\rangle \frac{1}{-m^2+s} \frac{1}{-m^2+s} (4 \times (-3+2 \text{eps}) S_{(1)}^4[\{\theta\}, \{m^2\}] + (-7+4 \text{eps}) (S_{(1,1)}^6[\{\theta, \theta\}, \{\theta, m^2\}] - \text{xIP} S_{(1,1)}^6[\{\theta, \theta\}, \{\theta, m^2 \text{xIP}\}])))$$

Figure 4.6.: Scalar expression of our loop diagram in Mathematica

The final reduction is obtained by further applying **ReduceScalarIntegral[...]** and expressing the matrix element as a series expansion in ϵ . It reads

$$-\frac{1}{8 (m^2-s)^2} g^4 [p1p4] \langle p2p3\rangle (3 \times (-6+5 \text{eps}) S_{(1)}^4[\{\theta\}, \{m^2\}] + (-6+\text{eps}) \text{xIP} S_{(1)}^4[\{\theta\}, \{m^2 \text{xIP}\}])$$

Figure 4.7.: Final reduced expression of our loop diagram in Mathematica

This reduced expression is the one we present in section (5.2.2), except that we flip $\langle 23\rangle = -\langle 32\rangle$ and add the factor $h(\epsilon)$ in (3.31) that we skip in Mathematica. The procedure is straightforward for all other diagrams, and the final expressions in terms of our scalar master integrals are presented in the following chapter.

5. Results

Here we provide the reduced invariant matrix elements and differential cross section at tree-level for the process $e_L^- e_L^+ \rightarrow \mu_L^- \mu_L^+$. The latter is presented in section (5.1). While the FMS expansion does not contribute at tree-level, the result already highlights many of the simplification rules of section (3.1). We continue with the regular matrix elements at NLO in section (5.2) and present the new loop contributions in section (5.3). Both sections are separated into the Feynman diagrams and the reduced algebraic expressions in the 't Hooft gauge. For the regular loop diagrams and the FMS loop diagrams we provide one example each where we carry out the calculation explicitly. Other results are given as an expansion in ϵ and the master integrals of section (3.2).

5.1. Tree level

At tree-level, there exists only one diagram with an intermediate neutral W -boson. It reads

$$i\mathcal{M}_{Tree} = \langle 2 | \left(-\frac{ig}{2} \gamma_\mu \right) | 1 \rangle \left(\frac{-i}{q^2 - m^2} \left(g^{\mu\nu} - \frac{q^\mu q^\nu}{q^2} \right) - \frac{q^\mu q^\nu}{q^2} \frac{\xi_W}{q^2 - \xi_W m^2} \right) \times \langle 3 | \left(-\frac{ig}{2} \gamma_\nu \right) | 4 \rangle \quad (5.1)$$

where the internal momentum is $q^\alpha = (p_1 + p_2)^\alpha = -(p_3 + p_4)^\alpha$. First we notice that all terms depending on $q^\mu q^\nu$ disappear since

$$\begin{aligned} \langle 2 | \gamma_\mu | 1 \rangle (p_1 + p_2)^\mu &= \langle 2 | \not{p}_1 | 1 \rangle + \langle 2 | \not{p}_2 | 1 \rangle \\ &= \langle 21 \rangle \langle 11 \rangle + \langle 21 \rangle [11] + \langle 22 \rangle \langle 21 \rangle + \langle 22 \rangle [21] = 0 \end{aligned} \quad (5.2)$$

where we used (3.8) and (3.9), which holds similarly for the final state spinors. The momentum can be expressed via the Mandelstam variable $q^2 = s$, and the simplified expression reads

$$\begin{aligned} \mathcal{M}_{Tree} &= \frac{g^2}{4} \frac{1}{s - m^2} \langle 2 | \gamma_\mu | 1 \rangle \langle 3 | \gamma^\mu | 4 \rangle \\ &= \frac{g^2}{2} \frac{1}{s - m^2} [14] \langle 32 \rangle \end{aligned} \quad (5.3)$$

by making use of the Fierz identity (3.10) in the final line. The higher n-point functions do not generate any diagrams at tree-level as we cannot construct any other connected diagrams without loops. All other chirality configurations are zero as the right-handed leptons do not couple to the weak vector boson W . The differential cross section yields

$$\begin{aligned} \left(\frac{d\sigma}{d\Omega}\right)_{CM} &= \frac{1}{64\pi^2 s} (\mathcal{M}_{Tree}^* \mathcal{M}_{Tree}) = \frac{g^4}{256\pi^2 s} \frac{1}{(s-m^2)^2} \langle 41 \rangle [14] [23] \langle 32 \rangle \\ &= \frac{g^4}{256\pi^2 s} \frac{u^2}{(s-m^2)^2} = \frac{g^4}{256\pi^2 s} \frac{(s+t)^2}{(s-m^2)^2} \end{aligned} \quad (5.4)$$

Formulating t in terms of s and the scattering angle θ leads to

$$\left(\frac{d\sigma}{d\Omega}\right)_{CM} = \frac{g^4}{1024\pi^2} \frac{s(1+\cos(\theta))^2}{(s-m^2)^2} \quad (5.5)$$

The differential cross section is shown in turns of the SM parameters $g \approx 0.64$ and $v \approx 247 GeV$ and the kinematical variables \sqrt{s} and θ in figure (5.1). Alternatively, we can express $d\sigma$ in terms of s and the pseudorapidity η , defined as

$$\eta \equiv -\ln\left(\tan\left(\frac{\theta}{2}\right)\right) \quad (5.6)$$

Figure (5.2) shows the differential cross section for the range $\eta \in \{-5, 5\}$. Furthermore, the differential cross section is plotted for fixed angles $\theta \in \{0, \frac{\pi}{2}, \frac{4\pi}{5}, \pi\}$ in (5.3) to highlight the strong angle dependence.

5. Results

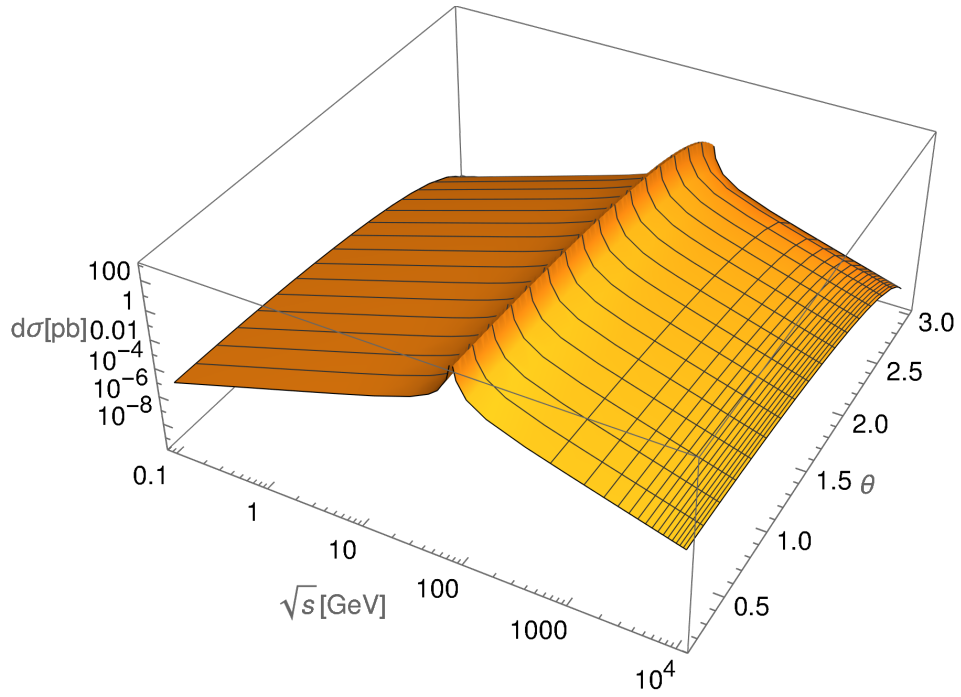


Figure 5.1.: Differential cross section of the tree-level process in terms of the CM-energy \sqrt{s} and the scattering angle θ

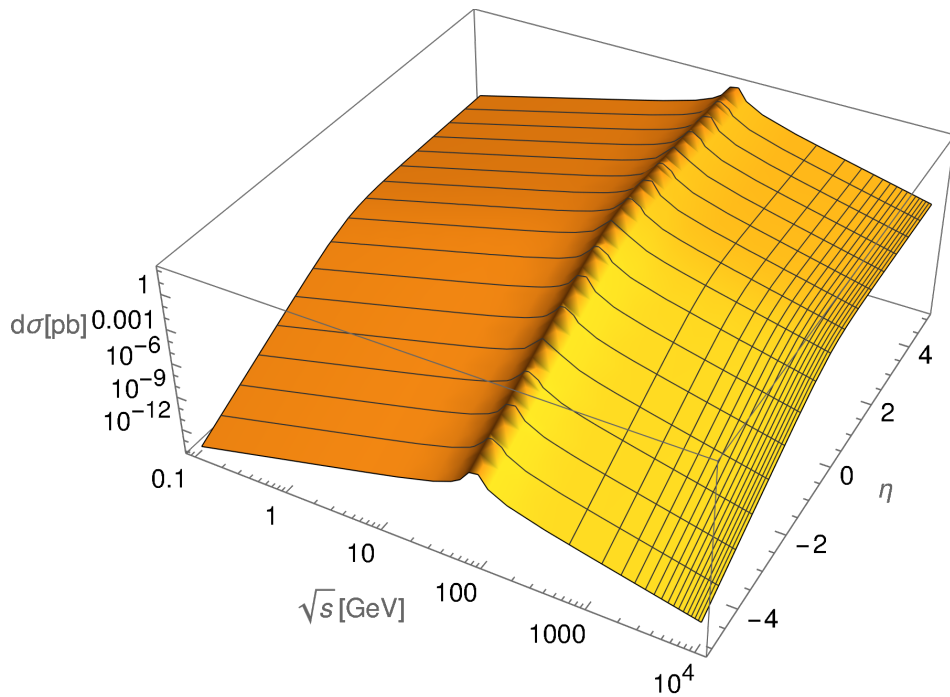


Figure 5.2.: Differential cross section of the tree-level process in terms of the CM-energy \sqrt{s} and the pseudorapidity η

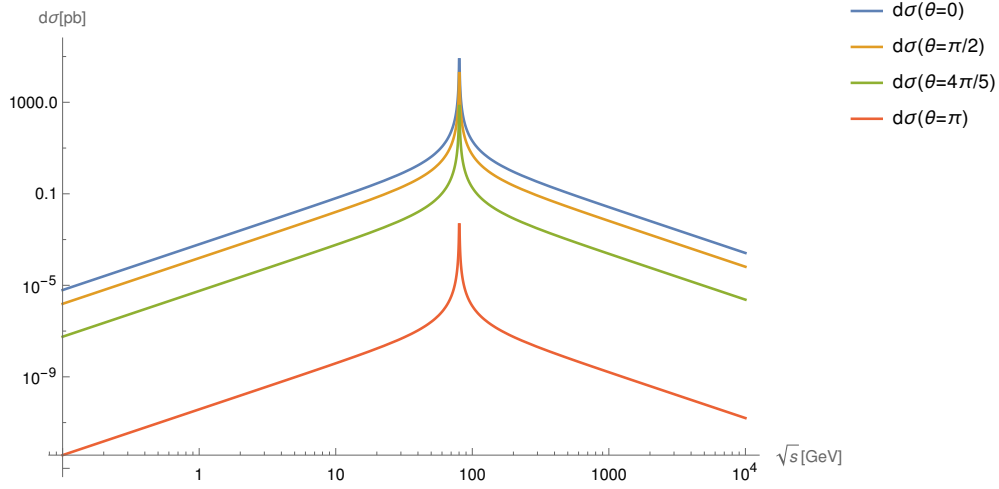


Figure 5.3.: Differential cross section of the tree-level process in terms of the CM-energy \sqrt{s} for fixed angles

The peak of $d\sigma$ appears at the location of the mass pole at $m = 79.04\text{GeV}$, slightly shifted from the Z-boson pole due to the disappearance of the photon. The asymmetry in forward and backward scattering is clearly visible in figures (5.1) and (5.3). The high-energy behaviour is very similar to the cross section obtained from the full massless EW sector containing the photon, see appendix (B).

5.2. Regular loop expressions

5.2.1. Feynman diagrams

At NLO, there exist 37 distinct Feynman diagrams that arise from the regular four-point function $\langle e_L^- e_L^+ \mu_L^- \mu_L^+ \rangle$. They are grouped based on their topology into bubble, snail, tadpole, triangle and box diagrams. All Feynman diagrams in terms of physical outgoing momenta are given in figures (5.4) to (5.8), where we used $\mathcal{M}_k^{\text{Type}}$ to refer to the k^{th} matrix element of topology $\text{Type} \in \{\text{Bubble}, \text{Snail}, \text{Tadpole}, \text{Triangle}, \text{Box}\}$. The corresponding algebraic expressions are given in the following section (5.2.2).

5. Results

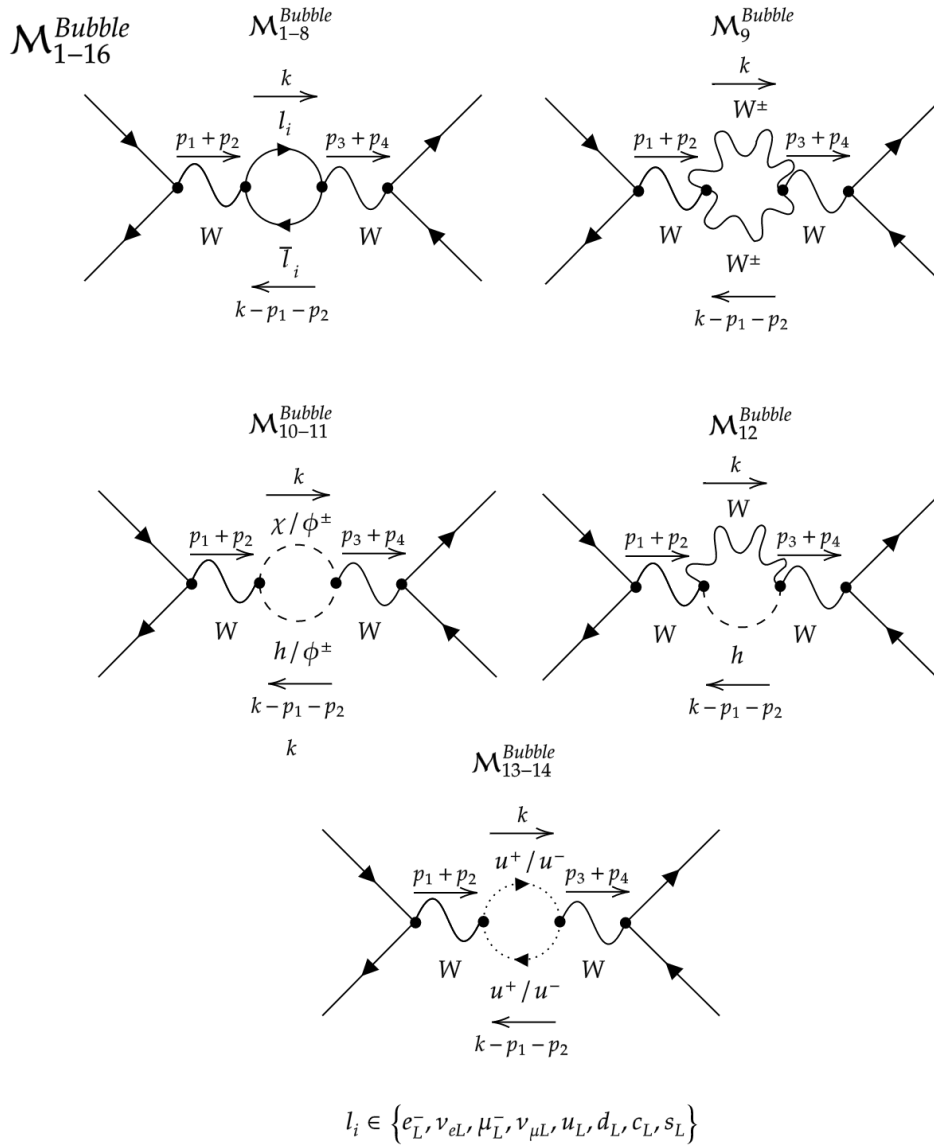


Figure 5.4.: Full list of all bubble diagrams

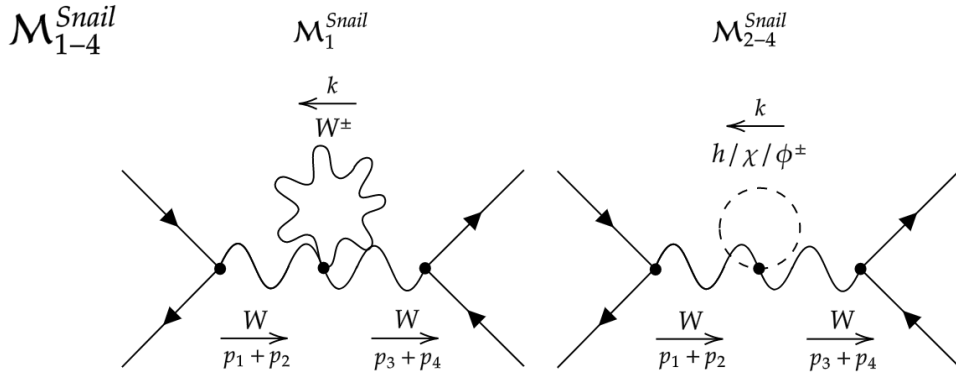


Figure 5.5.: Full list of all snail diagrams

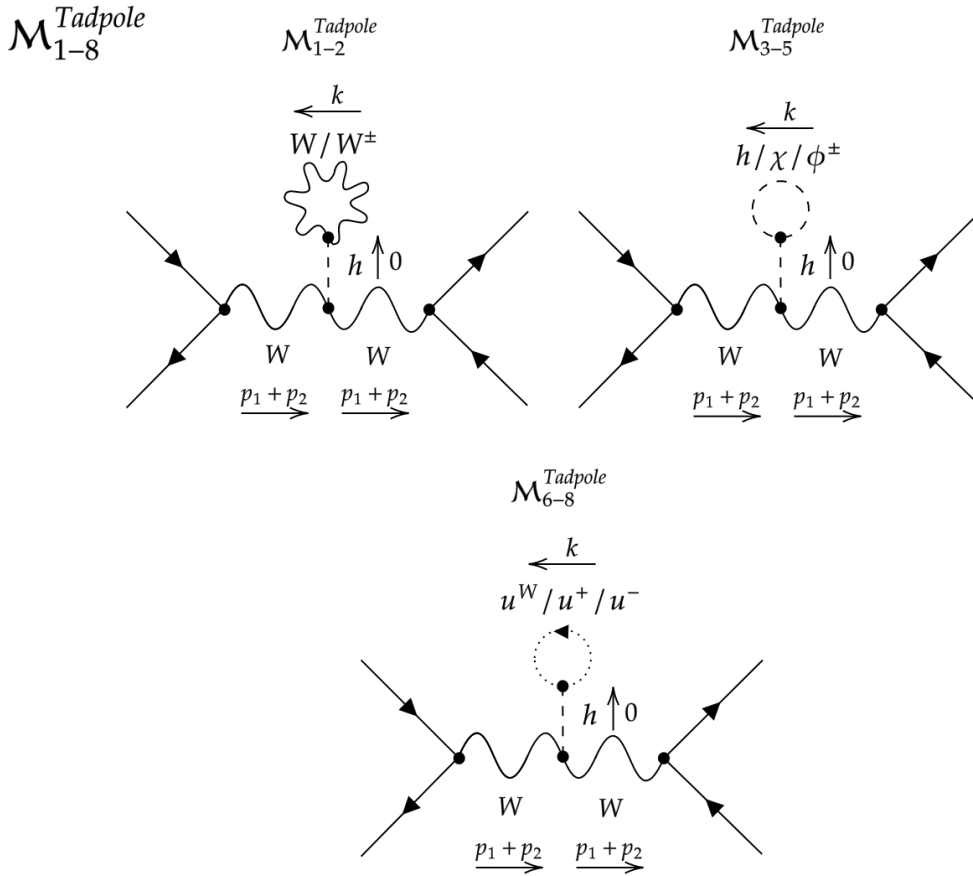


Figure 5.6.: Full list of all tadpole diagrams

5. Results

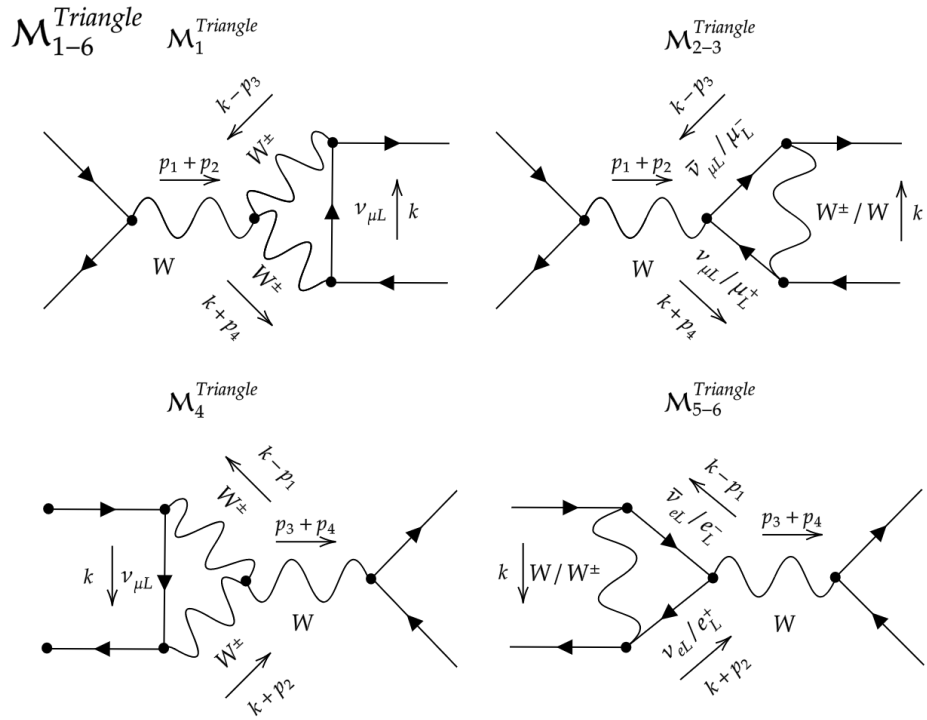


Figure 5.7.: Full list of all triangle diagrams

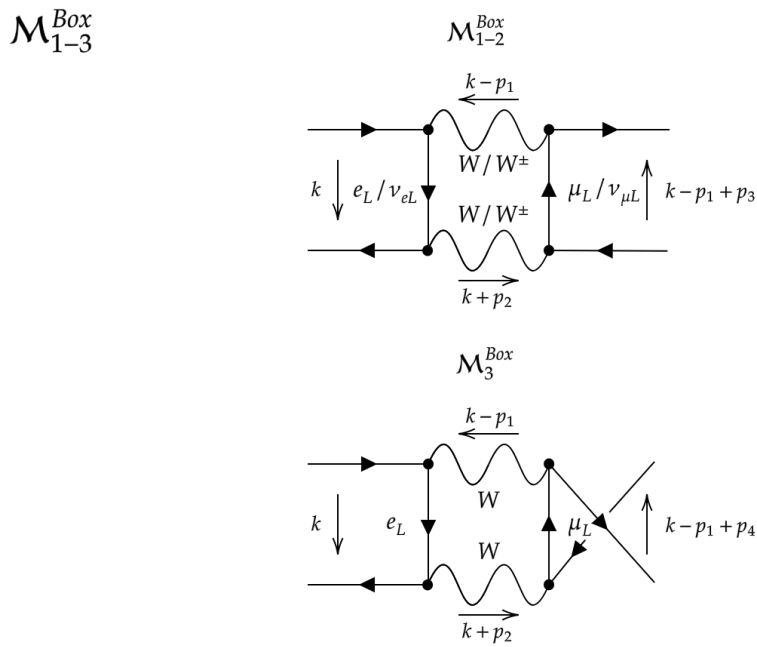


Figure 5.8.: Full list of all box diagrams

5.2.2. Reduced algebraic expressions

Bubble diagrams

The bubble diagrams for all eight leptonic loop diagrams have the same algebraic expression

$$\begin{aligned} \mathcal{M}_{1-8}^{Bubble} &= \frac{1}{16} \frac{g^4}{(s-m^2)^2} \langle 2|\gamma_\mu|1\rangle \langle 3|\gamma_\nu|4\rangle \\ &\times h(\epsilon) \frac{1}{i\pi^{d/2}} \int d^4k \frac{\text{Tr} \left[k \gamma^\mu (k - \not{p}_1 - \not{p}_2) \gamma^\nu \right]}{k^2 (k - p_1 - p_2)^2} \end{aligned} \quad (5.7)$$

since the weak isospin of each lepton is $\pm \frac{1}{2}$ with a sign that cancels since it appears exactly twice in each loop. Evaluating the trace in (5.7) gives

$$\begin{aligned} \frac{1}{4} \text{Tr} \left[k \gamma^\mu (k - \not{p}_1 - \not{p}_2) \gamma^\nu \right] &= 2k^\nu k^\mu - k^2 g^{\mu\nu} - k^\nu (p_1 + p_2)^\mu - k^\mu (p_1 + p_2)^\nu \\ &+ k(p_1 + p_2) g^{\mu\nu} \end{aligned} \quad (5.8)$$

The third and fourth term cancel, and the remaining expression in terms of tensor integrals reads

$$\begin{aligned} \mathcal{M}_{1-8}^{Bubble} &= \frac{g^4}{4(s-m^2)^2} \langle 2|\gamma_\mu|1\rangle \langle 3|\gamma_\nu|4\rangle h(\epsilon) \left(2S^{d,\mu\nu}(0, -p_1 - p_2|0, 0) \right. \\ &\left. - g^{\mu\nu} (S_{(1)}^4(-p_1 - p_2|0) - (p_1 + p_2)_\alpha S^{d,\alpha}(0, -p_1 - p_2|0, 0)) \right) \end{aligned} \quad (5.9)$$

Only tensor decompositions without external momenta will survive the full reduction in the massless case, and the final result reads

$$\mathcal{M}_{1-8}^{Bubble} = \frac{4g^4 s [14] \langle 32 \rangle}{9(s-m^2)^2} (3 - \epsilon) S_{(1,1)}^4(0, -p_1 - p_2|0, 0) \quad (5.10)$$

We do not need to consider the term in ϵ^2 here and in all further expressions since the scalar integrals are all IR-convergent. The reduced bosonic bubble diagram \mathcal{M}_9^{Bubble} is still rather lengthy in a full 't Hooft gauge, so we present here only the tensor expression and the reduced scalar form in the Feynman gauge where $\xi_W = \xi_+ = 1$. With the shorthand $q = -p_1 - p_2$ the tensor expression reads

$$\begin{aligned} \mathcal{M}_9^{Bubble}(\xi_W = \xi_+ = 1) &= \frac{g^4}{4(s-m^2)^2} \langle 2|\gamma_\mu|1\rangle \langle 3|\gamma_\nu|4\rangle h(\epsilon) \\ &\left[(-10 + 8\epsilon) S^{d,\mu\nu} + (5 - 8\epsilon) (q^\mu S^{d,\nu} + q^\nu S^{d,\mu}) + (2 - 2\epsilon) q^\mu q^\nu S_{(1,1)}^4 \right. \\ &\left. + g^{\mu\nu} \left(-2g_{\alpha\beta} S^{d,\alpha\beta} + 2q_\alpha S^\alpha - 5q^2 S_{(1,1)}^4 \right) \right] \end{aligned} \quad (5.11)$$

5. Results

where all integrals have the dependence $S = S(0, q|m^2, m^2)$.

The full decomposition up to order $\mathcal{O}(\epsilon)$ is

$$\begin{aligned} \mathcal{M}_9^{Bubble}(\xi_W = \xi_+ = 1) &= -\frac{g^4[14]\langle 32 \rangle}{36(s-m^2)^2} h(\epsilon) \left[(66 - 4\epsilon) S_{(1)}^4(0|m^2) \right. \\ &\quad \left. + (96m^2 - 93s + (8m^2 - 2s)\epsilon) S_{(1,1)}^4(0, -p_1 - p_2|m^2, m^2) \right] \end{aligned} \quad (5.12)$$

We continue with the bubble diagrams containing a scalar loop

$$\begin{aligned} \mathcal{M}_{10}^{Bubble} &= -\frac{g^4[14]\langle 32 \rangle}{72s(s-m^2)^2} (3 + 2\epsilon) h(\epsilon) \left[(m_h^2 + s - \xi_W m^2) S_{(1)}^4(0|m_h^2) \right. \\ &\quad - (m_h^2 - s - \xi_W m^2) S_{(1)}^4(0|\xi_W m^2) \\ &\quad \left. - (m_h^4 + (s - \xi_W m^2)^2 - 2m_h^2(s + \xi_W m^2)) S_{(1,1)}^4(0, -p_1 - p_2|m_h^2, \xi_W m^2) \right] \end{aligned} \quad (5.13)$$

$$\begin{aligned} \mathcal{M}_{11}^{Bubble} &= -\frac{g^4[14]\langle 32 \rangle}{72s(s-m^2)^2} (3 + 2\epsilon) h(\epsilon) \\ &\quad \times \left[2S_{(1)}^4(0|\xi_+ m^2) - (s - 4\xi_+ m^2) S_{(1,1)}^4(0, -p_1 - p_2|\xi_W m^2, \xi_W m^2) \right] \end{aligned} \quad (5.14)$$

The bubble diagram with a scalar and vector boson simplifies to

$$\begin{aligned} \mathcal{M}_{12}^{Bubble} &= \frac{g^4[14]\langle 32 \rangle}{72s(s-m^2)^2} (3 + 2\epsilon) h(\epsilon) \\ &\quad \left[(m^2 - m_h^2 + s) S_{(1)}^4(0|m^2) + m^2(\xi_W - 1) S_{(1)}^4(0|m_h^2) \right. \\ &\quad + (m_h^2 - s - \xi_W m^2) S_{(1)}^4(0|\xi_W m^2) \\ &\quad + (m_h^4 + (s - \xi_W m^2)^2 - 2m_h^2(s + \xi_W m^2)) S_{(1,1)}^4(0, -p_1 - p_2|m_h^2, \xi_W m^2) \\ &\quad \left. - \left(m^4 + (m_h^2 - s)^2 - 2m^2 \left(m_h^2 + \frac{-15 + 2\epsilon}{3 + 2\epsilon} s \right) \right) S_{(1,1)}^4(0, p_1 + p_2|m^2, m_h^2) \right] \end{aligned} \quad (5.15)$$

Finally, the reduced bubble diagrams containing ghosts read

$$\begin{aligned} \mathcal{M}_{13}^{Bubble} &= \frac{g^4[14]\langle 32 \rangle}{72(s-m^2)^2} (3 + 2\epsilon) h(\epsilon) \left[2S_{(1)}^4(0|\xi_+ m^2) \right. \\ &\quad \left. - (s - 4\xi_+ m^2) S_{(1,1)}^4(0, -p_1 - p_2|\xi_+ m^2, \xi_+ m^2) \right] \end{aligned} \quad (5.16)$$

$$\mathcal{M}_{14}^{Bubble} = \mathcal{M}_{13}^{Bubble} \quad (5.17)$$

Snail diagrams

The four distinct snail diagrams are

$$\mathcal{M}_1^{Snail} = \frac{g^4 [14] \langle 32 \rangle}{8(s-m^2)^2} h(\epsilon) \left[(18 - 15\epsilon) S_{(1)}^4(0|m^2) + (6 - \epsilon) S_{(1)}^4(0|\xi_+ m^2) \right] \quad (5.18)$$

$$\mathcal{M}_2^{Snail} = \frac{g^4 [14] \langle 32 \rangle}{4(s-m^2)^2} h(\epsilon) S_{(1)}^4(0|m_h^2) \quad (5.19)$$

$$\mathcal{M}_3^{Snail} = \frac{g^4 [14] \langle 32 \rangle}{4(s-m^2)^2} h(\epsilon) S_{(1)}^4(0|\xi_W m^2) \quad (5.20)$$

$$\mathcal{M}_4^{Snail} = \frac{g^4 [14] \langle 32 \rangle}{4(s-m^2)^2} h(\epsilon) S_{(1)}^4(0|\xi_+ m^2) \quad (5.21)$$

Tadpole diagrams

The algebraic expressions for the tadpole diagrams read

$$\mathcal{M}_1^{Tadpole} = \frac{g^4 m^2 [14] \langle 32 \rangle}{2m_h^2 (s-m^2)^2} h(\epsilon) \left[(3 - 2\epsilon) S_{(1)}^4(0|m^2) + \xi_W S_{(1)}^4(0|\xi_W m^2) \right] \quad (5.22)$$

$$\mathcal{M}_2^{Tadpole} = \frac{g^4 m^2 [14] \langle 32 \rangle}{2m_h^2 (s-m^2)^2} h(\epsilon) \left[(3 - 2\epsilon) S_{(1)}^4(0|m^2) + \xi_+ S_{(1)}^4(0|\xi_+ m^2) \right] \quad (5.23)$$

$$\mathcal{M}_3^{Tadpole} = \frac{3g^4}{4(s-m^2)^2} [14] \langle 32 \rangle h(\epsilon) S_{(1)}^4(0|m_h^2) \quad (5.24)$$

$$\mathcal{M}_4^{Tadpole} = \frac{g^4}{4(s-m^2)^2} [14] \langle 32 \rangle h(\epsilon) S_{(1)}^4(0|\xi_W m^2) \quad (5.25)$$

$$\mathcal{M}_5^{Tadpole} = \frac{g^4}{4(s-m^2)^2} [14] \langle 32 \rangle h(\epsilon) S_{(1)}^4(0|\xi_+ m^2) \quad (5.26)$$

and the corresponding three ghost diagrams are

$$\mathcal{M}_6^{Tadpole} = \frac{g^4 \xi_W m^2}{4m_h^2 (s-m^2)^2} [14] \langle 32 \rangle h(\epsilon) S_{(1)}^4(0|\xi_W m^2) \quad (5.27)$$

$$\mathcal{M}_7^{Tadpole} = \frac{g^4 \xi_+ m^2}{4m_h^2 (s-m^2)^2} [14] \langle 32 \rangle h(\epsilon) S_{(1)}^4(0|\xi_+ m^2) \quad (5.28)$$

$$\mathcal{M}_8^{Tadpole} = \mathcal{M}_7^{Tadpole} \quad (5.29)$$

Triangle diagrams

The triangle diagrams $\mathcal{M}_1^{Triangle}$ and $\mathcal{M}_4^{Triangle}$ containing the three-vector interaction WW^+W^- are lengthy and only presented in the Feynman gauge

$$\begin{aligned} \mathcal{M}_1^{Triangle}(\xi_W = \xi_+ = 1) &= -\frac{g^4}{8m^2s(s-m^2)} [14] \langle 32 \rangle h(\epsilon) \\ &\left[3sS_{(1)}^4(0|m^2) + m^2(m^2 + 6s)S_{(1,1)}^4(0, p_3|0, m^2) \right. \\ &+ m^2(7m^2 + 8s)S_{(1,1)}^4(0, -p_4|0, m^2) \\ &- (m^2s + 3s^2)S_{(1,1)}^4(0, p_3 + p_4|m^2, 0) \\ &- (8m^4 + 4m^2s - 3s^2)S_{(1,1)}^4(0, p_3 + p_4|m^2, m^2) \\ &\left. + 8m^4(m^2 + 2s)S_{(1,1,1)}^4(0, -p_4, p_3|0, m^2, m^2) \right] \end{aligned} \quad (5.30)$$

$$\begin{aligned} \mathcal{M}_4^{Triangle}(\xi_W = \xi_+ = 1) &= -\frac{g^4}{8m^2s(s-m^2)} [14] \langle 32 \rangle h(\epsilon) \\ &\left[3sS_{(1)}^4(0|m^2) + m^2(m^2 + 6s)S_{(1,1)}^4(0, p_2|0, m^2) \right. \\ &+ m^2(7m^2 + 8s)S_{(1,1)}^4(0, -p_1|0, m^2) \\ &- (m^2s + 3s^2)S_{(1,1)}^4(0, p_1 + p_2|m^2, 0) \\ &- (8m^4 + 4m^2s - 3s^2)S_{(1,1)}^4(0, p_1 + p_2|m^2, m^2) \\ &\left. + 8m^4(m^2 + 2s)S_{(1,1,1)}^4(0, -p_1, p_2|0, m^2, m^2) \right] \end{aligned} \quad (5.31)$$

The full expressions for the other four triangle diagrams are simpler in nature, and their full reduction reads

$$\begin{aligned}
 \mathcal{M}_2^{Triangle} &= \frac{g^4}{96s(s-m^2)} [14] \langle 32 \rangle h(\epsilon) \\
 &\times \left[(18s + 12s\epsilon) S_{(1)}^4(0|m^2) - \zeta_+ (18s + 12s\epsilon) S_{(1)}^4(0|\zeta_+ m^2) \right. \\
 &+ (18m^4 + 78m^2s + (21m^4 - 3m^2s - 48s^2)\epsilon) S_{(1,1)}^4(0, p_3|m^2, 0) \\
 &+ (18m^4 + 30m^2s + (21m^4 + 45m^2s - 48s^2)\epsilon) S_{(1,1)}^4(0, -p_4|m^2, 0) \\
 &- \zeta_+^2 (30m^2s + 18m^4\zeta_+ + 21m^2(s + \zeta_+ m^2)\epsilon) \\
 &\quad \times (S_{(1,1)}^4(0, p_3|\zeta_+ m^2, 0) + S_{(1,1)}^4(0, -p_4|\zeta_+ m^2, 0)) \\
 &+ (-36m^3 - 126m^2s + 24s^2\zeta_+ + 78m^2s\zeta_+^2 + 36m^4\zeta_+^3 \\
 &+ (-42m^4 - 63m^2s + 32s^2 + 16s^2\zeta_+ + 63m^2s\zeta_+^2 + 42m^4\zeta_+^3)\epsilon) \\
 &\quad \times S_{(1,1)}^4(0, p_3 + p_4|0, 0) \\
 &+ (-36m^6 + 144m^4s + 60m^2s^2) S_{(1,1,1)}^4(0, -p_4, p_3|m^2, 0, 0) \\
 &\left. + \zeta_+^2 (60m^2s^2 + 96m^4s + 36m^6) S_{(1,1,1)}^4(0, -p_4, p_3|\zeta_+ m^2, 0, 0) \right] \quad (5.32)
 \end{aligned}$$

$$\mathcal{M}_3^{Triangle} = 2\mathcal{M}_2^{Triangle} \quad (5.33)$$

$$\begin{aligned}
 \mathcal{M}_5^{Triangle} &= \frac{g^4}{8s^2m^2(s-m^2)} [14] \langle 32 \rangle h(\epsilon) \\
 &\left[2s(m^2 + 2s) S_{(1)}^4(0|m^2) - 2s(m^2\zeta_W + 2s) S_{(1)}^4(0|\zeta_W m^2) \right. \\
 &+ (m^6 + m^4 - 4m^2s^2 - 2m^4s\epsilon) S_{(1,1)}^4(0, -p_1|m^2, 0) \\
 &- m^4\zeta_W^2 (s + m^2\zeta_W) S_{(1,1)}^4(0, -p_1|\zeta_W m^2, 0) \\
 &- m^2(m^4 + 7m^2s + 6s^2 - m^2s\epsilon) S_{(1,1)}^4(0, p_2|m^2, 0) \\
 &+ m^2\zeta_W (2s^2 + 3m^2s\zeta_W + m^4\zeta_W^2) S_{(1,1)}^4(0, p_2|\zeta_W m^2, 0) \\
 &+ 2m^2s(2m^2 + 3s + 2s\epsilon) S_{(1,1)}^4(0, p_1 + p_2|0, 0) \\
 &\left. + 4m^2s(m^2 + s)^2 S_{(1,1,1)}^4(0, -p_1, p_2|m^2, 0, 0) \right] \\
 \mathcal{M}_6^{Triangle} &= 2\mathcal{M}_5^{Triangle} \quad (5.34)
 \end{aligned}$$

Box Diagrams

The full tensor expression of the first box diagram in the 't Hooft gauge is

$$\mathcal{M}_1^{Box} = \frac{g^4}{16} \langle 2 | \gamma_\rho \gamma_\alpha \gamma_\mu | 1 \rangle \langle 3 | \gamma_\nu \gamma_\beta \gamma_\eta | 4 \rangle h(\epsilon) \left(\sum_{i=1}^6 T_i^1 \right)^{\rho\alpha\mu\nu\beta\eta} \quad (5.35)$$

where the tensor contributions $T_i^{1,\rho\alpha\mu\nu\beta\eta}$ correspond to Lorentz invariants multiplied by tensor integrals. Using the short forms of the following integrals

$$\begin{aligned} S_4^{d,\alpha\dots} &\equiv S^{d,\alpha\dots}(0, -p_1, p_2, p_2 - p_4 | 0, m^2, m^2, 0) \\ S_5^{d,\alpha\dots} &\equiv S^{d,\alpha\dots}(0, 0, -p_1, p_2, p_2 - p_4 | 0, 0, m^2, m^2, 0) \\ S_{5(1)}^{d,\alpha\dots} &\equiv S^{d,\alpha\dots}(0, -p_1, -p_1, p_2, p_2 - p_4 | 0, 0, \xi_W m^2, m^2, 0) \\ S_{5(2)}^{d,\alpha\dots} &\equiv S^{d,\alpha\dots}(0, p_2, -p_1, p_2, p_2 - p_4 | 0, 0, m^2, \xi_W m^2, 0) \\ S_6^{d,\alpha\dots} &\equiv S^{d,\alpha\dots}(0, -p_1, p_2, -p_1, p_2, p_2 - p_4 | 0, 0, 0, m^2, m^2, 0) \\ S_{6(1)}^{d,\alpha\dots} &\equiv S^{d,\alpha\dots}(0, -p_1, p_2, -p_1, p_2, p_2 - p_4 | 0, 0, 0, \xi_W m^2, m^2, 0) \\ S_{6(2)}^{d,\alpha\dots} &\equiv S^{d,\alpha\dots}(0, -p_1, p_2, -p_1, p_2, p_2 - p_4 | 0, 0, 0, m^2, \xi_W m^2, 0) \\ S_{6(12)}^{d,\alpha\dots} &\equiv S^{d,\alpha\dots}(0, -p_1, p_2, -p_1, p_2, p_2 - p_4 | 0, 0, 0, \xi_W m^2, \xi_W m^2, 0) \end{aligned} \quad (5.36)$$

allows us to express the kinematical factors in a relatively compact way

$$T_1^{1,\rho\alpha\mu\nu\beta\eta} = (p_2 - p_4)^\beta g^{\mu\nu} g^{\rho\eta} S_4^{d,\alpha} \quad (5.37)$$

$$\begin{aligned} T_2^{1,\rho\alpha\mu\nu\beta\eta} &= g^{\mu\nu} g^{\rho\eta} S_4^{d,\alpha\beta} \\ &\quad + (p_2 - p_4)^\beta \left[p_1^\nu g^{\rho\eta} \left(S_5^{d,\alpha\mu} - \xi_W S_{5(1)}^{d,\alpha\mu} \right) \right. \\ &\quad \left. - p_2^\eta g^{\mu\nu} \left(S_5^{d,\alpha\mu} - \xi_W S_{5(2)}^{d,\alpha\mu} \right) \right] \end{aligned} \quad (5.38)$$

$$\begin{aligned} T_3^{1,\rho\alpha\mu\nu\beta\eta} &= (p_2 - p_4)^\beta \left[g^{\mu\nu} \left(S_5^{d,\alpha\rho\eta} - \xi_Z S_{5(1)}^{d,\alpha\rho\eta} \right) + g^{\rho\eta} \left(S_5^{d,\alpha\mu\nu} - \xi_W S_{5(1)}^{d,\alpha\mu\nu} \right) \right. \\ &\quad \left. + p_1^\nu p_2^\eta \left(-S_6^{d,\alpha\mu\rho} + \xi_W \left(S_{6(1)}^{d,\alpha\mu\rho} + S_{6(2)}^{d,\alpha\mu\rho} \right) - \xi_W^2 S_{6(12)}^{d,\alpha\mu\rho} \right) \right] \end{aligned} \quad (5.39)$$

$$\begin{aligned} T_4^{1,\rho\alpha\mu\nu\beta\eta} &= g^{\mu\nu} \left(-S_5^{d,\alpha\beta\rho\eta} + \xi_W S_{5(1)}^{d,\alpha\beta\rho\eta} \right) + g^{\rho\eta} \left(-S_5^{d,\alpha\beta\mu\nu} + \xi_W S_{5(2)}^{d,\alpha\beta\mu\nu} \right) \\ &\quad + p_1^\nu p_2^\eta \left(-S_6^{d,\alpha\beta\mu\rho} + \xi_Z \left(S_{6(1)}^{d,\alpha\beta\mu\rho} + S_{6(2)}^{\alpha\beta\mu\rho} \right) - \xi_W^2 S_{6(12)}^{d,\alpha\beta\mu\rho} \right) \\ &\quad + (p_2 - p_4)^\beta \left[p_1^\nu \left(-S_6^{d,\alpha\mu\rho\eta} + \xi_W \left(S_{6(1)}^{d,\alpha\mu\rho\eta} + S_{6(2)}^{d,\alpha\mu\rho\eta} \right) - \xi_W^2 S_{6(12)}^{d,\alpha\mu\rho\eta} \right) \right. \\ &\quad \left. + p_2^\eta \left(S_6^{d,\alpha\mu\rho\nu} - \xi_W \left(S_{6(1)}^{d,\alpha\mu\rho\nu} + S_{6(2)}^{d,\alpha\mu\rho\nu} \right) + \xi_W^2 S_{6(12)}^{d,\alpha\mu\rho\nu} \right) \right] \end{aligned} \quad (5.40)$$

$$T_5^{1,\rho\alpha\mu\nu\beta\eta} = p_1^\nu \left(-S_6^{d,\alpha\beta\mu\rho\eta} + \xi_W \left(S_{6(1)}^{\alpha\beta\mu\rho\eta} + S_{6(2)}^{d,\alpha\beta\mu\rho\eta} \right) - \xi_W^2 S_{6(12)}^{d,\alpha\beta\mu\rho\eta} \right)$$

$$\begin{aligned}
 & + p_2^\eta \left(-S_6^{d,\alpha\beta\mu\nu\rho} + \xi_W (S_{6(1)}^{\alpha\beta\mu\nu\rho} + S_{6(2)}^{d,\alpha\beta\mu\nu\rho}) - \xi_W^2 S_{6(12)}^{d,\alpha\beta\mu\nu\rho} \right) \\
 & + (p_2 - p_4)^\beta \left(S_6^{d,\alpha\mu\nu\rho\eta} - \xi_W (S_{6(1)}^{\alpha\mu\nu\rho\eta} + S_{6(2)}^{d,\alpha\mu\nu\rho\eta}) + \xi_W^2 S_{6(12)}^{d,\alpha\mu\nu\rho\eta} \right) \\
 T_6^{1,\rho\alpha\mu\nu\beta\eta} = & S_6^{d,\alpha\beta\mu\nu\rho\eta} - \xi_W (S_{6(1)}^{d,\alpha\beta\mu\nu\rho\eta} + S_{6(2)}^{d,\alpha\beta\mu\nu\rho\eta}) + \xi_W^2 S_{6(12)}^{d,\alpha\beta\mu\nu\rho\eta} \quad (5.41)
 \end{aligned}$$

The second box diagram only differs by a factor of four due to the similar vertex rules in appendix (C.4)

$$\mathcal{M}_2^{Box} = 4\mathcal{M}_1^{Box} \quad (5.42)$$

The final box diagram with twisted external legs \mathcal{M}_3^{Box} can be obtained from \mathcal{M}_1^{Box} by exchanging p_4 with p_3 and flipping the second tensor chain

$$\mathcal{M}_3^{Box} = \frac{g^4}{16} \langle 2|\gamma_\rho\gamma_\alpha\gamma_\mu|1\rangle \langle 3|\gamma_\eta\gamma_\beta\gamma_\nu|4\rangle h(\epsilon) \left(\sum_{i=1}^6 T_i^1(p_4 \rightarrow p_3) \right)^{\rho\alpha\mu\nu\beta\eta} \quad (5.43)$$

The evaluation of all tensor contractions and scalar reductions would be extremely tiresome by hand, so especially for these kinds integrals our package becomes almost indispensable.

5. Results

For clarity, the final reduction is again only given in the Feynman gauge

$$\begin{aligned}
\mathcal{M}_1^{Box}(\zeta_W = \zeta_+ = 1) &= -\frac{g^4}{8(s+t)^2} [14] \langle 32 \rangle h(\epsilon) \\
&\times \left[-2(s+t) (S_{(1,1)}^4(0, p_1 + p_2 | m^2, m^2) - S_{(1,1)}^4(0, p_2 - p_4 | 0, 0)) \right. \\
&+ (2m^2s + st - (s+t)(s+2t) + (2m^2s - s^2)\epsilon) S_{(1,1,1)}^4(0, -p_1, p_2 | 0, m^2, m^2) \\
&+ (t(2m^2 + s + 2t) - s(2m^2 + t)\epsilon) \\
&\quad \times (S_{(1,1,1)}^4(0, -p_1, p_2 - p_4 | 0, m^2, 0) + S_{(1,1,1)}^4(0, p_2, p_2 - p_4 | 0, m^2, 0)) \\
&+ (2m^2s - s^2 - 2t(s+t) + (2m^2s + s^2)\epsilon) S_{(1,1,1)}^4(-p_1, p_2, p_2 - p_4 | m^2, m^2, 0) \\
&+ (m^4(t-s) + s^2t + 4m^2t^2 + 2t^2(s+t) + (s^2t - 4m^2s(m^2+t))\epsilon) \\
&\quad \left. \times S_{(1,1,1,1)}^4(0, -p_1, p_2, p_2 - p_4 | 0, m^2, m^2, 0) \right] \tag{5.44}
\end{aligned}$$

$$\mathcal{M}_2^{Box} = 4\mathcal{M}_1^{Box} \tag{5.45}$$

$$\begin{aligned}
\mathcal{M}_3^{Box}(\zeta_W = \zeta_+ = 1) &= -\frac{g^4}{8t} [14] \langle 32 \rangle h(\epsilon) \\
&\times \left[2(-t + (s - 2m^2)\epsilon) S_{(1,1,1)}^4(0, -p_1, p_2 | 0, m^2, m^2) \right. \\
&+ 2(2m^2 - s - t) \\
&\quad \times (S_{(1,1,1)}^4(0, -p_1, p_2 - p_3 | 0, m^2, 0) + S_{(1,1,1)}^4(0, p_2, p_2 - p_3 | 0, m^2, 0)) \\
&- 2(t + (2m^2 - s)\epsilon) S_{(1,1,1)}^4(-p_1, p_2, p_2 - p_3 | m^2, m^2, 0) \\
&- 2(t(s+t) - (5m^4 - 4m^2(s+t) + s(s+t))\epsilon) \\
&\quad \left. \times S_{(1,1,1,1)}^4(0, -p_1, p_2, p_2 - p_3 | 0, m^2, m^2, 0) \right] \tag{5.46}
\end{aligned}$$

5.3. FMS loop expressions

5.3.1. Feynman diagrams

The full bound-state treatment at NLO yields twelve matrix elements from the six-point functions and nine matrix elements from the eight-point functions. The twelve six-point functions, scaled by v^2 , read

$$\begin{aligned} & \frac{1}{4} \langle e_L^- e_L^- [h\mu_L^-] [h\mu_L^-] \rangle, \quad \frac{1}{4} \langle e_L^- e_L^- [\chi\mu_L^-] [\chi\mu_L^-] \rangle, \\ & \frac{i}{4} \langle e_L^- e_L^- [h\mu_L^-] [\chi\mu_L^-] \rangle, \quad -\frac{i}{4} \langle e_L^- e_L^- [\chi\mu_L^-] [h\mu_L^-] \rangle, \quad \frac{1}{2} \langle e_L^- e_L^- [\phi^- v_{\mu L}] [\phi^+ \bar{v}_{\mu L}] \rangle, \\ & \frac{1}{4} \langle [he_L^-] [he_L^-] \mu_L^- \mu_L^- \rangle, \quad \frac{1}{4} \langle [\chi e_L^-] [\chi e_L^-] \mu_L^- \mu_L^- \rangle, \\ & \frac{i}{4} \langle [he_L^-] [\chi e_L^-] \mu_L^- \mu_L^- \rangle, \quad -\frac{i}{4} \langle [\chi e_L^-] [he_L^-] \mu_L^- \mu_L^- \rangle, \quad \frac{1}{2} \langle [\phi^- v_{eL}] [\phi^+ \bar{v}_{eL}] \mu_L^- \mu_L^- \rangle \end{aligned} \quad (5.47)$$

Each of the contributions containing h and χ generates exactly one triangle diagram, whereas the terms involving ϕ^\pm yield two triangle diagrams, as seen in figure (5.9).

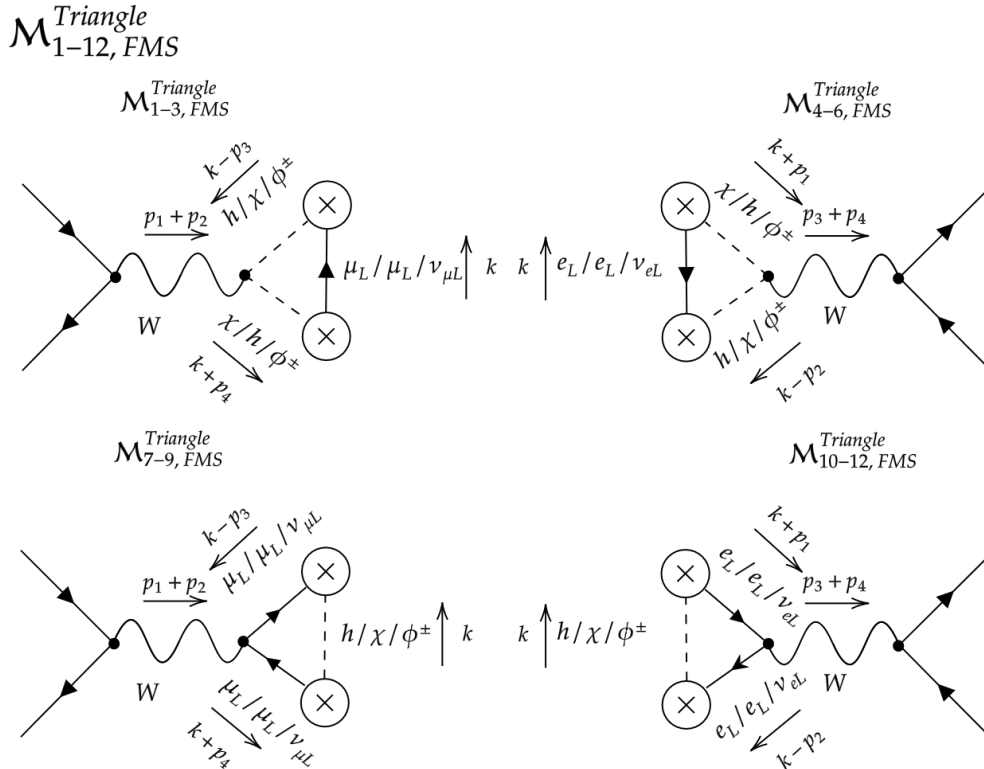


Figure 5.9.: Full list of all triangle diagrams arising from six-point functions

5. Results

Furthermore, the nine different eight-point functions

$$\begin{aligned}
 & \frac{1}{4} \langle [he_L^-][he_L^-][h\mu_L^-][h\mu_L^-] \rangle, \quad -\frac{1}{4} \langle [he_L^-][\chi e_L^-][h\mu_L^-][\chi\mu_L^-] \rangle, \\
 & -\frac{1}{4} \langle [\chi e_L^-][he_L^-][\chi\mu_L^-][h\mu_L^-] \rangle, \quad \frac{1}{4} \langle [\chi e_L^-][\chi e_L^-][\chi\mu_L^-][\chi\mu_L^-] \rangle, \\
 & \langle [\phi^- v_{eL}][\phi^+ \bar{v}_{eL}][\phi^- v_{\mu L}][\phi^+ \bar{v}_{\mu L}] \rangle
 \end{aligned} \tag{5.48}$$

yield the box diagrams presented in (5.10).

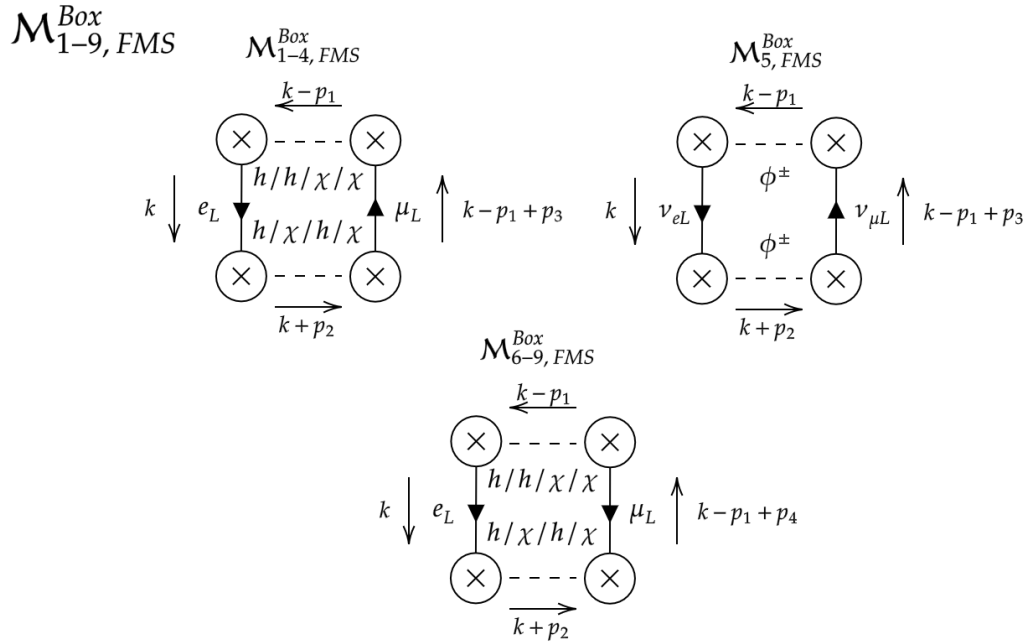


Figure 5.10.: Full list of all box diagrams arising from eight-point functions

No other diagram at NLO appears for our process. The same holds for all other chirality combinations of external states. Overall, this means that there are a total of 21 new matrix elements in addition to the 37 regular matrix elements. How do their algebraic expressions look like?

5.3.2. Reduced algebraic expressions

Triangle diagrams

We start off with a step-by-step decomposition of the triangle diagram seen in figure (5.11), corresponding to the six-point function $-\frac{i}{4v^2}\langle e_L^- e_L^- [\chi\mu_L^-][h\mu_L^-]\rangle$.

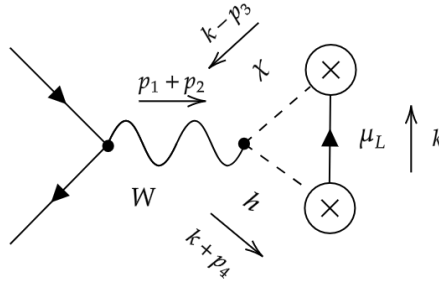


Figure 5.11.: Exemplary FMS contribution

Applying all Feynman rules and extracting all Dirac chains results in

$$i\mathcal{M}_{1,FMS}^{Triangle} = \frac{K_3 K_4}{4v^2} \langle 2 | \left(-\frac{ig}{2} \gamma_\mu \right) | 1 \rangle \left(\frac{-ig^{\mu\alpha}}{s-m^2} \right) \langle 3 | \gamma_\beta | 4 \rangle \\ \times \frac{(\mu)^{4-d}}{(2\pi)^d} \int d^d k g k_\alpha \frac{k^\beta}{k^2} \frac{i}{(k-p_3)^2 - \xi_W m^2} \frac{i}{(k+p_4)^2 - m_h^2} \quad (5.49)$$

where we introduced the external wavefunction renormalizations K_3 and K_4 for the compound final states. They carry mass dimension one and ensure that the whole diagram stays dimensionless. We can compactify this expression by contracting the metric tensor and by using the notation from equation (3.41) to write

$$\mathcal{M}_{1,FMS}^{Triangle} = \frac{g^2 K_3 K_4}{8v^2} \frac{1}{s-m^2} \langle 2 | \gamma_\alpha | 1 \rangle \langle 3 | \gamma_\beta | 4 \rangle h(\epsilon) S_{(1,1,1)}^{\alpha\beta}(0, -p_3, p_4 | 0, \xi_W m^2, m_h^2) \quad (5.50)$$

The explicit tensor decomposition of $S_{(1,1,1)}^{\alpha\beta}$ is derived from equation (3.42) and yields

$$S_{(1,1,1)}^{\alpha\beta}(0, -p_3, p_4 | 0, \xi_W m^2, m_h^2) = -\frac{1}{2} g^{\alpha\beta} S_{(1,1,1)}^6 + 2p_3^\alpha p_3^\beta S_{(1,3,1)}^8 + 2p_4^\alpha p_4^\beta S_{(1,1,3)}^8 \\ - (p_3^\alpha p_4^\beta + p_4^\alpha p_3^\beta) S_{(1,2,2)}^8 \quad (5.51)$$

The terms containing four-momenta vanish again for our massless Weyl spinors, and the remaining expression reads

$$\mathcal{M}_{1,FMS}^{Triangle} = -\frac{g^2 K_3 K_4 [14] \langle 32 \rangle}{8v^2 (s-m^2)} h(\epsilon) S_{(1,1,1)}^6(0, -p_3, p_4 | 0, \xi_W m^2, m_h^2) \quad (5.52)$$

5. Results

Finally, we apply the recursion relation (3.47) to the scalar integral in order to express it in terms of our master integrals

$$\begin{aligned} \mathcal{M}_{1,FMS}^{Triangle} &= \frac{g^2 K_3 K_4 [14] \langle 32 \rangle}{16s v^2 (s - m^2)} h(\epsilon) (1 + \epsilon) \\ &\times \left[\xi_W m^2 S_{(1,1)}^4(0, -p_3 | 0, \xi_W m^2) + m_h^2 S_{(1,1)}^4(0, p_4 | 0, m_h^2) \right. \\ &+ (s - m_h^2 - \xi_W m^2) S_{(1,1)}^4(0, p_3 + p_4 | \xi_W m^2, m_h^2) \\ &\left. + 2\xi_W m^2 m_h^2 S_{(1,1,1)}^4(0, -p_3, p_4 | 0, \xi_W m^2, m_h^2) \right] \end{aligned} \quad (5.53)$$

Similarly, we obtain for $\frac{i}{4v^2} \langle e_L^- e_L^- [h\mu_L^-] [\chi\mu_L^-] \rangle$ and $\frac{1}{2v^2} \langle e_L^- e_L^- [\phi^- \nu_{\mu L}] [\phi^+ \bar{\nu}_{\mu L}] \rangle$

$$\mathcal{M}_{2,FMS}^{Triangle} = \mathcal{M}_{1,FMS}^{Triangle} (m_h^2 \rightarrow \xi_W m^2) \quad (5.54)$$

$$\mathcal{M}_{3,FMS}^{Triangle} = 2\mathcal{M}_{1,FMS}^{Triangle} (m_h^2 \rightarrow \xi_+ m^2) \quad (5.55)$$

The three triangle diagrams with one scalar line, corresponding to $\frac{1}{4v^2} \langle e_L^- e_L^- [h\mu_L^-] [h\mu_L^-] \rangle$, $\frac{1}{4v^2} \langle e_L^- e_L^- [\chi\mu_L^-] [\chi\mu_L^-] \rangle$ and again $\frac{1}{2v^2} \langle e_L^- e_L^- [\phi^- \nu_{\mu L}] [\phi^+ \bar{\nu}_{\mu L}] \rangle$, result in the expressions

$$\begin{aligned} \mathcal{M}_{4,FMS}^{Triangle} &= \frac{g^2 K_3 K_4 [14] \langle 32 \rangle}{8s(s - m^2)v^2} h(\epsilon) \\ &\times \left[-m_h^2 \epsilon S_{(1,1)}^4(0, -p_4 | m_h^2, 0) - (2m_h^2 + m_h^2 \epsilon) S_{(1,1)}^4(0, p_3 | m_h^2, 0) \right. \\ &+ (2\xi_W m^2 - s + (s + 2\xi_W m^2)\epsilon) S_{(1,1)}^4(0, p_3 + p_4 | 0, 0) \\ &\left. + 2\xi_W^2 m^4 S_{(1,1,1)}^4(0, -p_4, p_3 | m_h^2, 0, 0) \right] \end{aligned} \quad (5.56)$$

$$\mathcal{M}_{5,FMS}^{Triangle} = \mathcal{M}_{4,FMS}^{Triangle} (m_h^2 \rightarrow \xi_W m^2) \quad (5.57)$$

$$\mathcal{M}_{6,FMS}^{Triangle} = -2\mathcal{M}_{5,FMS}^{Triangle} (m_h^2 \rightarrow \xi_+ m^2) \quad (5.58)$$

The same line of reasoning follows for the other six triangle diagrams with bound-state contributions to the initial states. We only need to exchange $p_3 \rightarrow p_1$, $p_4 \rightarrow p_2$ and $K_{3,4} \rightarrow K_{1,2}$.

$$\mathcal{M}_{7,FMS}^{Triangle} = \mathcal{M}_{1,FMS}^{Triangle} (p_3 \rightarrow p_1, p_4 \rightarrow p_2, K_{3,4} \rightarrow K_{1,2}) \quad (5.59)$$

$$\mathcal{M}_{8,FMS}^{Triangle} = \mathcal{M}_{7,FMS}^{Triangle} (m_h^2 \rightarrow \xi_W m^2) \quad (5.60)$$

$$\mathcal{M}_{9,FMS}^{Triangle} = 2\mathcal{M}_{7,FMS}^{Triangle} (m_h^2 \rightarrow \xi_+ m^2) \quad (5.61)$$

$$\mathcal{M}_{10,FMS}^{Triangle} = \mathcal{M}_{4,FMS}^{Triangle} (p_1 \rightarrow p_3, p_2 \rightarrow p_4) \quad (5.62)$$

$$\mathcal{M}_{11,FMS}^{Triangle} = \mathcal{M}_{10,FMS}^{Triangle} (m_h^2 \rightarrow \xi_W m^2) \quad (5.63)$$

$$\mathcal{M}_{12,FMS}^{Triangle} = -2\mathcal{M}_{10,FMS}^{Triangle} (m_h^2 \rightarrow \xi_+ m^2) \quad (5.64)$$

Box diagrams

The box diagrams arising from the full FMS treatment contain two scalar and two fermionic lines that are integrated over. Their full reductions are listed below, and contain again wave-function renormalization factors K_i . The first five diagrams (upper two diagrams in 5.10) can be derived in terms of diagram $\mathcal{M}_{2,FMS}^{Box}$ by replacing the masses accordingly. They simplify to

$$\begin{aligned}
 \mathcal{M}_{2,FMS}^{Box} &= -\frac{K_1 K_2 K_3 K_4}{8(s+t)^2 v^4} [14] \langle 32 \rangle h(\epsilon) \\
 &\times \left[-2(s+t) S_{(1,1)}^4(0, -p_1 + p_3 | 0, 0) + 2(s+t) S_{(1,1)}^4(0, p_1 + p_2 | \xi_W m^2, m_h^2) \right. \\
 &+ t(s - m_h^2 - \xi_W m^2) \\
 &\quad \times (S_{(1,1,1)}^4(0, -p_1, -p_1 + p_3 | 0, \xi_W m^2, 0) + S_{(1,1,1)}^4(0, p_2, -p_1 + p_3 | 0, m_h^2, 0)) \\
 &+ s(s - m_H^2 - \xi_W m^2) \\
 &\quad \times (S_{(1,1,1)}^4(0, -p_1, p_2 | 0, \xi_W m^2, m_h^2) + S_{(1,1,1)}^4(0, -p_3, p_4 | 0, \xi_W m^2, m_h^2)) \\
 &- (m_h^2 t + t(s - \xi_W m^2)^2 - 2m^2 s(t + \xi_W m^2)) \\
 &\quad \left. \times S_{(1,1,1,1)}^4(0, -p_1, p_2, -p_1 + p_3 | 0, \xi_W m^2, m_h^2, 0) \right] \tag{5.65}
 \end{aligned}$$

$$\mathcal{M}_{1,FMS}^{Box} = -\mathcal{M}_{2,FMS}^{Box}(\xi_W m^2 \rightarrow m_h^2) \tag{5.66}$$

$$\mathcal{M}_{3,FMS}^{Box} = \mathcal{M}_{2,FMS}^{Box}(\xi_W m^2 \rightarrow m_h^2, m_h^2 \rightarrow \xi_W m^2) \tag{5.67}$$

$$\mathcal{M}_{4,FMS}^{Box} = -\mathcal{M}_{2,FMS}^{Box}(m_h^2 \rightarrow \xi_W m^2) \tag{5.68}$$

$$\mathcal{M}_{5,FMS}^{Box} = -4\mathcal{M}_{2,FMS}^{Box}(\xi_W m^2 \rightarrow \xi_+ m^2, m_h^2 \rightarrow \xi_+ m^2) \tag{5.69}$$

The different prefactors originate from the expansion of the elementary constituents within the FMS expansion of the compound leptons in equation (2.23) and (2.25).

5. Results

The other four box diagrams with a flipped fermion line in the final states can most easily be expressed in terms of $\mathcal{M}_{7,FMS}^{Box}$

$$\begin{aligned}
\mathcal{M}_{7,FMS}^{Box} = & -\frac{1}{8t(s+t)v^4} [14] \langle 32 \rangle h(\epsilon) \\
& \times \left[6tS_{(1,1)}^4(0, -p_1 + p_4 | 0, 0) - 2tS_{(1,1)}^4(0, p_1 + p_2 | m_h^2, \xi_W m^2) \right. \\
& - 2tS_{(1,1)}^4(0, p_1 + p_2 | \xi_W m^2, m_h^2) - 2tS_{(1,1)}^4(0, p_1 + p_2 | \xi_W m^2, \xi_W m^2) \\
& + st(S_{(1,1,1)}^4(0, -p_1, p_2 | 0, m_h^2, \xi_W m^2) + S_{(1,1,1)}^4(0, -p_1, p_2 | 0, \xi_W m^2, \xi_W m^2)) \\
& + s(m_h^2 - s + \xi_W m^2)S_{(1,1,1)}^4(0, -p_1, p_2 | 0, \xi_W m^2, m_h^2) \\
& + t(2m_h^2 - s - t)S_{(1,1,1)}^4(0, -p_1, -p_1 + p_4 | 0, \xi_W m^2, 0) \\
& + t(s + 2t)(S_{(1,1,1)}^4(-p_1, p_2, -p_1 + p_4 | m_h^2, \xi_W m^2, 0) \\
& \quad + S_{(1,1,1)}^4(-p_1, p_2, -p_1 + p_4 | \xi_W m^2, \xi_W m^2, 0)) \\
& + s(m_h^2 - s + \xi_W m^2)S_{(1,1,1)}^4(-p_1, p_2, -p_1 + p_4 | \xi_W m^2, m_h^2, 0) \\
& + (t(s + t)(s - \xi_W m^2) - m_h^2 t(s + t - 2\xi_W m^2)) \\
& \quad \times S_{(1,1,1,1)}^4(0, -p_1, p_2, -p_1 + p_4 | 0, m_h^2, \xi_W m^2, 0) \\
& + 2\xi_W m^2 m_h^2 t S_{(1,1,1,1)}^4(0, -p_1, p_2, -p_1 + p_4 | 0, \xi_W m^2, m_h^2, 0) \\
& + t(s^2 + s(t - 2\xi_W m^2) + 2\xi_W m^2(\xi_W m^2 - t)) \\
& \quad \times S_{(1,1,1,1)}^4(0, -p_1, p_2, -p_1 + p_4 | 0, \xi_W m^2, \xi_W m^2, 0) \left. \right] \tag{5.70}
\end{aligned}$$

$$\mathcal{M}_{6,FMS}^{Box} = -\mathcal{M}_{7,FMS}^{Box}(\xi_W m^2 \rightarrow m_h^2) \tag{5.71}$$

$$\mathcal{M}_{8,FMS}^{Box} = \mathcal{M}_{7,FMS}^{Box}(\xi_W m^2 \rightarrow m_h^2, m_h^2 \rightarrow \xi_W m^2) \tag{5.72}$$

$$\mathcal{M}_{9,FMS}^{Box} = -\mathcal{M}_{7,FMS}^{Box}(m_h^2 \rightarrow \xi_W m^2) \tag{5.73}$$

The signs originate again from the prefactors of the FMS expansion.

6. Conclusion and Future Work

We have showcased a novel approach to perturbative calculations of leptonic scattering processes by using an augmented gauge-invariant description for the weak sector of the SM. After summarizing the usual picture of the weak interaction in sections (2.1) and (2.2), we show how this so-called FMS formalism leads to a change in particle phenomenology (2.3) with bound-state external leptons composed of scalar Higgs particles and the usual leptons. These composite-state objects were linked to higher n-point functions in terms of elementary particles via a FMS expansion through splitting the Higgs doublet into the vev v and its fluctuation fields. The leading term of this expansion is the usual elementary four-point function, with higher Green's functions yielding new invariant matrix elements that can potentially effect the perturbative description of scattering process at NLO (2.4). We investigated a bound-state formulation of the leptonic scattering process $e_L^- e_L^+ \rightarrow \mu_L^- \mu_L^+$ at NLO via an augmented perturbation theory (APT) by employing the SH formalism (3.1) and the Davydychev reduction (3.2) to express matrix elements in terms of spinor products and scalar master integrals. We developed a toolkit to automatically create Feynman diagrams via QGraf (4.1) and calculate the corresponding matrix elements using Mathematica (4.2). We presented the tree-level differential cross section (5.1) and loop corrections in (5.2) and (5.3). New invariant matrix elements \mathcal{M}_{FMS} occur due to higher n-point functions, with twelve non-vanishing triangle diagrams that arise from the six-point functions

$$\begin{aligned}
 & \langle e_L^- e_L^- [h\mu_L^-] [h\mu_L^-] \rangle, \langle e_L^- e_L^- [\chi\mu_L^-] [\chi\mu_L^-] \rangle, \\
 & \langle e_L^- e_L^- [h\mu_L^-] [\chi\mu_L^-] \rangle, \langle e_L^- e_L^- [\chi\mu_L^-] [h\mu_L^-] \rangle, \langle e_L^- e_L^- [\phi^- \nu_{\mu L}] [\phi^+ \bar{\nu}_{\mu L}] \rangle, \\
 & \langle [he_L^-] [he_L^-] \mu_L^- \mu_L^- \rangle, \langle [\chi e_L^-] [\chi e_L^-] \mu_L^- \mu_L^- \rangle, \\
 & \langle [he_L^-] [\chi e_L^-] \mu_L^- \mu_L^- \rangle, \langle [\chi e_L^-] [he_L^-] \mu_L^- \mu_L^- \rangle, \langle [\phi^- \nu_{e L}] [\phi^+ \bar{\nu}_{e L}] \mu_L^- \mu_L^- \rangle \quad (6.1)
 \end{aligned}$$

and nine box diagrams that arise from the eight-point functions

$$\begin{aligned}
&\langle [he_L^-][he_L^-][h\mu_L^-][h\mu_L^-] \rangle, \langle [he_L^-][\chi e_L^-][h\mu_L^-][\chi\mu_L^-] \rangle, \\
&\langle [\chi e_L^-][he_L^-][\chi\mu_L^-][h\mu_L^-] \rangle, \langle [\chi e_L^-][\chi e_L^-][\chi\mu_L^-][\chi\mu_L^-] \rangle, \\
&\langle [\phi^- \nu_{eL}][\phi^+ \bar{\nu}_{eL}][\phi^- \nu_{\mu L}][\phi^+ \bar{\nu}_{\mu L}] \rangle
\end{aligned} \tag{6.2}$$

These contributions can be treated the same way as the standard one-loop diagrams, with a modified wave functional renormalization appearing for each bound-state insertion. A visual summary of the higher n-point functions with non-vanishing Feynman diagrams is given in figure (6.1). All diagrams in our model are IR-convergent, and the reduced forms of the diagrams in section (5.3.2) yield the same types of scalar integrals that appear for the standard matrix elements. We successfully expanded on the effects of the Higgs constituents in a perturbative setting [14], where no discrepancy between our results and the formulation of leptonic bound states in terms of PDFs appears.

6. Conclusion and Future Work

Topology	$\langle e_L^- e_L^+ \mu_L^- \mu_L^+ \rangle$	$\langle [\phi_i] I [\phi_j] \mu_L^- \mu_L^+ \rangle$ $\langle e_L^- e_L^+ [\phi_i] I [\phi_j] \rangle$	$\langle [\phi_i] I [\phi_j] I [\phi_k] I [\phi_s] \rangle$
Bubble		\times	\times
Tadpole		\times	\times
Snail		\times	\times
Triangle			\times
Box		\times	

Figure 6.1.: Summary of all types of matrix elements due to the gauge-invariant description of external leptons. Red lines symbolize all possible propagator types that are consistent with Feynman rules of the weak sector, and crosses correspond to operator insertions of the composite scalar-lepton fields. The terms $\phi_a \in \{h, \chi, \phi^\pm\}$ represent the would-be Goldstone bosons in (6.1) and (6.2).

Future studies will involve the clarification of the exact kinematical dependence of the external factors K_i , allowing us to obtain a first glimpse into the damping prefactors of the higher n-point functions. The final evaluation of all scalar integrals in our matrix elements and counterterms will be done via LoopTools [42, 43], with its code extension allowing for a full calculation of all scalar integrals with complex masses, as long as one external particle is massless [44]. Additionally, an extension to the massive weak (or electroweak) sector is obvious, where we could compare different non-vanishing helicity configurations for collision experiments in future lepton colliders.

Bibliography

- [1] G't Hooft. "Why do We Need Local Gauge Invariance in Theories with Vector Particles? An Introduction." In: *Recent Developments in Gauge Theories*. Springer, 1980, pp. 101–115.
- [2] Thomas Banks and Eliezer Rabinovici. "Finite-temperature behavior of the lattice abelian Higgs model." In: *Nuclear Physics B* 160.2 (1979), pp. 349–379.
- [3] J Fröhlich, G Morchio, and F Strocchi. "Higgs phenomenon without a symmetry breaking order parameter." In: *Physics Letters B* 97.2 (1980), pp. 249–252.
- [4] Axel Maas. "BOUND-STATE/ELEMENTARY-PARTICLE DUALITY IN THE HIGGS SECTOR AND THE CASE FOR AN EXCITED" HIGGS" WITHIN THE STANDARD MODEL." In: *Modern Physics Letters A* 28.28 (2013), p. 1350103.
- [5] Manfred Böhm, Ansgar Denner, and Hans Joos. *Gauge theories of the strong and electroweak interaction*. Springer Science & Business Media, 2012.
- [6] Masaharu Tanabashi et al. "Review of Particle Physics: particle data groups." In: *Physical Review D* 98.3 (2018), pp. 1–1898.
- [7] J Fröhlich, G Morchio, and F Strocchi. "Higgs phenomenon without symmetry breaking order parameter." In: *Nuclear Physics B* 190.3 (1981), pp. 553–582.
- [8] Benjamin W Lee and Jean Zinn-Justin. "Spontaneously broken gauge symmetries. I. Preliminaries." In: *Physical Review D* 5.12 (1972), p. 3121.
- [9] Axel Maas and Tajdar Mufti. "Two- and three-point functions in Landau gauge Yang-Mills-Higgs theory." In: *Journal of High Energy Physics* 2014.4 (2014), pp. 1–45.
- [10] Vincenzo Afferrante et al. "Testing the mechanism of lepton compositeness." In: *SciPost Physics* 10.3 (2021), p. 062.
- [11] Pascal Törek and Axel Maas. "On observable particles in theories with a Brout-Englert-Higgs effect." In: *arXiv preprint arXiv:1806.11373* (2018).
- [12] Axel Maas and René Sondheimer. "Gauge-invariant description of the Higgs resonance and its phenomenological implications." In: *Physical Review D* 102.11 (Dec. 2020). ISSN: 2470-0029. DOI: 10.1103/physrevd.102.113001. URL: <http://dx.doi.org/10.1103/PhysRevD.102.113001>.

-
- [13] David Dudal et al. "Spectral properties of local gauge invariant composite operators in the SU (2) Yang–Mills–Higgs model." In: *The European Physical Journal C* 81.3 (2021), p. 222.
- [14] Larissa Egger, Axel Maas, and René Sondenheimer. "Pair production processes and flavor in gauge-invariant perturbation theory." In: *Modern Physics Letters A* 32.38 (Dec. 2017), p. 1750212. ISSN: 1793-6632. DOI: 10.1142/s0217732317502121. URL: <http://dx.doi.org/10.1142/S0217732317502121>.
- [15] Axel Maas and Franziska Reiner. "Restoring the Bloch-Nordsieck theorem in the electroweak sector of the standard model." In: *Physical Review D* 108.1 (July 2023). DOI: 10.1103/physrevd.108.013001. URL: <https://doi.org/10.1103%2Fphysrevd.108.013001>.
- [16] Sheldon L Glashow. "The renormalizability of vector meson interactions." In: *Nuclear Physics* 10 (1959), pp. 107–117.
- [17] Abdus Salam and John Clive Ward. "Weak and electromagnetic interactions." In: *Il Nuovo Cimento (1955-1965)* 11 (1959), pp. 568–577.
- [18] Steven Weinberg. "A model of leptons." In: *Physical review letters* 19.21 (1967), p. 1264.
- [19] Peter W Higgs. "Broken symmetries and the masses of gauge bosons." In: *Physical review letters* 13.16 (1964), p. 508.
- [20] François Englert and Robert Brout. "Broken symmetry and the mass of gauge vector mesons." In: *Physical review letters* 13.9 (1964), p. 321.
- [21] Ansgar Denner and Stefan Dittmaier. "Electroweak radiative corrections for collider physics." In: *Physics Reports* 864 (2020), pp. 1–163.
- [22] Albert S Schwarz. *Quantum field theory and topology*. Vol. 307. Springer Science & Business Media, 2013.
- [23] Shmuel Elitzur. "Impossibility of spontaneously breaking local symmetries." In: *Physical review d* 12.12 (1975), p. 3978.
- [24] Vladimir Naumovich Gribov. "Quantization of non-Abelian gauge theories." In: *Nuclear Physics B* 139.1-2 (1978), pp. 1–19.
- [25] Axel Maas. "Brout–Englert–Higgs physics: From foundations to phenomenology." In: *Progress in Particle and Nuclear Physics* 106 (May 2019), pp. 132–209. ISSN: 0146-6410. DOI: 10.1016/j.pnpnp.2019.02.003. URL: <http://dx.doi.org/10.1016/j.pnpnp.2019.02.003>.
- [26] René Sondenheimer. "Analytical relations for the bound state spectrum of gauge theories with a Brout-Englert-Higgs mechanism." In: *Physical Review D* 101.5 (2020), p. 056006.
- [27] Matthew D Schwartz. *Quantum field theory and the standard model*. Cambridge university press, 2014.

- [28] Lance J Dixon. “A brief introduction to modern amplitude methods.” In: *Journeys Through the Precision Frontier: Amplitudes for Colliders: TASI 2014 Proceedings of the 2014 Theoretical Advanced Study Institute in Elementary Particle Physics*. World Scientific, 2016, pp. 39–97.
- [29] Simon Plätzer and Fabian Veider. *SpinorHelicity*. Version 1.0. 2023.
- [30] Simon Plätzer and Fabian Veider. *Oneloop*. Version 1.0. 2023.
- [31] C. Gnendiger et al. “To $\{d\}$ d , or not to $\{d\}$ d : recent developments and comparisons of regularization schemes.” In: *The European Physical Journal C* 77.7 (July 2017). DOI: 10.1140/epjc/s10052-017-5023-2. URL: <https://doi.org/10.1140%2Fepjc%2Fs10052-017-5023-2>.
- [32] Joakim Alnefjord et al. “The chirality-flow formalism for the standard model.” In: *The European Physical Journal C* 81.4 (Apr. 2021). DOI: 10.1140/epjc/s10052-021-09055-2. URL: <https://doi.org/10.1140%2Fepjc%2Fs10052-021-09055-2>.
- [33] R Keith Ellis and Giulia Zanderighi. “Scalar one-loop integrals for QCD.” In: *Journal of High Energy Physics* 2008.02 (2008), p. 002.
- [34] Giampiero Passarino and M J G 1979 NuPhB Veltman. “One-loop corrections for $e^+ e^-$ annihilation into $\mu^+ \mu^-$ in the Weinberg model.” In: *Nuclear Physics B* 160.1 (1979), pp. 151–207.
- [35] Andrei I Davydychev. *A simple formula for reducing Feynman diagrams to scalar integrals*. Tech. rep. Moskovskij Gosudarstvennyj Univ., 1991.
- [36] Walter T Giele and EW Nigel Glover. “A calculational formalism for one-loop integrals.” In: *Journal of High Energy Physics* 2004.04 (2004), p. 029.
- [37] Vladyslav Shtabovenko, Rolf Mertig, and Frederik Orellana. “FeynCalc 9.3: New features and improvements.” In: *Computer Physics Communications* 256 (Nov. 2020), p. 107478. ISSN: 0010-4655. DOI: 10.1016/j.cpc.2020.107478. URL: <http://dx.doi.org/10.1016/j.cpc.2020.107478>.
- [38] Vladyslav Shtabovenko, Rolf Mertig, and Frederik Orellana. “New developments in FeynCalc 9.0.” In: *Computer Physics Communications* 207 (Oct. 2016), pp. 432–444. ISSN: 0010-4655. DOI: 10.1016/j.cpc.2016.06.008. URL: <http://dx.doi.org/10.1016/j.cpc.2016.06.008>.
- [39] Rolf Mertig, Manfred Böhm, and Ansgar Denner. “Feyn Calc-Computer-algebraic calculation of Feynman amplitudes.” In: *Computer Physics Communications* 64.3 (1991), pp. 345–359.
- [40] Paulo Nogueira. “Automatic Feynman graph generation.” In: *Journal of Computational Physics* 105.2 (1993), pp. 279–289.
- [41] John Ellson et al. “Graphviz and dynagraph—static and dynamic graph drawing tools.” In: *Graph drawing software* (2004), pp. 127–148.

-
- [42] T. Hahn and M. Pérez-Victoria. “Automated one-loop calculations in four and D dimensions.” In: *Computer Physics Communications* 118.2-3 (May 1999), pp. 153–165. DOI: 10.1016/s0010-4655(98)00173-8. URL: <https://doi.org/10.1016%2Fs0010-4655%2898%2900173-8>.
- [43] GJ Van Oldenborgh and Jos AM Vermaseren. “New algorithms for one-loop integrals.” In: *Zeitschrift für Physik C Particles and Fields* 46 (1990), pp. 425–437.
- [44] Dao Thi Nhung and Le Duc Ninh. “DoC: A code to calculate scalar one-loop four-point integrals with complex masses.” In: *Computer Physics Communications* 180.11 (Nov. 2009), pp. 2258–2267. DOI: 10.1016/j.cpc.2009.07.012. URL: <https://doi.org/10.1016%2Fj.cpc.2009.07.012>.
- [45] Gerard t Hooft and MJD1979NuPhB Veltman. “Scalar one-loop integrals.” In: *Nuclear Physics B* 153 (1979), pp. 365–401.

Appendix

Appendix A.

Conventions

A.1. Units

We make use of natural units throughout this paper, setting $c = \hbar = 1$. This allows for all quantities to be defined on a simple mass scale. We introduced the unit barn (b) to express the cross sectional area. It is related to GeV^{-2} via

$$1GeV^{-2} = 0.389379 \times 10^9 pb \quad (\text{A.1})$$

A.2. Minkowski space

We use the following convention for the metric tensor

$$g_{\mu\nu} = g^{\mu\nu} = \text{diag}(1, -1, -1, -1) \quad (\text{A.2})$$

The spacetime vectors are then given by

$$x^\mu = (x^0, \mathbf{x}) = (t, x, y, z), \quad x_\mu = (x^0, -\mathbf{x}) = (t, -x, -y, -z) \quad (\text{A.3})$$

and the usual summation convention over repeated (Greek) Lorentz indices is used

$$ab = a_\mu b^\mu = a^\mu b_\mu = \eta_{\mu\nu} a^\mu b^\nu = a^0 b^0 - \mathbf{ab} \quad (\text{A.4})$$

A.3. Mandelstam variables

We frequently make use of Mandelstam variables to simplify kinematics of our scattering process. For initial momenta p_1 and p_2 and final momenta p_3 and p_4 all pointing inward, they are

$$\begin{aligned} s &= (p_1 + p_2)^2 = (p_3 + p_4)^2 \\ t &= (p_1 + p_3)^2 = (p_2 + p_4)^2 \\ u &= (p_1 + p_4)^2 = (p_2 + p_3)^2 \end{aligned} \quad (\text{A.5})$$

The corresponding diagrams are often coined channels corresponding to tree-level interactions with one exchange particle. As they are the only Lorentz-invariant quantities one can create from external momenta, every cross section can be expressed in terms of s , t and u . They are not linearly independent since

$$s + t + u = \sum_{i=1}^4 m_i^2 \quad (\text{A.6})$$

If all masses are zero, we can simply express the scalar products of external momenta in terms of Mandelstam variables

$$\begin{aligned} p_1 \cdot p_2 &= p_3 \cdot p_4 = \frac{s}{2} \\ p_1 \cdot p_3 &= p_2 \cdot p_4 = \frac{t}{2} \\ p_1 \cdot p_4 &= p_2 \cdot p_3 = \frac{u}{2} \end{aligned}$$

The variables t and u can also be represented by s and the scattering angle θ

$$\begin{aligned} t &= -\frac{s}{2}(1 - \cos \theta) \\ u &= -\frac{s}{2}(1 + \cos \theta) \end{aligned}$$

A.4. Dirac & Pauli matrices

Dirac matrices γ^μ are generators of matrix representation of the Clifford algebra $Cl_{1,3}(\mathbb{R})$, acting on the space of Dirac spinors. They are given in the Weyl representation as

$$\gamma^\mu = \begin{pmatrix} 0 & \sigma^\mu \\ \bar{\sigma}^\mu & 0 \end{pmatrix}, \quad \gamma_5 = \begin{pmatrix} -\mathbb{1} & 0 \\ 0 & \mathbb{1} \end{pmatrix} \quad (\text{A.7})$$

and are expressed by the hermitian Pauli matrices

$$\begin{aligned} \sigma^\mu &= (\sigma^0, \vec{\sigma}) = (\sigma^0, \sigma^1, \sigma^2, \sigma^3) \\ &= \left(\begin{pmatrix} 1 & 0 \\ 0 & 1 \end{pmatrix}, \begin{pmatrix} 0 & 1 \\ 1 & 0 \end{pmatrix}, \begin{pmatrix} 0 & -i \\ i & 0 \end{pmatrix}, \begin{pmatrix} 1 & 0 \\ 0 & -1 \end{pmatrix} \right) \end{aligned} \quad (\text{A.8})$$

$$\bar{\sigma}^\mu = (\sigma^0, -\vec{\sigma}) \quad (\text{A.9})$$

that fulfill $(\sigma^\mu)^2 = \mathbb{1}_{2 \times 2}$ for all μ . In four spacetime dimensions, relevant contraction identities for Dirac matrices are

$$\gamma^\alpha \gamma_\alpha = 4\mathbb{1}_4 \quad (\text{A.10})$$

$$\gamma^\alpha \gamma^\beta \gamma_\alpha = -2\gamma^\beta \quad (\text{A.11})$$

$$\gamma^\alpha \gamma^\beta \gamma^\delta \gamma_\alpha = 4g^{\beta\delta} \quad (\text{A.12})$$

$$\gamma^\alpha \gamma^\beta \gamma^\delta \gamma^\epsilon \gamma_\alpha = -2\gamma^\epsilon \gamma^\delta \gamma^\beta \quad (\text{A.13})$$

and trace identities in four dimensions are

$$\text{Tr}(1) = 4 \quad (\text{A.14})$$

$$\text{Tr}(\gamma_\alpha) = 0 \quad (\text{A.15})$$

$$\text{Tr}(\gamma_\alpha \gamma_\beta) = 4g_{\alpha\beta} \quad (\text{A.16})$$

$$\text{Tr}(\gamma_\alpha \gamma_\beta \gamma_\delta \gamma_\omega) = 4(g_{\alpha\beta} g_{\delta\omega} - g_{\alpha\delta} g_{\beta\omega} + g_{\alpha\omega} g_{\beta\delta}) \quad (\text{A.17})$$

$$\text{Tr}(\text{odd } \# \gamma_\alpha) = 0 \quad (\text{A.18})$$

In case of dimensional regularization they need to be extended to $d = 4 - 2\epsilon$

$$\gamma^\alpha \gamma_\alpha = (4 - 2\epsilon)\mathbb{1} \quad (\text{A.19})$$

$$\gamma^\alpha \gamma^\beta \gamma_\alpha = -(2 - 2\epsilon)\gamma^\beta \quad (\text{A.20})$$

$$\gamma^\alpha \gamma^\beta \gamma^\delta \gamma_\alpha = 4g^{\beta\delta} - 2\epsilon\gamma^\beta \gamma^\delta \quad (\text{A.21})$$

$$\gamma^\alpha \gamma^\beta \gamma^\delta \gamma^\epsilon \gamma_\alpha = -2\gamma^\epsilon \gamma^\delta \gamma^\beta + 2\epsilon\gamma^\beta \gamma^\delta \gamma^\epsilon \quad (\text{A.22})$$

These identities are incorporated in the simplification of our tensor integrals, where careful cancellation of ϵ -parameters arising from loop reductions is necessary in order to ensure a consistent series expansion up to order $\mathcal{O}(\epsilon)$.

Appendix B.

Tree level for the full EW model

The calculations of the differential cross section of $e_L^- e_L^+ \rightarrow \mu_L^- \mu_L^+$ for the massless electroweak sector are summarized here. This time, there are two matrix elements that contribute to the tree-level interaction due to an interaction with the neutral Z-boson and the photon γ

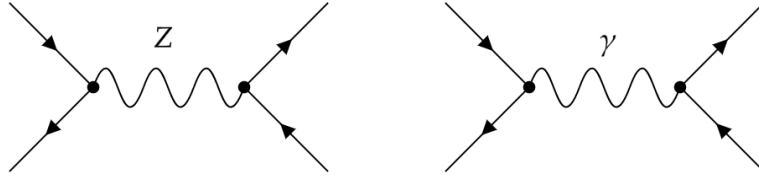


Figure B.1.: Tree level diagrams for the scattering process in the full EW sector

Converting these into algebraic expressions using Feynman rules of the EW standard model [5] yields

$$\mathcal{M}^Z = g^2 s_W^2 C_L^2 \frac{1}{s - m_Z^2} [14] \langle 32 \rangle \quad (\text{B.1})$$

$$\mathcal{M}^\gamma = g^2 s_W^2 \frac{1}{s} [14] \langle 32 \rangle \quad (\text{B.2})$$

where s_W and c_W are the sine and cosine of the weak mixing angle θ_W that rotates the vector field B_μ of the $U_Y(1)$ group and our vector field W_μ^3 from $SU_W(2)$ in the broken electroweak sector. The term

$$C_L = \frac{s_W^2 - \frac{1}{2}}{s_W c_W} \quad (\text{B.3})$$

originates from the interaction of the Z-boson with an left-handed fermion-antifermion pair and can be derived by expanding the electroweak Lagrangian in terms of the rotated vector fields. The Z-boson mass

$$m_Z = \frac{g v}{2 c_W} \quad (\text{B.4})$$

differs by a factor of c_W from the mass of our neutral vector boson W . Squaring the sum of matrix elements and adding the prefactor $\frac{1}{64\pi^2 s}$ leads to the differential cross section

$$\left(\frac{d\sigma}{d\Omega}\right)_{CM}^{EW} = \frac{g^4 s}{1024\pi^2} \left(\frac{s_W^2}{s} + \frac{(s_W^2 - \frac{1}{2})}{c_W^2 (s - m_Z^2)} \right)^2 (1 + \cos(\theta))^2 \quad (\text{B.5})$$

The plots (B.2) and (B.3) show the behaviour of the EW sector compared to our $SU(2)$ model for the measured values $s_W^2 \approx 0.223$ and $c_W^2 \approx 0.7777$. The difference is only noticeable at energies around and lower than the mass pole of the Z -boson.

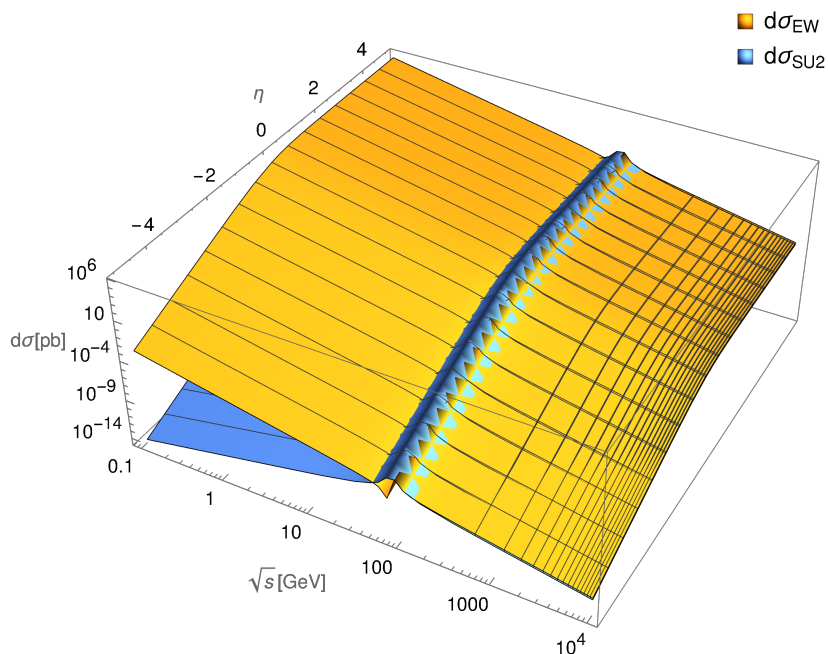


Figure B.2.: Differential cross sections at tree-level for the full EW model and our $SU(2)$ model in terms of the CM-energy \sqrt{s} and the pseudorapidity η

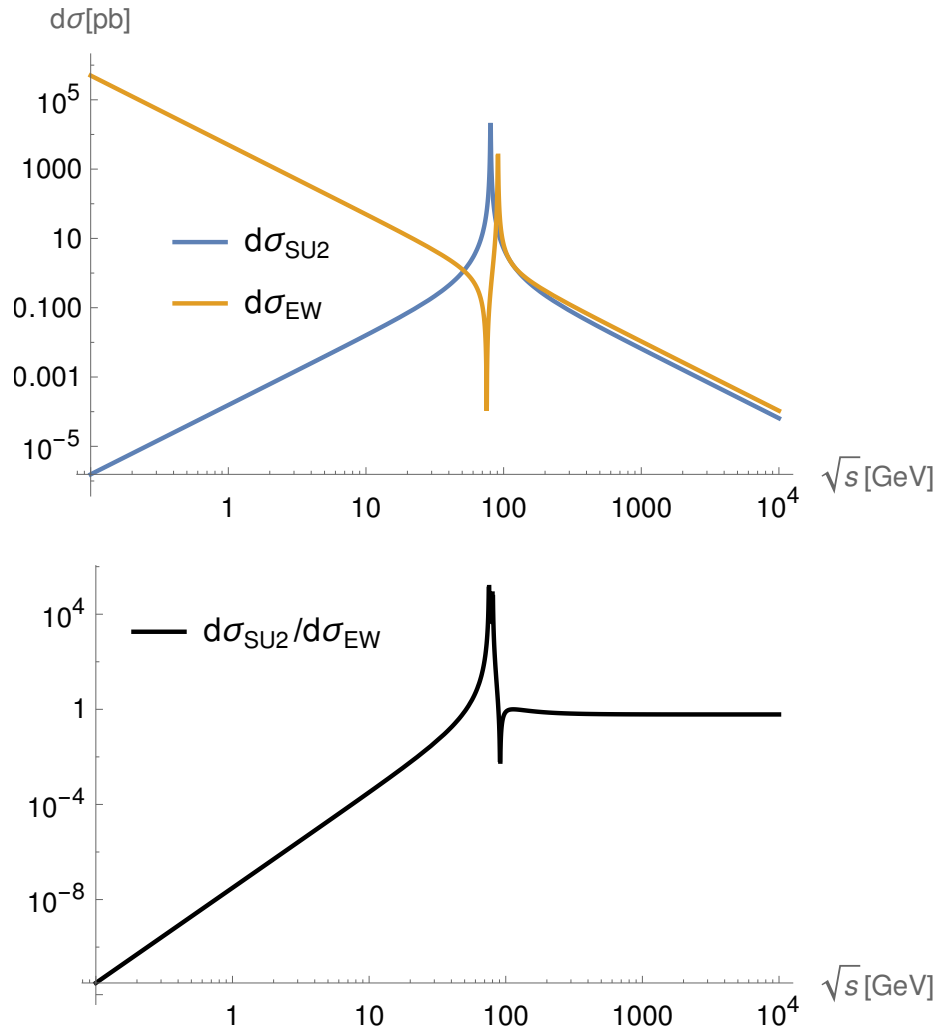


Figure B.3.: Differential cross section of the tree-level process in terms of the CM-energy \sqrt{s} and fixed angle $\theta = 0$ of the full EW model and our $SU(2)$ model (above). The comparison $d\sigma_{SU(2)}/d\sigma_{EW}$ shows strong agreement for energies far above the pole of the vector boson (below).

Appendix C.

Feynman rules in Weyl representation

We give a full list of all the leptonic external legs, all propagators and all relevant interaction vertices for our process in an arbitrary 't Hooft gauge.

C.1. Elementary external legs

The elementary external leptons $l = e, \mu$ are given in terms of Dirac and Weyl spinors.

$$\begin{array}{c}
 \begin{array}{c}
 l_L \\
 \longrightarrow \\
 l_R
 \end{array}
 \xrightarrow{p_i}
 \begin{array}{c}
 \text{---} \\
 \text{---} \\
 \text{---}
 \end{array}
 = \frac{P_L u(p_i)}{P_R u(p_i)} \equiv \begin{array}{l} |i\rangle \\ |i\rangle \end{array}
 = \begin{array}{c}
 \begin{array}{c}
 \text{---} \\
 \text{---} \\
 \text{---}
 \end{array}
 \xleftarrow{p_i} \\
 \bar{l}_L \\
 \bar{l}_R
 \end{array}
 \\
 \hline
 \begin{array}{c}
 \bar{l}_L \\
 \xrightarrow{p_i} \\
 \bar{l}_R
 \end{array}
 \xrightarrow{p_i}
 \begin{array}{c}
 \text{---} \\
 \text{---} \\
 \text{---}
 \end{array}
 = \frac{\bar{v}(p_i) P_L}{\bar{v}(p_i) P_R} = \frac{\overline{v(p_i) P_R}}{\overline{v(p_i) P_L}} \equiv \begin{array}{l} \langle i| \\ [i] \end{array}
 = \begin{array}{c}
 \begin{array}{c}
 \text{---} \\
 \text{---} \\
 \text{---}
 \end{array}
 \xleftarrow{p_i} \\
 l_L \\
 l_R
 \end{array}
 \end{array}
 \end{array}$$

Figure C.1.: Full list of all leptonic external legs

C.2. External bound states

The bound-state insertions for our compound leptons $L = E, M$ are denoted by a cross that corresponds to an elementary spinor with two internal propagators and an integration over the constituent momentum. The BS-amplitude is taken to be an elementary spinor in our NLO description, and a renormalization of the wave function K_i in terms of momentum p_i with mass dimension one is added.

$$\begin{aligned}
 & L_L \text{ (cross)} \begin{array}{l} \nearrow k \\ \searrow p_i - k \end{array} = -\frac{K_i \mu^{4-d}}{(2\pi)^d} \int d^d k \frac{\gamma^\alpha k_\alpha}{k^2 [(p-k)^2 - m_S^2]} |p], \quad S = h, \chi, \phi^\pm \\
 & \bar{L}_L \text{ (cross)} \begin{array}{l} \nearrow k \\ \searrow p_i - k \end{array} = -\langle p| \frac{K_i \mu^{4-d}}{(2\pi)^d} \int d^d k \frac{\gamma^\alpha k_\alpha}{k^2 [(p-k)^2 - m_S^2]}, \quad S = h, \chi, \phi^\pm \\
 & \begin{array}{l} \nearrow p_i - k \\ \searrow k \end{array} \text{ (cross)} L_L = -\langle p| \frac{K_i \mu^{4-d}}{(2\pi)^d} \int d^d k \frac{\gamma^\alpha k_\alpha}{k^2 [(p-k)^2 - m_S^2]}, \quad S = h, \chi, \phi^\pm \\
 & \begin{array}{l} \nearrow p_i - k \\ \searrow k \end{array} \text{ (cross)} \bar{L}_L = -\frac{K_i \mu^{4-d}}{(2\pi)^d} \int d^d k \frac{\gamma^\alpha k_\alpha}{k^2 [(p-k)^2 - m_S^2]} |p], \quad S = h, \chi, \phi^\pm
 \end{aligned}$$

Figure C.2.: Operator insertion of the bound states

C.3. Propagators

$$\begin{aligned}
 V_\mu \overset{q}{\curvearrowright} V_\nu &= \frac{-i}{q^2 - m^2} \left(g_{\mu\nu} - \frac{q_\mu q_\nu}{q^2} \right) - \frac{q_\mu q_\nu}{q^2} \frac{i\xi_V}{q^2 - \xi_V m^2}, \quad V = W, + \\
 f \overset{q}{\longrightarrow} \bar{f} &= \frac{i\gamma^\mu q_\mu}{q^2} \\
 S \overset{q}{\cdots\cdots} S &= \frac{i}{q^2 - m_S}, \quad S = h, \chi, \phi^\pm \\
 G \overset{q}{\dashrightarrow} \bar{G} &= \frac{i}{q^2 - m_G}, \quad G = u^W, u^\pm
 \end{aligned}$$

Figure C.3.: Full list of all propagators.

C.4. Interaction vertices

$$\begin{aligned}
 \begin{array}{ccc}
 S_1 & & S_3 \\
 & \times & \\
 S_2 & & S_4
 \end{array} &= -i\lambda C^{S_1 S_2 S_3 S_4}, \quad C^{hhhh} = C^{\chi\chi\chi\chi} = \frac{3}{2}, \quad C^{\phi^+\phi^-\phi^+\phi^-} = 1 \\
 & \quad C^{hh\chi\chi} = C^{hh\phi^+\phi^-} = C^{\chi\chi\phi^+\phi^-} = \frac{1}{2} \\
 \begin{array}{ccc}
 W_\mu^+ & & W_\rho^3 \\
 \curvearrowright & & \curvearrowright \\
 & \times & \\
 W_\nu^- & & W_\sigma^3
 \end{array} &= -ig^2(2g_{\mu\nu}g_{\sigma\rho} - g_{\nu\rho}g_{\mu\sigma} - g_{\rho\mu}g_{\nu\sigma}) \\
 \begin{array}{ccc}
 S_1 & & V_{1,\mu} \\
 & \times & \\
 S_2 & & V_{2,\nu}
 \end{array} &= ig^2 g_{\mu\nu} C^{S_1 S_2 V_1 V_2}, \quad C^{WWhh} = C^{WW\chi\chi} = C^{W^+W^-hh} \\
 & \quad = C^{W^+W^-\chi\chi} = C^{W^+W^-\phi^+\phi^-} = C^{WW\phi^+\phi^-} = \frac{1}{2}
 \end{aligned}$$

Figure C.4.: Full list of all interactions containing four particles.

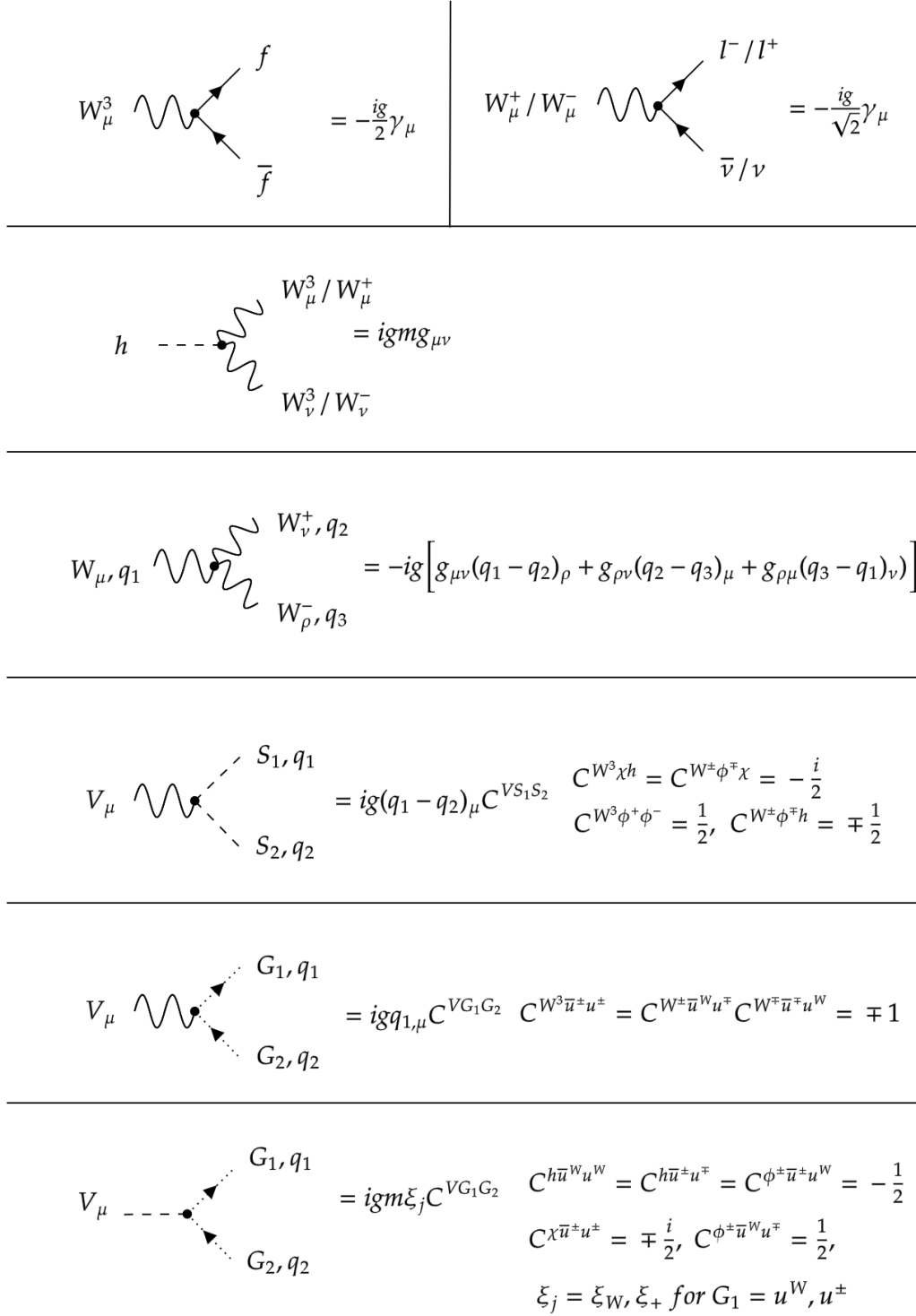


Figure C.5.: Full list of all interactions containing three particles.

Appendix D.

Scalar integrals

D.1. Convention

The logarithm has a cut along the negative real axis, and the products of logarithms are

$$\ln(ab) = \ln(a) + \ln(b) + \eta(a, b) \quad (\text{D.1})$$

$$\eta(a, b) = 2\pi i \left(\theta(-\text{Im}(a))\theta(-\text{Im}(b))\theta(\text{Im}(ab)) \right. \\ \left. - \theta(\text{Im}(a))\theta(\text{Im}(b))\theta(-\text{Im}(ab)) \right) \quad (\text{D.2})$$

For $a, b \in \mathbb{C}$ and $c, d \in \mathbb{R}$ this simplifies to

$$\ln(ab) = \ln(a) + \ln(b) \quad (\text{D.3})$$

$$\ln\left(\frac{a}{b}\right) = \ln(a) - \ln(b) \quad (\text{D.4})$$

$$\ln(cd - i\delta) = \ln(a - i\delta_2) + \ln\left(B - i\frac{\delta}{A}\right) \quad (\text{D.5})$$

for infinitesimal δ and δ_2 . The dilogarithm appears for reduced algebraic expression of triangle and box integrals

$$Sp(x) = - \int_0^1 dt \frac{\ln(1 - xt)}{t} \quad (\text{D.6})$$

which has a cut along the positive real axis starting at $x = 1$. We can expand it around $\ln(1 - x)$ and obtain an infinite sum in terms of Bernouilly numbers B_n

$$Sp(x) = \sum_{n=0}^{\infty} B_n \frac{z^{n+1}}{(n+1)!}, \quad z = -\ln(1 - x) \quad (\text{D.7})$$

D.2. Tadpole integral

The tadpole integral contains an UV-divergence and needs to be regulated. It is independent of external momenta and reads

$$\begin{aligned}
S_{(1)}^4(0|m^2) &= -\mu^{2\epsilon}\Gamma(-1+\epsilon)(m^2-i\delta)^{1-\epsilon} \\
&= m^2\left(\frac{\mu^2}{m^2-i\delta}\right)^\epsilon\left(\frac{1}{\epsilon}-\gamma_E+1\right)+\mathcal{O}(\epsilon) \\
&= m^2\left(\frac{1}{\epsilon}-\gamma_E+1-\ln\left(\frac{m^2}{\mu^2}\right)\right)+\mathcal{O}(\epsilon)
\end{aligned} \tag{D.8}$$

D.3. Bubble integrals

The most general massive bubble integral reads

$$\begin{aligned}
S_{(1,1)}^4(0,q^2|m_1^2,m_2^2) &= \\
&\left(\frac{\mu^2}{q^2-i\delta}\right)^\epsilon\left(\frac{1}{\epsilon}-\gamma_E+2+\sum_{k=\pm}\left(\gamma_k\log\left(\frac{\gamma_k-1}{\gamma_k}\right)-\ln(\gamma_k-1)\right)\right)+\mathcal{O}(\epsilon)
\end{aligned} \tag{D.9}$$

with γ_\pm being the solutions of the quadratic equation

$$-\gamma^2q^2+\gamma(q^2+m_2^2-m_1^2)+m_1^2-i\delta=0 \tag{D.10}$$

$$\gamma_\pm=\frac{q^2-m_2^2+m_1^2\pm\sqrt{(q^2-m_2^2+m_1^2)^2-4q^2(m_1^2-i\delta)}}{2q^2} \tag{D.11}$$

that appears in the final integration step of bubble diagrams.

There are two different special cases for non-vanishing q^2 and for one or two massless particles

$$\begin{aligned}
 S_{(1,1)}^{4-2\epsilon}(0, q^2 | 0, m^2) &= \\
 & \left(\frac{\mu^2}{m^2} \right)^\epsilon \left(\frac{1}{\epsilon} - \gamma_E + 2 + \frac{m^2 - q^2}{q^2} \ln \left(\frac{m^2 - q^2 - i\delta}{m^2} \right) \right) + \mathcal{O}(\epsilon) \\
 &= \frac{1}{\epsilon} - \gamma_E + 2 + \frac{m^2 - q^2}{q^2} \ln \left(\frac{m^2 - q^2 - i\delta}{m^2} \right) + \ln \left(\frac{\mu^2}{m^2} \right) + \mathcal{O}(\epsilon) \quad (\text{D.12})
 \end{aligned}$$

$$\begin{aligned}
 S_{(1,1)}^{4-2\epsilon}(0, q^2 | 0, 0) &= \left(\frac{\mu^2}{-q^2 - i\delta} \right)^\epsilon \left(\frac{1}{\epsilon} - \gamma_E + 2 \right) + \mathcal{O}(\epsilon) \\
 &= \frac{1}{\epsilon} - \gamma_E + 2 + \ln \left(\frac{-\mu^2}{q^2 + i\delta} \right) + \mathcal{O}(\epsilon) \quad (\text{D.13})
 \end{aligned}$$

If the momentum dependence vanishes, as is the case for pinched bubble integrals that appear in our integral reduction, the solution simplifies to

$$\begin{aligned}
 S_{(1,1)}^{4-2\epsilon}(0, 0 | m_1^2, m_2^2) &= \\
 & \left(\frac{\mu^2}{m_2^2 - m_1^2 - i\delta} \right)^\epsilon \left(\frac{1}{\epsilon} - \gamma_E + 2 + \left(\gamma_0 \log \left(\frac{\gamma_0 - 1}{\gamma_0} \right) - \ln(\gamma_0 - 1) \right) \right) + \mathcal{O}(\epsilon) \\
 & \quad (\text{D.14})
 \end{aligned}$$

with γ_0 being the solution of the linear equation

$$\gamma_0(m_2^2 - m_1^2) + m_1^2 - i\delta = 0, \quad \gamma_0 = \frac{m_1^2 - i\delta}{m_1^2 - m_2^2} \quad (\text{D.15})$$

In case both masses are equal, there remains a very simple solution

$$S_{(1,1)}^{4-2\epsilon}(0, 0 | m^2, m^2) = \left(\frac{\mu^2}{m^2 - i\delta} \right)^\epsilon \left(\frac{1}{\epsilon} - \gamma_E + 2 \right) \quad (\text{D.16})$$

Both masses being zero would lead to an IR-divergence [45], but this case does not appear in our calculations.

Appendix E.

QGRAF

E.1. Model file

```
%_authors:_Simon_Plaetzer_<simon.plaetzer@uni-graz.at>
%_Fabian_Veider_<fabian.veider@edu.uni-graz.at>
%_weak_standard_model_including_FMS_contributions
%_no_QCD_yet
%_only_includes_two_fermion_generations
%_no_Yukawa_coupling,_no_photon_interaction
%_tested_with_qgraf_3.5.1

%_leptons_--_mind:_fermion_--_antifermion

[_eL,_eL_bar,_-_]
[_nueL,_nueL_bar,_-_]
[_eR,_eR_bar,_-_]
[_mL,_mL_bar,_-_]
[_numL,_numL_bar,_-_]
[_mR,_mR_bar,_-_]

%_quarks_--_mind:_fermion_--_antifermion

[_uL,_uL_bar,_-_]
[_dL,_dL_bar,_-_]
[_uR,_uR_bar,_-_]
[_dR,_dR_bar,_-_]
[_cL,_cL_bar,_-_]
[_sL,_sL_bar,_-_]
[_cR,_cR_bar,_-_]
[_sR,_sR_bar,_-_]

%_quark_mass_terms_--_mind:_fermion_--_antifermion

%_physical_bosons
```

```

[w,w,+]
[w_plus,w_minus,+]
[h,h,+]

%goldstones

[chi,chi,+]
[phi_plus,phi_minus,+]

%ghosts

[vw,vw_bar,-]
[v_plus,v_plus_bar,-]
[v_minus,v_minus_bar,-]

%gauge_invariant_perturbation_theory:bound_states

[UL,UL_bar,-,external]
[DL,DL_bar,-,external]
[CL,CL_bar,-,external]
[SL,SL_bar,-,external]
[EL,EL_bar,-,external]
[NueL,NueL_bar,-,external]
[ML,ML_bar,-,external]
[NumL,NumL_bar,-,external]
[H,H,+,external]

[W,W,+,external]
[W_plus,W_minus,+,external]

%vector_vertices

[w,w_plus,w_minus;gpow='1',vpow='0']

[w,w,w_plus,w_minus;gpow='2',vpow='0']
[w_plus,w_minus,w_plus,w_minus;gpow='2',vpow='0']

%scalar_vertices

[h,h,h;gpow='1',vpow='0']
[h,chi,chi;gpow='1',vpow='0']
[h,phi_plus,phi_minus;gpow='1',vpow='0']

```

```
[_h,_h,_h,_h;_gpow=_2',_vpow=_0']
[_chi,_chi,_chi,_chi;_gpow=_2',_vpow=_0']
[_h,_h,_chi,_chi;_gpow=_2',_vpow=_0']
[_h,_h,_phi_plus,_phi_minus;_gpow=_2',_vpow=_0']
[_chi,_chi,_phi_plus,_phi_minus;_gpow=_2',_vpow=_0']
[_phi_plus,_phi_minus,_phi_plus,_phi_minus;_gpow=_2',_vpow=_0']
```

%_vector/scalar_vertices

```
[_w,_h,_chi;_gpow=_1',_vpow=_0']
[_w,_phi_plus,_phi_minus;_gpow=_1',_vpow=_0']
[_w_plus,_phi_minus,_h;_gpow=_1',_vpow=_0']
[_w_minus,_phi_plus,_h;_gpow=_1',_vpow=_0']
[_w_plus,_phi_minus,_chi;_gpow=_1',_vpow=_0']
[_w_minus,_phi_plus,_chi;_gpow=_1',_vpow=_0']
```

```
[_w,_w,_h,_h;_gpow=_2',_vpow=_0']
[_w,_w,_chi,_chi;_gpow=_2',_vpow=_0']
[_w_plus,_w_minus,_h,_h;_gpow=_2',_vpow=_0']
[_w_plus,_w_minus,_chi,_chi;_gpow=_2',_vpow=_0']
[_w_plus,_w_minus,_phi_plus,_phi_minus;_gpow=_2',_vpow=_0']
[_w,_w,_phi_plus,_phi_minus;_gpow=_2',_vpow=_0']
[_w_plus,_w,_phi_minus,_h;_gpow=_2',_vpow=_0']
[_w_plus,_w,_phi_minus,_chi;_gpow=_2',_vpow=_0']
[_w_minus,_w,_phi_plus,_h;_gpow=_2',_vpow=_0']
[_w_minus,_w,_phi_plus,_chi;_gpow=_2',_vpow=_0']
```

```
[_h,_w,_w;_gpow=_1',_vpow=_0']
[_h,_w_plus,_w_minus;_gpow=_1',_vpow=_0']
[_phi_plus,_w_minus,_w;_gpow=_1',_vpow=_0']
[_phi_minus,_w_plus,_w;_gpow=_1',_vpow=_0']
```

%_fermion_vertices--_mind:_antifermion-_fermion-_boson

```
[_eL_bar,_eL,_w;_gpow=_1',_vpow=_0']
[_eR_bar,_eR,_w;_gpow=_1',_vpow=_0']
[_mL_bar,_mL,_w;_gpow=_1',_vpow=_0']
[_mR_bar,_mR,_w;_gpow=_1',_vpow=_0']
[_uL_bar,_uL,_w;_gpow=_1',_vpow=_0']
[_uR_bar,_uR,_w;_gpow=_1',_vpow=_0']
[_dL_bar,_dL,_w;_gpow=_1',_vpow=_0']
[_dR_bar,_dR,_w;_gpow=_1',_vpow=_0']
```

```

[ucL_bar,ucL,uw;ugpow=u'1',uvpow=u'0']
[ucR_bar,ucR,uw;ugpow=u'1',uvpow=u'0']
[usL_bar,usL,uw;ugpow=u'1',uvpow=u'0']
[usR_bar,usR,uw;ugpow=u'1',uvpow=u'0']

[unueL_bar,unueL,uw;ugpow=u'1',uvpow=u'0']
[unumL_bar,unumL,uw;ugpow=u'1',uvpow=u'0']

[uuL_bar,udL,uw_plus;ugpow=u'1',uvpow=u'0']
[udL_bar,uuL,uw_minus;ugpow=u'1',uvpow=u'0']
[ucL_bar,usL,uw_plus;ugpow=u'1',uvpow=u'0']
[usL_bar,ucL,uw_minus;ugpow=u'1',uvpow=u'0']
[unueL_bar,ueL,uw_plus;ugpow=u'1',uvpow=u'0']
[ueL_bar,unueL,uw_minus;ugpow=u'1',uvpow=u'0']
[unumL_bar,umL,uw_plus;ugpow=u'1',uvpow=u'0']
[umL_bar,unumL,uw_minus;ugpow=u'1',uvpow=u'0']

%fermion_mass_term_vertices(1)--mind:antifermion-fermion-boson

%fermion_mass_term_vertices(2)--mind:antifermion-fermion-boson

%ghost_vertices--mind:antighost-ghost-boson

[uv_plus_bar,uv_plus,uw;ugpow=u'1',uvpow=u'0']
[uv_minus_bar,uv_minus,uw;ugpow=u'1',uvpow=u'0']

[uvw_bar,uv_minus,uw_plus;ugpow=u'1',uvpow=u'0']
[uvw_bar,uv_plus,uw_minus;ugpow=u'1',uvpow=u'0']
[uv_plus_bar,uvw,uw_plus;ugpow=u'1',uvpow=u'0']
[uv_minus_bar,uvw,uw_minus;ugpow=u'1',uvpow=u'0']

[uvw_bar,uvw,uh;ugpow=u'1',uvpow=u'0']
[uv_plus_bar,uv_plus,uh;ugpow=u'1',uvpow=u'0']
[uv_minus_bar,uv_minus,uh;ugpow=u'1',uvpow=u'0']
[uv_plus_bar,uv_plus,uchi;ugpow=u'1',uvpow=u'0']
[uv_minus_bar,uv_minus,uchi;ugpow=u'1',uvpow=u'0']

[uv_plus_bar,uvw,phi_plus;ugpow=u'1',uvpow=u'0']
[uv_minus_bar,uvw,phi_minus;ugpow=u'1',uvpow=u'0']
[uvw_bar,uv_plus,phi_minus;ugpow=u'1',uvpow=u'0']
[uvw_bar,uv_minus,phi_plus;ugpow=u'1',uvpow=u'0']

%gauge_invariant_perturbation_theory:bound_state_constituents

```



```

[eL_bar,NueL,phi_minus;ugpow=u'0',uvpow=u'1']

[numL_bar,NumL,h;ugpow=u'0',uvpow=u'1']
[numL_bar,NumL,chi;ugpow=u'0',uvpow=u'1']
[mL_bar,NumL,phi_minus;ugpow=u'0',uvpow=u'1']

[eL_bar,eL,h;ugpow=u'0',uvpow=u'1']
[eL_bar,eL,chi;ugpow=u'0',uvpow=u'1']
[eL_bar,nueL,phi_minus;ugpow=u'0',uvpow=u'1']

[mL_bar,mL,h;ugpow=u'0',uvpow=u'1']
[mL_bar,mL,chi;ugpow=u'0',uvpow=u'1']
[mL_bar,numL,phi_minus;ugpow=u'0',uvpow=u'1']

[eL_bar,eL,h;ugpow=u'0',uvpow=u'1']
[eL_bar,eL,chi;ugpow=u'0',uvpow=u'1']
[nueL_bar,eL,phi_plus;ugpow=u'0',uvpow=u'1']

[mL_bar,mL,h;ugpow=u'0',uvpow=u'1']
[mL_bar,mL,chi;ugpow=u'0',uvpow=u'1']
[numL_bar,mL,phi_plus;ugpow=u'0',uvpow=u'1']

[H,h,h;ugpow=u'0',uvpow=u'1']
[H,chi,chi;ugpow=u'0',uvpow=u'1']
[H,phi_plus,phi_minus;ugpow=u'0',uvpow=u'1']

```